Theses   Electronic Theses and Dissertations

2004

Structural Studies of the Role of Iron Oxide in Environmental Catalysis

Aisha Ali Saif Rashid Al-Nayeli

Follow this and additional works at: https://scholarworks.uaeu.ac.ae/all_theses

Part of the Environmental Sciences Commons

United Arab Emirates University
Deanship of Graduate Studies
M.Sc. Program in Environmental Sciences

"STRUCTURAL STUDIES OF THE ROLE OF IRON OXIDE IN ENVIRONMENTAL CATALYSIS"

By

Aisha Ali Saif Rashid Al-Nayeli

A thesis
Submitted to

United Arab Emirates University
In partial fulfillment of the requirements
For the Degree of M.Sc. in Environmental Sciences

Supervisors

Brian Murphy	Abbas Khaleel
Assistant Professor	Assistant Professor
Department of Chemistry	Department of Chemistry
Faculty of Science	Faculty of Science
UAEU	UAEU

2004

United Arab Emirates University

Deanship of Graduate Studies

M.Sc. Program in Environmental Science

CERTIFICATE OF APPROVAL

M.Sc. THESIS

This is to certify that the M.Sc. thesis of

Aisha Ali Saif Al-Nayeli

Has been approved by the Examining Committee for the thesis requirement for the Degree

of M.Sc. in Environmental Sciences

At the May 2004 graduation.

	Date	Signature

Thesis Committee:

1-

2-

3-

Dean of Graduate studies
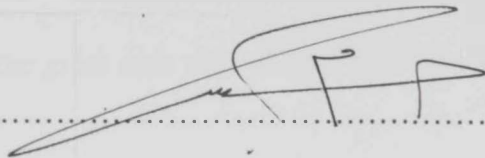
The Thesis of Aisha Ali Al-Nayeli for the Degree of Master of Science in Environmental is approved.

Examining Committee Member, Dr. Brian Murphy

Examining Committee Member, Dr. Maryam Al-Yousef

Examining Committee Member, Prof. Mike Hursthouse

Dean of the Graduate Studies, Dr. Hadef Rashed Al-Owais

United Arab Emirates University
2003/2004

Dedication

.

.

To the very special person who resides deep in my heart ..

To the great man who offered me every thing while I offered him little in return

.

.

.

.

To my father..

In whose eyes I always see the happiness for my happiness..

and the sadness for my sadness..

and the tears for my cry..

.

.

.

.

To my beloved father I dedicate this work ..

.

.

.

Acknowledgement

Praise and thanks to *Allah* who granted me the health and the ability to complete this thesis under his mercy. *Allah*, the Almighty, is the one who deserves sincere worship and complete obedience.

My sincere thanks to Dr. Brian Murphy, Assistant Professor of Inorganic Chemistry, for his continuous and active contribution to my thesis, especially, in the final stages involving the editing and formatting. Without his efforts and encouragement this work would not have been completed. In addition, my sincere and deep thanks to Dr. Abbas Khalil, Assistant Professor of Inorganic Chemistry, for his continuous efforts in helping me complete the experimental part of this work. He stood with me in the laboratory solving several technical problems and provided me with all the necessary equipment and technical assistance I needed for the experiments. Dr. Khalil devoted a whole summer period for the completion of this work.

My deep thanks also to all of the faculty members in the Department of Chemistry for their generous and helpful advice as well as their words of encouragement, which was a great help for me in completing this project. I would also like to thank all the specialists in the Central Laboratory Unit (CLU) at UAEU.

I thank everyone who taught me up at all stages in my career and education. Some of them sadly have passed away; may *Allah* grant them Paradise; some of them have left the country, may Allah protect them; and some of them are still here with us; may *Allah* grant them happiness. I will never forget any of them and their efforts.

I would like also to thank Dr. Mohammad Khatab for his help especially with his efforts in helping me in my literature search and for his gentle encouragement and words of moral support, when he used to say "you are the best".

Very special thanks to my very close friend, Lina Al-Kaabi, for her love and support. She was with me at all times, the happy as well as the sad moments. I will never forget the summer vacation she sacrificed to stay with me in the laboratory everyday. Just being there was a great help and support. Lina: My deep thanks and sincere love to you.

My deepest and most sincere thanks are to my sisters who always stood with me and were patient with me all the time even during the tense periods when I was writing this thesis. My deep thanks to my brother Mohammad who was the first one to stand by me and encourage me to continue in higher education.

Finally, all of my love and thanks are to my mother, who devoted her life for our success and happiness. We were always her hope and pride.

ABSTRACT

This thesis presents several fundamental studies of structure-reactivity relationships between pure iron oxides, supported and composite oxides specifically in relation to the decomposition of carbon tetrachloride, CCl_4. A series of iron oxides were synthesized and characterized using infrared (FT-IR) spectroscopy to establish their composition spectroscopically, using BET surface area measurements to determine their surface areas and X-ray diffraction powder (XRD) experiments to measure their structural parameters.

A new method was then developed to decompose CCl_4 at a lower temperature than previously found, choosing the optimum catalyst. The effects of varying the temperature on the CCl_4 decomposition was then studied in this work. Some suggested possible structural inferences were explored based on the empirical results obtained *via* surface area measurements and FT-IR methods of characterization. The optimum catalyst was found to be Fe_2O_3/Al_2O_3 with a high surface area. Small amount of CCl_4 decomposed at 100 °C which then increased as the temperature increased progressively with a concomitant decrease in the amount of $COCl_2$. In this work, binary systems generally showed higher reactivity, especially the Fe_2O_3/Al_2O_3 system than pure iron oxides. Among the pure iron oxides, magnetite showed the highest reactivity and an ability to adsorb water which could be the main reason behind its reactivity. Tentative reaction mechanisms were suggested, based on the new empirical results, outlining what may be taking place structurally on the surface.

In the final part of this work, some of the characteristics of metal oxides in general, including both main-group and transition metal oxides were firstly considered. Recently reported structural models (2002) from the literature were then examined, specifically in relation to iron oxides and the role of carbon tetrachloride on the surface, which has been the example chosen for this work. Specifically in the case of magnetite (Fe_3O_4), the

products were found to be significantly different. The major observed products were CO_2, $COCl_2$, C_2Cl_4 and small traces of CO and HCl. This different behavior may indicate a different reaction mechanism due to different structures. However, further continued work using advanced structural techniques (not available at UAEU) need to be carried out to ascertain these observations.

This work may pave the way for the future development of a newer and simpler technique for the treatment of carbon tetrachloride, which has huge implications environmentally, if fully exploited and developed at a later stage.

TABLE OF CONTENTS

LISTS OF TABLES

LIST OF FIGURES

CHAPTER 1.

167 g/l, pH = 4.8.

CHAPTER 1

INTRODUCTION AND REVIEW OF THE LITERATURE

CHAPTER 1: INTRODUCTION AND REVIEW OF THE LITERATURE.

1.0 The Iron Oxides and Hydroxides

Iron oxides are common in the environment, occurring either naturally or as a result of human activities [1]. The most common Fe(III)-hydroxides, oxides and oxyhydroxides include ferrihydrite ($Fe_5HO_8.4H_2O$, often written as $Fe(OH)_3$) which changes to hematite (α-Fe_2O_3) and/or goethite (α-FeOOH), depending on solution composition, temperature and pH. ''Green rust'' is the name given to the layered Fe(II,III)-hydroxides which contain anions such as CO_3^{2-}, SO_4^{2-} or Cl^- in the interlayers [1]. Depending on the composition of the solid and the solution, oxidation can transform green rust to lepidocrocite (γ-FeOOH) or magnetite ($Fe(II)Fe(III)_2O_4$). Magnetite can also be present as detrital grains or as relics of biological activity. Weathering can degrade magnetite to maghemite (γ-Fe_2O_3) and all of the iron oxides (Fe-oxides) are subject to attack and dissolution by organic acids and ligands that are formed during breakdown of biological material. Specially, close to the water table, seasonal fluctuation of the redox boundary promotes alternation of oxidised and reduced forms [2].

The red or brown colour that iron-oxides impart to soil often makes it look as if they dominate composition, but they are frequently present only in minor concentrations, even when the colour is intense [1]. In rocks, soil and sediments, Fe-oxides can be present as discrete particles or as coatings on grains of quartz, clay or other minerals. Fractures through rocks and unconsolidated sediments are often observed to be lined with red or brown Fe-oxides. In such cases, where coatings cover particles or fracture walls, Fe-oxides often make up less than the weight percentage (wt. %) of bulk composition but, they can shield the underlying material from contact with the groundwater [1]. Thus, interaction with the major components, quartz, feldspar, clay, sulfides or other minerals is limited, meaning that Fe-oxide

mineralogy plays the dominant role in controlling groundwater composition in these situations (1).

Macroscopic investigations have led to a broad understanding of the uptake behaviour of Fe-oxides (2,3). More recently, spectroscopic studies have provided new information about the respective bonding environments for contaminants incorporated within the bulk as well as adsorbed at the mineral/solution interface (4-7). It is well known that Fe-oxides, with their high surface area and strong affinity, sequester cations such as the transition metals and radio-nuclides, in proportions that are strongly a function of solution composition and pH (1). Under appropriate conditions, Fe-oxides are also strong adsorbers of anionic complexes such as AsO_4^{3-} (7), CrO_4^{2-} (8) and PO_4^{3-} (9-11) and organic molecules such as pesticides (11-13) and humic or fulvic acids (14). Thus, the Fe-compounds are useful for retarding transport or immobilizing contaminants in groundwater systems. For components that are susceptible to biological breakdown, Fe-oxides can serve as a substrate to make them more available to bacteria (1). Because of these properties, as well as the low cost, involved easy availability and lack of health risk, such compounds are frequently chosen for use in the treatment of drinking water and for waste (15-18). Treatment of waste before disposal can help to decrease the leaching of contaminants from the waste facility. One method for such treatment makes use of the precipitation of Fe-oxides to trap heavy metals. In the Ferrox process (18), ash residue from municipal incineration is mixed with $FeSO_4$ solutions and aerated. Many of the contaminants, which were present in the original ash as salts, are dissolved in the solution and then incorporated into the solid Fe(III)-oxide precipitate as the solution is bubbled with air. Their immobilisation in the solid product prevents leaching to the groundwater beneath the waste disposal site. In the design of waste disposal sites, reactive barriers are often used to insure that contaminants do not escape. One simple, effective and inexpensive type of barrier is made with zero-valent iron (19,20). Redox-sensitive contaminants are reduced while they

oxidise the Fe(0). Some organic molecules can be broken down in this way, giving degradation products that are not dangerous and some transition metals which are soluble and toxic in oxidised form, such as Cr(VI), can be reduced to a nonsoluble form, Cr(III), which precipitates (1). The Fe-hydroxides produced in the barrier material can also offer reactive surface area for adsorption of other contaminants (1).

The potential of Fe-oxides to take up contaminants by adsorption or by incorporation within the bulk, and likewise to release them again to solution, depends on their behaviour during three major stages: their initial formation by precipitation or coprecipitation, their transformation to a more stable phase, and their susceptibility to dissolve again or to exsolve incorporated trace components. Improved understanding of the processes involved in each of these stages will lead to diminished uncertainty in models that assess the risk of contaminants in the environment, and will promote development of strategies for waste treatment or containment that are more effective and less expensive (1). There are thirteen iron oxides known to date. The most important oxides are listed in Table 1-1. In addition to these, $Fe(OH)_2$, FeO (wustite), β-Fe_2O_3 and ϵ-Fe_2O_3 and high pressure FeOOH also exist. Except for ferrihydrite ($Fe_5HO_8.4H_2O$) and feroxyhyte (δ'-FeOOH), all the other iron oxides can be obtained in a well crystallized form. Green rusts are not true oxides but are iron hydroxide salts (21).

Table 1-1: The main iron oxides and oxyhydroxides.

Oxides		Oxyhydroxides	
Formula	Mineral	Formula	Mineral
$Fe_5HO_8.4H_2O$	Ferrihydrite	α-FeOOH	Goethite
α-Fe_2O_3	Hematite	B-FeOOH	Akaganeite
γ-Fe_2O_3	Maghemite	Γ-FeOOH	Lepidocrocite
Fe_3O_4	Magnetite	δ'-FeOOH	Feroxyhyte

1.1 The Major Iron Oxides

The basic structural unit for all iron oxides is an octahedron, in which each Fe atom is surrounded either by six O's or by both O and OH ions. The O and OH ions form layers which involve either a hexagonally close-packed (hcp) arrangement, seen in goethite and hematite, or a cubic close-packed (ccp), arrangement observed in lepidocrocite and maghemite. In both the hcp and ccp structures, tetrahedral interstices also exist between the three O's or OH in one plane and the anion in the plane above this. The two hcp-forms, lepidocrocite and maghemite, are termed γ-phases. The α-phases are more stable than the γ-phases (22).

The Fe^{3+} in the octahedral position may be partially replaced by other trivalent metal cations of smilar size (Table 1-2), such as Al^{3+}, Mn^{3+} and Cr^{3+}, without modifying the structure (isomorphous substitution). In this way, solid solutions between pure and species such as FeOOH and AlOOH are formed. Other cations, *e.g.* Ni, Ti, Co, Cu and Zn can also be incorporated into the iron oxide structure (22).

Table 1-2. Ionic radii of Fe and metal substituents.

Ion	Ionic radius[a] nm
Fe^{2+}	0.077
Fe^{3+}	0.064
Al^{3+}	0.053
Cr^{3+}	0.061
Cu^{2+b}	0.073
Mn^{2+}	0.082
Mn^{3+b}	0.065

[a] The ionic radius depends on whether the ion is in the high spin or low spin state. In the iron oxide structure (and where a choice exists), the ions listed here adopt the high spin state.

[b] These ions display the Jahn-Teller effect which leads to a distortion of the coordination sphere of the ion (22).

The various iron oxides differ mainly in the arrangement of the $Fe(O,OH)_6$ octahedra. Goethite, lepidocrocite and akaganeite, *i.e.* the FeOOH forms, all consist of double bands of wedge-sharing $FeO_3(OH)_3$ octahedron (Figure 1-1). In goethite (α-FeOOH), as in diaspore (α-AlOOH) the double bands are linked by corner-sharing in such way as to form 2x1 octahedra "tunnels" crossed by hydrogen bridges. Akaganeite (β-FeOOH) contains channels bounded by double octahedra, resulting in a 2x2 arrangement. These channels are stabilized by being filled with variable amounts of chloride anions and water. In lepidocrocite (γ -FeOOH), as in boehmite, (γ-AlOOH), the double bands of octahedra share edges to form zig-zag layers which are connected to each other by hydrogen bonds (OH-O). In all these FeOOH structures only half of the octahedral interstices are filled with Fe^{3+} (22).

Hematite (α-Fe_2O_3) consists of layers of FeO_6 octahedra which are connected by edge- and face-sharing (as observed in corundum, α-Al_2O_3) and stacked perpendicular to the *c* direction. Two thirds of the octahedral interstices are filled with Fe^{3+}. The face-sharing (shaded in Figure 1-1) is accomplished by a slight distortion of the octahedra which causes a regular displacement of the Fe ions. The distortion and the absence of hydrogen bonds yields a compact structure which is responsible for the high density of 5.26 g cm^{-3} (22).

In the cubic structure of both magnetite and maghemite one-third of the interstices are tetrahedrally coordinated with oxygen and two-thirds are octahedrally coordinated. In magnetite, all of these positions are filled with iron. Magnetite is an inverse spinel: the tetrahedral positions are completely occupied by Fe^{3+}, the octahedral sites by equal amounts of Fe^{3+} and Fe^{2+}. In maghemite only five-sixths of the total available positions are filled and only by Fe^{3+}, with the rest are vacant. Maghemite can have different symmetries depending on the degree of ordering of the vacancies (23). Completely ordered maghemite has a tetragonal symmetry; otherwise it is cubic.
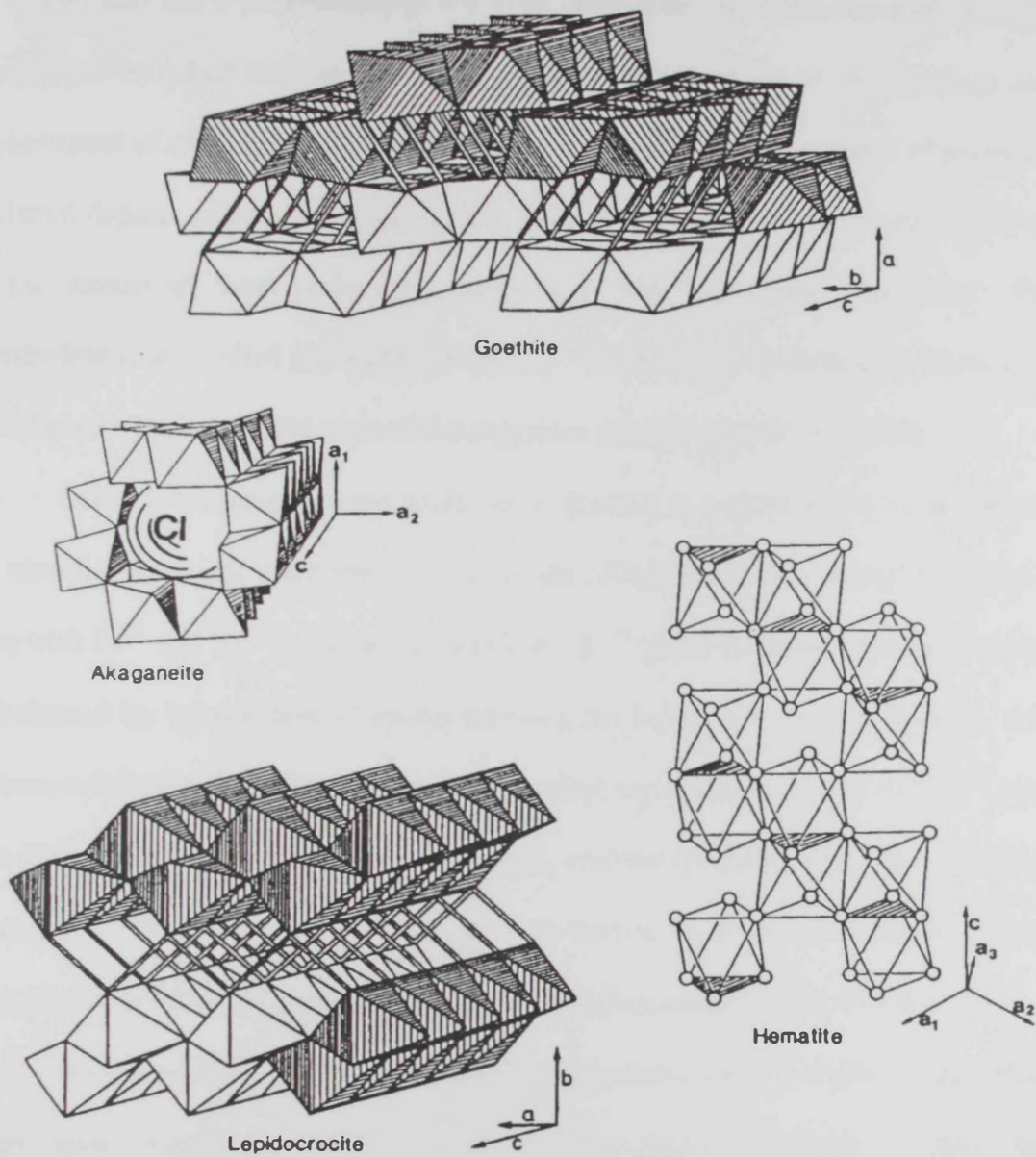
Figure 1-1: Idealized models of goethite, lepidocrocite, akaganeite and hematite structures. The double lines in the goethite and lepidocrocite structures represent H bonds.

Although the structures of ferrihydride (Fe_5HO_8) and feroxyhyte (δ'-FeOOH) are not yet fully understood, both compounds are considered to have a hematite-like structure consisting of hcp oxygen planes with Fe ions in the octahedral interstices. The periodicity of the octahedral sheets along the z-direction is 2 for feroxyhyte ($c = 0.46$ nm), 4 for ferrihydrite

($c = 0.94$ nm) and 6 for hematite ($c = 1.3752$ nm). The low crystallinity of ferrihydride and feroxyhyte is linked both to the presence of vacant iron sites in the structure and to the replacement of some oxygen by H_2O and/or OH. For ferrihydrite, a range of compounds with different degrees of structural order exists; these compounds are sometimes named according to the number of X-ray peaks they exhibit: *e.g.* 2-line and 6-line ferrihydrite. The 2-line ferrihydrite is also called protoferrihydrite (23). The formula of ferrihydrite has not been fully established. Table 1-3 lists some of the suggested formula of such acids (22).

Green rust species are not oxides or hydroxides in a strict sense but contain anions as an essential structural component. They consist of hcp layers of OH and O of the $Fe(OH)_2$ type with Fe^{2+} and Fe^{3+} in the interstices (2, 4). Fe^{3+} gives the layers a positive charge which is balanced by intercalation of anions between the layers. Forms with chloride, sulfate and carbonate between the layers are known. The first two forms may have Fe^{2+}/Fe^{3+} ratios of up to 4 (25) depending on the degree of oxidation, whereas the carbonate form was found to have a ratio of 2 (26, 27) or 3 (28). The name is derived from the blueish-green colour of the compounds and their occurrence as anaerobic oxidation products of steel (22).

Interconversions between the different compounds listed in Table 1-1 are possible and often occur readily. In particular, the hydroxy-oxides dehydrate to their anhydrous counterparts and ultimately to hematite on heating. At lower temperatures and in solution interconversions often involve dissolution followed by reprecipitation of the new phase. Oxidation or reduction reactions are also possible. An overview of possible interconversions is presented in Figure 1-2.

Fe³⁺

Deprotonation

$Fe(OH)_x^{3-x}$

dissolved

hexagonal – close packing

cubic – close packing

Hydrolysis, Nucleation, Crystallization

pH ⩾1   +Cl⁻   pH ⩾2

Goethite   Akaganeite   Ferrihydrite   Dehydration   Hematite
α – FeOOH   β – FeOOH Fe_5HO_8 · $4H_2O$ Rearrangement   α –Fe_2O_3

Thermal transformation 200 – 400°C

Therm. transfmn.

Oxidation + carbonate   pH 5 – 7

Thermal transformation

Maghemite
γ –Fe_2O_3

Dehydroxylation   Oxidn. higher temp.

Green rusts   Oxidn. pH5–7   Lepido- crocite γ–FeOOH   Magnetite Fe_3O_4 Feroxyhyte δ⁻FeOOH

Oxidn. + dehydn. pH >8

Precipitation $Fe(OH)_x^{3-x}$ $Fe(OH)_y^{2-y}$ Rapid oxidation

Oxidn., Deprotnn.

Fe²⁺

Figure 1-2: Schematic representation of formation and transformation pathways of common iron oxides together with the approximate transformation conditions (22).

1.1.2 Less Common or Rare Iron Oxides

The minor iron oxides are $Fe(OH)_2$, FeO (wustite) β-Fe_2O_3, ε-Fe_2O_3 and the high pressure form of FeOOH. $Fe(OH)_2$ is prepared from Fe^{2+} solutions by precipitation with alkali. When freshly precipitated under an inert atmosphere (in a Schlenck apparatus, for example) $Fe(OH)_2$ is white (23). It is however, readily oxidized by air or even water upon which it develops a brown color. $Fe(OH)_2$ has a well defined crystal structure and composition. The layer

8

structure is of the CdI_2 type with hcp anions. The Fe^{2+} ions fill half of the octahedral interstices, thus filled layers alternate with the empty layers. The crystals are in the form of hexagonal platelets. In solution, $Fe(OH)_2$ transforms by a combination of oxidation/dehydration/hydrolysis reactions to other iron oxides and hydroxides. The actual product formed is dependent both on the order in which these processes occur and upon their rates (22).

Recently a high pressure synthetic form of FeOOH has been prepared by hydrothermal conversion of α-Fe_2O_3 in NaOH at $500^{\circ}C$ at a pressure of 80-90 kbar for one hour (29,30). The crystal structure is that of InOOH. It consists of single chains of octahedra running parallel to the c axis and linked by hydrogen bonds.

β-Fe_2O_3 has been obtained by dehydration of β-FeOOH in high vacuum at $170^{\circ}C$ (31) as shown by Mossbauer spectroscopy (32). ε-Fe_2O_3 can be produced by the reaction of alkaline potassium ferricyanide solution with sodium hypochlorite. It is also obtained (together with a mixture of other iron oxides) in an electric arc under an oxidizing atmosphere (33). Its magnetic and thermal properties have been investigated by Dezsi and Coey (34).

Wustite, FeO, is obtained by heating $Fe(OH)_2$ to dryness at $200^{\circ}C$ under an atmosphere of N_2 (22). It is non-stoichiometric and contains defect clusters approaching the Fe_3O_4 structure of magnetite. Wustite is stable only at a temperature greater than $570^{\circ}C$. At lower temperatures it decomposes to Fe_3O_4 and Fe (23).

1.1.3 Iron Oxides in the Environment

Iron oxides are widespread in nature. They are found in soil and rocks, lakes and rivers, on the seafloor, in air (*e.g.* admixed in Aeolian Sahara dust) and in organisms. It is also known that maghemite is a constituent of the reddish-brown, magnetic dust on the planet Mars (22). Iron oxides are of great significance for many of the processes taking place in ecosystems.

9

They are ubiquitous in soils and sediments where they are important regulators of the concentration and distribution of plant nutrients and pollutants such as heavy metals. Iron oxides may be either beneficial or undesirable (22). Everyone is familiar with rust (a mixture of FeOOH and γ–Fe_2O_3) as the end product of the corrosion of iron. The modern steel industry, on the other hand, relies on the huge deposits of hematite (α-Fe_2O_3) and magnetite (Fe_3O_4) found in many parts of the world. In living organisms, iron oxides may form unwanted deposits in the human body (22). In the following section, a brief survey of the occurrence and properties of iron oxides in the environment is presented (22).

Iron oxides and hydroxides are introduced into the environment during rock weathering. Iron is the fourth most abundant element of the earth's crust (5.1 mass %). In primary (magmatic) rocks most of the iron is located in iron(II) silicates such as pyroxenes, amphiboles, biotites and olivines; it can also be found in sulfides such as pyrite, FeS_2. During weathering the silicates are decomposed by oxidation and hydrolysis according to the Eq.1:

$$-Fe(II)-O-SiO_3 \xrightarrow{+O_2/+H_2O} -Fe(III)-OH + H_4SiO_4 \qquad (1)$$

For example, the formation of goethite (α-FeOOH) from an olivine (fayalite) (Eq. 2) or from pyrite (eq. 3) can be written as:

$$Fe_2SiO_4 + 1/2O_2 + 3H_2O \longrightarrow 2\alpha\text{-}FeOOH + H_4SiO_4 \qquad (2)$$

$$4FeS_2 + 15O_2 + 10H_2O \longrightarrow 4\alpha\text{-}FeOOH + 8H_2SO_4 \qquad (3)$$

$$4FeOOH + CH_2O + 8H^+ \longrightarrow 4Fe^{2+} + CO_2 + 7H_2O \qquad (4)$$
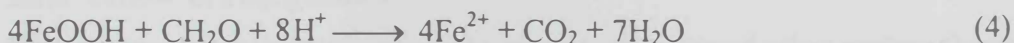
In these reactions oxygen serves as the electron acceptor. The resultant iron(III) oxides have a very low solubility, and hence measurable concentrations of Fe^{3+} ions in solution are only present under strongly acidic conditions, $e.g.$ those resulting from pyrite oxidation (Eq. 3). Once in the weathered zone, $i.e.$ the soil mantle, iron(III) oxides may, however, be remobilized under anaerobic conditions

by microbial reduction (Eq. 4) (22). This process involves enzymatic transfer of electrons by the microorganisms from the organic biomass (written as CH_2O) to iron(III). The resulting Fe^{2+} concentration in solution increases with decreasing redox potential (increasing "electron concentration" and decreasing the pH (eq. 4)) (22). Once mobilized by microbial reduction, the Fe^{2+} can be redistributed in the environment (*e.g.* within a soil or from a soil into a lake). It can also enter the biocycle (plants, animals and humans).

Iron oxides formed by surface weathering display three major characteristics. They colour the material with which they are mixed in a sticking manner; they are present only as very small crystals (5-100 nm in size) and they exhibit a large and reactive surface area. In addition, there is often substantial replacement of Fe by Al in the iron oxide structures (22).

Precipitation, dissolution and reprecipitation of Fe oxides in the environment depends very much on factors such as pH, Eh, temperature and water activity. For this reason, the different iron oxides may serve as indicators of the type of environment which they were formed. Goethite and hematite are thermodynamically the most stable iron oxides under aerobic surface conditions and they are, therefore, the most widespread iron oxides in soils and sediments. Other iron oxides are, however, also found in the environment because, although they are thermodynamically less stable, their formation is kinetically favored (22).

1.1.4 Yellow-brown goethite

The yellow-brown goethite occurs in almost all soils and other surface formations (*e.g.* lakes, streams), whereas the red hematite often colours soils of tropical and subtropical regions. Higher temperatures and lower water activities in the latter regions are important parameters which partly account for this phenomenon. The ratio of goethite to hematite varies greatly with local conditions and is therefore, an environmental indicator. The same is true for the

extent of Al for Fe substitution; this ranges from 0 to 33 mol% for goethite and from 0 to 16 mol% for hematite. Its extent reflects, among other things, the availability of aluminum during iron oxide formation. Goethite has also been found in the teeth of certain mollusks (limpetsm chitons), but as yet, hematite has not been found in living organisms (22). It is now generally accepted that goethite precipitates directly in solution *via* a nucleation-crystal growth process, whereas formation of hematite requires the presence of ferrihydrite particles by a dehydration/rearrangement mechanism. No direct, solid-state transformation of goethite to hematite by simple dehydration has so far been observed under surface conditions; it may, however, take place after sediment burial. Although soil goethites may be acicular or fibrous and hematites may appear as hexagonal plates, both oxides are most frequently isometric and irregularly shaped (22).

1.1.5 Lepidocrocite

Lepidocrocite is generally less widespread than its polymorph, goethite but it does occur frequently as orange accumulations in certain environments. These are characterized by the presence of Fe^{2+} from which lepidocrocrocite forms upon oxidation. The presence of this mineral, therefore, indicates a deficiency of oxygen; in soils this is due mainly to excessive moisture. Lepidocrocite may exist on a pedogenic time scale (10^3 years) because, although it is metastable with respect to goethite, its formation may be kinetically favored and, furthermore, its transformation to goethite is extremely slow. In carbonate-rich solutions, formation of lepidocrocite is prevented and goethite forms (from Fe^{2+}) instead. Soil lepidocrocites resemble the lathlike crystals produced in the laboratory. Lepidocrocite is found in various biota including sponge spicules and the teeth of chitons (22).

The occurance of ferrihydrite appears to be limited to those situations where Fe^{2+} is oxidized rapidly (in comparison with lepidocrocite formation) and/or where crystallization inhibitors are present. Such inhibitors include organics, phosphate and silicate species, all of which are widespread in natural environments and have a high affinity for the iron oxide surface. Because of the high rate of oxidation during its formation and/or the presence of inhibitors, ferrihydrite is poorly crystalline with a very small particle size (and hence a surface area greater than 200 m^2g^{-1}). Inhibitors stabilize ferrihydrite and retard its transformation to more stable minerals (22).

Typical environments in which ferrihydrite exists are iron containing springs, drainage lines, lake oxide precipitates, ground water and stagnant-water soils, river sediments and in the oceans, deep sea crusts and manganese nodules. Oxidation of Fe^{2+} to ferrihydrite can proceed *via* an inorganic pathway, but may also be assisted by micro-organisms such as Gallionella and Lepthotrix (22). The oxidation reaction (termed iron respiration) supplies the micro-organism with energy. Where micro-organisms have been involved, sheaths of bacteria filled with ferrihydrite particles may be found. Ferrihydrite is related to ferritin, an iron oxyhydroxide-phosphate association which acts as an iron reservoir in living organisms(22). The micelles of ferritin are encapsulated in a shell of protein molecules which may prevent conversion to more crystalline, less active iron oxides thus maintaining the ability of the core to supply iron (22). In nature, ferrihydrite is considered to be a necessary precursor to the solid state formation of hematite. It may, however, also transform to goethite over a wide pH range by a dissolution/reprecipitation process (see Figure 1-2). Such a mechanism is feasible in view of the much higher solubility of ferrihydrite (pK_s 37-39) in comparison with that of goethite ($pK_s \geq 42$). The transformation is slow at neutral pH (months to years), but can be greatly accelerated (days) by organic reducing agents such as cysteine its occurrence in lakes, streams and hydromophic

13

soils, *i.e.* environments where oxidizing and reducing conditions alternate and hence an active iron turnover exists (22).

1.1.6 Maghemite

Maghemite is among those iron oxides found invariably in the soils of the tropics and subtropics, but can also occur occasionally in soils of more temperate regions of the world. Maghemite may form during pedogenesis (soil formation) by several pathways. One is by oxidation involving magnetite inherited from the parent rock or formed in soils. If derived from a titano-magnetite, maghemite may contain titanium in the structure. Another, probably more widespread, mechanism involves conversion of other iron oxides such as goethite; the essential prerequisites are heat (from bush or forest fires) and the present of organic matter. This mechanism may operate in temperature regions, but it is more common in the laboratory, involving dehydration of lepidocrocite. However, this is the least likely to be operative in nature (22). Maghemite formed by oxidation of maghemite may be well ordered and may display superstructure lines, whereas a poorly ordered material without superstructure lines and often containing structural aluminum, results from the firing of other iron oxides (22).

1.1.7 Magnetite

Magnetite in soils is often of lithogenic origin. It can, however, be formed in surface environments by biological processes and has been detected in various biota including bacteria (magnetotactic bacteria), bees and pigeons. The presence of magnetite is considered to be related to the directional sense of these organisms. Magnetotactic bacteria have been identified in marine, limnic and soil environments. In constrast to the comparatively large size of magnetite crystals in rocks, the magnetite crystals in bacteria are only in the 0.1 μm range (22).

14

Table 1-3: General physical and chemical characteristics of iron-oxide mineral.

Mineral name: / Formula:	Hematite / α-Fe$_2$O$_3$	Maghemite / γ-Fe$_2$O$_3$	Magnetite / Fe$_3$O$_4$	Goethite / α-FeOOH	Lepidocrocite / γ-FeOOH	Ferrihydrite 5Fe$_2$O$_3$.9H$_2$O Fe$_5$HO$_8$.4H$_2$O[a] Fe$_6$(O$_4$H$_3$)$_3$[b] Fe$_2$O$_3$±2FeOOH. 2.6H$_2$O[c]	Feroxyhyte / δ'-FeOOH	Akaganeite / β-FeOOH
Crystal system	Trigonal	Cubic or Tetragonal	Cubic	Orthorhombic	Orthorhombic	Trigonal	Hexagonal	Tetragonal
Cell dimensions[d] (nm)	$a = 0.5034$ $c = 1.3752$	$a = 0.834$ or $a = 0.8338$ $c = 2.5014$	$a = 0.839$	$a = 0.4608$ $b = 0.9956$ $c = 0.30215$	$a = 0.88$ $b = 1.254$ $c = 0.307$	$a = 0.508$ $b = 0.94$	$a = 0.293$ $b = 0.460$	$a = 1.048$ $b = 0.3023$
Formula units, per unit cell, Z	6	8	8	4	4	4	2	8
Density (gcm^{-3})	5.26	4.87	5.18	4.26	4.09	3.96	4.20	3.56
Octaheddral occupancy	2/3	-	-	½	½	>2/3	1/2	1/2
Maximal Al-for-Fe substitution	1/6	[e]	[e]	1/3	[e]	n. k.	n. k.	n. k.
Standard free energy of formation ΔG° (KJ mol^{-1})	-742.8[f]	-683.8[g] -727.4[h]	-1016.2[g]	-489[h]	-476.5[h]	-696.0[g]	n. k.	n. k.
Solubility product [h] (pFe + 3 pOH)	42.2-43.3	40.5		43.3-44.0	40.6-42.5	37.0-39.4	n. k.	n. k.
Type of magnestism	Weakly ferromag. Or antiferromg.	Ferrimag.	Antiferromag.	Antiferromag.	Speromg.	Ferrimag.	Ferrimag.	Antiferromag.
Néel temperature (K)	955	n. k.	850	400	77	25-115[k]	440	295

Points of zero degree (pzc) are generally between pH 7-8.
[a] After towe and Bradley (1987), (35)
[c] After Russell (1979), (36)
[e] Al-substitution possible but max not known.
[g] After Garrels and Christ (1965), (38)
[l] Depends on particle size.
n. k. = not known.

[b] After Chukhrov et. al. (1973), (24)
[d] Changes with substituation for Fe by cations of different radii.
[f] After Robie and Waldbaum (1967), (37)
[h] After Mohr et. Al. (1972), (39)
[k] Bloking temp (Murad et. al., 1988), (40)

1.1.8 Other types of iron oxides

Other iron oxides do occur in the environment, but are rare. Akaganeite (β-FeOOH) is formed in nature under the same conditions used in the laboratory synthesis, *i.e.* in the presence of high chloride concentrations and at a high temperature (*e.g.* 60 °C). Examples are the hot brines of the Atlantis Deep of the Red Sea and the hot springs of similar composition of the White Island volcano, New Zealand. Natural and synthetic akaganeites frequently display similar morphologies (22).

Only a few occurrences of feroxyhyte have been reported so far; these were in some soils, in ochreous bands of Pleistocene sediments and in marine concretion. Nothing is known about the mechanism of formation in nature, although rapid oxidation may be presumed to be involved (22).

The as yet unnamed Fe(III) oxyhydroxysulfate seems to be a common ochreous precipitate in the presence of air. The Fe^{2+} in this sulfate containing, extremely acidic (pH<3) waters can only be oxidized with the assistance of a micro-organism, Thiobacillus ferroxydans. Formation of the Fe(III) oxyhydroxysulfate requires the presence of high sulfate concentrations (> 1000 mg L^{-1}) and associated iron products may be goethite and jarosite, $KFe_3(SO_4)_2(OH)_6$ (22).

1.2 Catalytic behaviour of iron oxides

Surface chemistry is of vital importance in numerous processes, including corrosion, adsorption, oxidation, reduction and catalysis. Particles in the 1-10 nm range open a new vista in surface chemistry because surface-reactant intersections can become stoichiometric. This is for two reasons. First, the large surface areas of nanostructured materials dictate that many of the atoms are on the surface, thus allowing good "atom economy" in surface-gas, surface-liquid, or even surface-solid reactions. Figure 1-3 illustrates the calculated numbers of iron atoms on spherical iron metal nanoparticles that are surface or bulk (interior) atoms. Relatively small sizes are necessary; *e.g.* a 3 nm particle has 50% of the atoms on the surface,

while a 20 nm particle has fewer than 10%. Hence, in order to benefit from the desired atom economy, small nanosized particles are needed (41). A second aspect of surface chemistry involving nanoparticles is the enhanced intrinsic chemical reactivity as the size gets smaller. The reason for this enhanced reactivity is most likely due to changes in the crystal shape: for example, changes from cubic to polyhedral shapes, when the surface concentration of edges and corner sites increases considerably, as demonstrated in Figure 1-4 for MgO crystals (42).

However, there are other features that can affect the surface energy. As the crystal size becomes smaller, anion/cation vacancies of Frenkel or Schottky type become prevalent. In addition, atoms on the surface can be distorted in their bonding patterns (43). Since surface chemistry is of such major importance in aspects of nanoparticles (44-46), atom economy (47,48) and surface chemical reactions, (either stoichiometric or catalytic) must be considered. Adsorption, catalysis, medication utilization, acid-base reactions and neutralizations, and reactions in which solids are consumed can all be significantly affected by such factor.
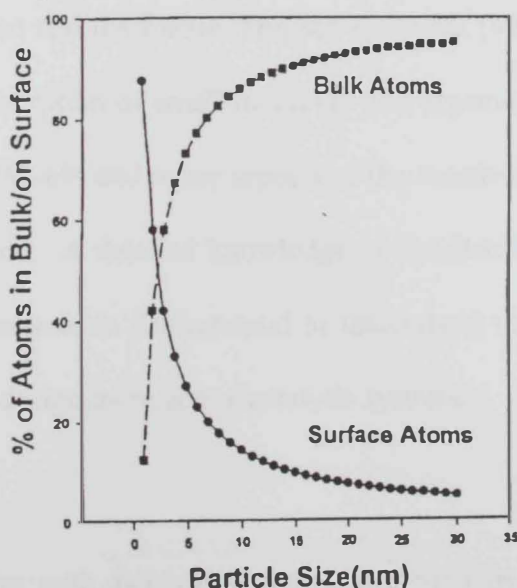
Figure 1-3: Calculated surface to bulk atom ratios for spherical iron nanocrystals(1).

17

AP-MgO

(a)

CP-MgO

(b)

CM-MgO

(c)
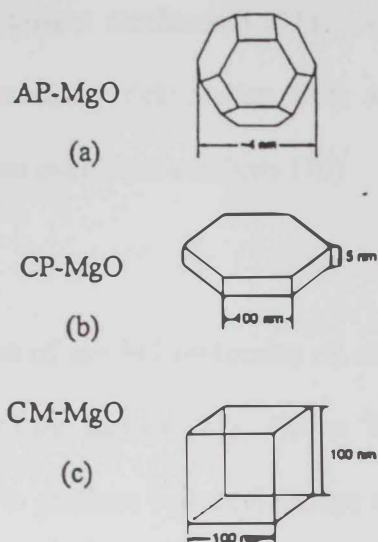
Figure 1-4: Models of (a) nanocrystalline (AP-MgO); (b) microcrystalline (CP-MgO); (c) normal commercially available (CM-MgO) magnesium oxide crystals (2).

1.3 Reactivity of some compounds on pure iron oxide

1.3.1 Reactivity of simple molecules on iron oxide powder

Iron and iron oxide based catalysts have been widely used in several industrial processes such as dehydrogenation, oxidation and the Fisher–Tropsch synthesis (49,50). Nevertheless, only a few studies about the chemisorption of small inorganic and organic molecules on iron oxides have been so far published (51-69) and many aspects of the reactivity of hematite surfaces are not yet completely understood. A detailed knowledge of the distribution and strength of the active sites of iron oxide surfaces is fundamental to understand the reactivity of iron oxide based catalysts as well as to design more active catalytic systems.

1.3.2 Alcohols

The reactivity of iron oxides with alcohols is interesting for two reasons: (a) alcohols are important intermediates in several chemical processes; and (b) the interaction between alcohols and oxide surfaces can help in understanding the relationships between surface

18

acidity and the alcohol decomposition mechanism (51). As an example, decomposition of butan-2-ol generally yields butanes by dehydration over acidic catalysts and yields ethyl methyl ketone by dehydrogenation over basic catalysts (70).

1.3.3 Reaction with methanol

The mechanism of chemisorption of alcohol molecules on an oxide surface strongly depends on the degree of hydroxylation of the surface (71). On an 'ideal' dehydroxylated surface the mechanism can be dissociative, to produce hydroxyl groups and alkoxy groups, or molecular, by interaction of the alcohol molecules with the Lewis acidic and basic sites. Three further types of chemisorption modes can be possible for a 'real' hydroxylated surface: replacement of molecular water present on the surface, esterification with acidic surface hydroxy groups and reversible adsorption on the surface hydroxyl groups or on methoxy groups, through hydrogen bonds (72). In order to characterize the species formed during the decomposition of methanol on an Fe_2O_3 catalyst in the high vacuum environment, XP spectra of the iron oxide surface before and after chemisorption have been compared (71).

The methanol is chemisorbed at RT on the Fe_2O_3 both dissociatively and molecularly. Around 400 K the molecularly chemisorbed methanol partially dissociates, giving rise to coordinated methoxy groups, and partially decomposes. The decomposition path is *via* oxidation if oxygen is present and *via* fragmentation when oxygen is absent. In the high vacuum system the temperatures at which methanol and methoxy groups decompose (420 K for methanol and 550-570 K for methoxide) are higher than in the high temperature and high pressure (HTHP) reactor (380 K for methanol and 500-550 K for methoxide, respectively). The presesnce of H_2CO, CO_2 and H_2O around 600-625 K may be due to the reaction path and/or to the decomposition of formate ions Figure 1-5 (71).
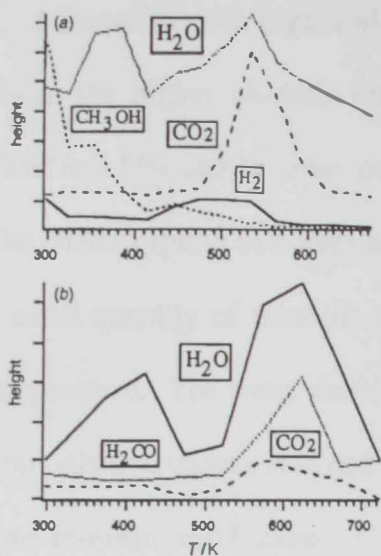
Figure 1-5: Desorption peaks obtained by the MS spectrum for the systems: (a) Fe_2O_3-methanol studied in the HTHP reactor; (b) Fe_2O_3 + (O_2-methanol) studied in the HV system.

1.3.4 Reaction with ethanol

Ethanol begins to be desorbed from the surface around 320-340 K; between 450 and 500 K both ethanol and ethoxy groups are desorbed from the surface and decompose, giving rise to C_2H_4, C_2H_6, C_3H_6, C_3H_8 and H_2O. The formation of these species is also evident at 630 K. Traces of ethanoate are present and increase with the temperature. At high temperature the formation of propane is evident, Figure 1-6 (69).
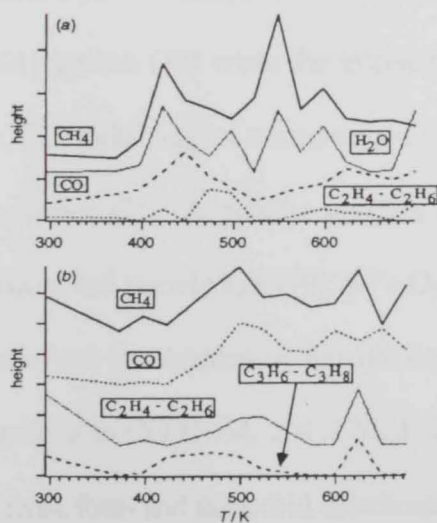
Figure 1-6: Desorption peaks obtained by the MS spectrum for: (a) Fe_2O_3-methanol and (b) Fe_2O_3-ethanol, studied under high vacuum conditions.

1.3.5 Reaction with higher alcohols

When the higher alcohols (propan-1-ol and butan-1-ol) are taken into consideration, both FTIR and MS data become more complex and their interpretation is not always unambiguous. The chemisorption of higher alcohols on hematite is mainly molecular, even in the presence of a small quantity of alkoxide. The dissociated form becomes more relevant with increasing temperature. The main chemisorption products are hydrocarbons: linear chain hydrocarbons from ethanol, unsaturated and saturated hydrocarbons with three and four carbon atom chains from propanol and butanol (71).

1.3.6 Reaction with carbon monoxide and carbon dioxide

The exact nature of the interaction between CO and α-Fe_2O_3 is still unresolved and several authors have reported different results (73-76). Several authors have attempted to compare the behavior of polycrystalline samples and well-defined model surfaces. This comparison is not so straightforward for hematite. Natural growth faces of α-Fe_2O_3 are (001) and (012) respectively (77). The reactivities of the α-Fe_2O_3 (001) surface and of a powder sample are different: as an example, methanol adsorbs molecularly on the α-Fe_2O_3 (001) surface (78) while the interaction is mainly dissociative on the nanopowders (71). In addition, IR results suggest a mechanism of esterification involving the OH groups distributed on the oxide surface (71). In powder samples, the predominantly exposed faces depend on the preparation procedure and particle size (79); α-Fe_2O_3 microcrystals with preferentially low index faces (mainly prismatic) can be obtained by thermal decomposition of α-FeO(OH) (74). The IR peak observed after exposure to CO (2054, 2041, 2024 and 2012 cm^{-1}) can be tentatively assigned to the interaction with five-, four- and three-fold coordinated Fe^{3+} ions respectively. The IR spectrum obtained after exposing the α-Fe_2O_3 to CO_2 at RT is shown in Figure 1-7.
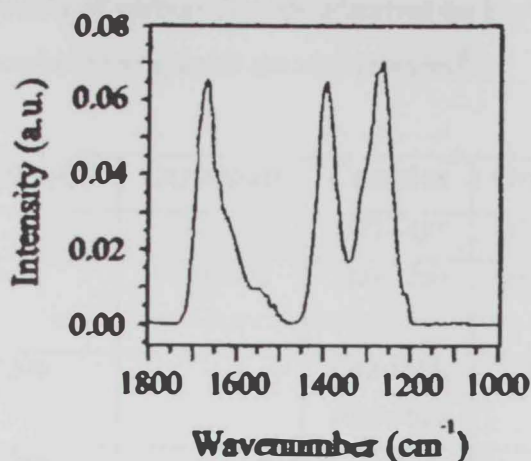
Figure 1-7: IR spectrum obtained after the exposure of the α–Fe_2O_3 (hematite) powder to the CO_2 at RT; region between 1000 and 1800 cm^{-1}.

The region between 1200 and 1750 cm^{-1} includes several peaks at *ca.* 1671 (with shoulders around 1650 and 1620 cm^{-1}), 1556, 1396 and 1269 cm^{-1} (with a shoulder around 1316 cm^{-1}). The position of the bands at 1671, 1396 and 1269 (Table 1-4) is indicative of the formation of surface bicarbonate species (80,81) as a consequence of the interaction between CO_2 and the surface OH. In contrast, the weak contributions around 1556 and 1316 cm^{-1} agree with the formation of surface bidentate carbonate species (81,82) as a consequence of the adsorption of CO_2 on a Lewis acid/base site constituted by the metal ion and the neighbouring oxide ion (83).

Rochester *et al.* (52) studied the interaction between CO_2 and an α-Fe_2O_3 (hematite) powder synthesized by decomposition of a ferrigel precipitate (obtained by mixing aqueous solution of NaOH and $FeCl_3$). These authors observed a peak centred around 1320 cm^{-1} after the exposure at CO_2 of an hematite powder heated at 713 K while no evidence for the adsorption of CO_2 could be detected on hematite heated at 973 K. The presence of the bicarbonate species is clearly evident and suggests a high hydroxylation of the surface; the surface bidentate carbonate species form to a lesser extent (56).

Table 1-4: FTIR data (cm^{-1}) of carbon dioxide adsorbed on Fe_2O_3 powder; the reference data for the carbonate and bicarbonated species are also reported[a].

	CO_2/Fe_2O_3[b]	Carbonate	Complex	Organic	Bicarbonate
C=O stretching			1577-1493	1870-1750	1630-1620
Asymmetrical stretching C-O	1671	1420-1470	1338-1260	1280-1252	1410-1400; 1370-1290
Symmetrical stretching C-O	1396		1082-1055; 1050-1021	1021-969	1050-1010; 1000-990
O-H bending	1269				

[a] 80, [b] 58

The chemisorption of carbon dioxide was also carried out under high vacuum conditions and followed by means of XPS and QMS. The Fe 2p and O 1s XPS peaks position, their shape as well as the surface atomic composition, do not change after the exposure to CO_2 at RT or at higher temperatures (Figure 1-8). This suggests that the interaction between α-Fe_2O_3 and CO_2 is weak and cannot withstand the vacuum conditions.
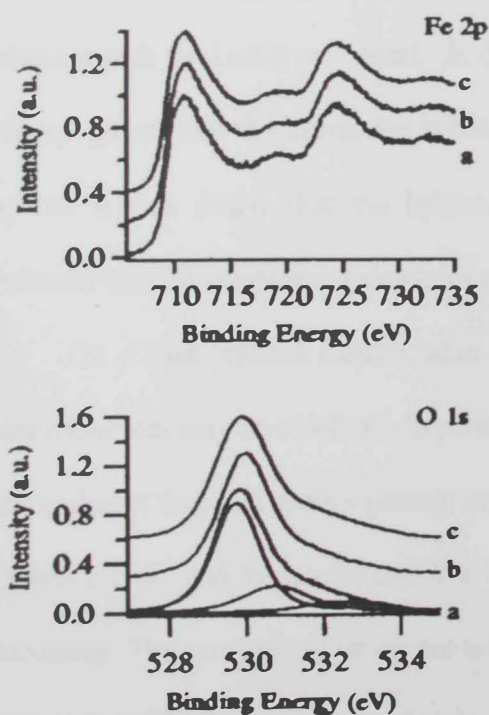
Figure 1-8: Fe 2p and O1s XPS spectra obtained for the −Fe_2O_3 (hematite) powder (a) before the chemisorptions, after the chemisorption of (b) pyridine and (c) carbon dioxide at RT. The fitting results obtained processing the O1s XP peak are also shown.

Furthermore, it was found that the QMS results never showed, at temperatures lower than 473 K, species derived from the decomposition of the carbon dioxide (56).

1.3.7 Reaction with formic acid

Glisenti has investigated the interaction of formic acid with Fe_2O_3 (67). She studied the interaction between iron oxide and molecules characterized by a more acidic behavior than the alcohols in order to investigate the acid-base properties of the catalytic surface. The selectivity for dehydration *versus* dehydrogenation of carboxylic acids and alcohols has been used as a probe for the acid-base properties of metal oxide surfaces. Basic oxides are generally assumed to have a high selectivity for dehydrogenation, while acidic oxides favor dehydration (50, 84, 85). Several Brönsted and Lewis acid sites are present on the hematite surface: their distribution and number change as a consequence of chemisorption and heating.

The chemisorption of formic acid molecules on a dehydroxylated surface can be dissociative (to produce hydroxyl groups and formate groups) or molecular (by interaction of the formic acid molecules with the Lewis acid sites). In the HV experiment the iron oxide surface is almost free of hydroxyl groups and the interaction between these groups and the formic acid molecules cannot be relevant. It was found that the hydroxy groups increase after chemisorption (Figure 1-9) in agreement with the interaction mechanisms suggested for the dehydroxylated surfaces (56).

On a hydroxylated surface other mechanisms are possible, in which hydroxy groups and water molecules may be involved. In particular, the formic acid chemisorption abruptly decreases the free or almost free OH groups present on the surface (Figure 1-10) suggesting that the interaction between formic acid molecules and free hydroxy groups is an important step in the chemisorption mechanism. The existence of strong contributions due to the formic acid and formate species does not allow us to verify whether water molecules are perturbed by the chemisorption of formic acid (56).

These results suggest the importance of the interaction between formic acid and/or Lewis acid sites present on the surface of the catalyst. Formic acid chemisorbs, at room temperature, molecularly and dissociatively, both in HV and at atmospheric pressure. The dissociation of the formic acid with the formation of the formate moieties becomes more important when the temperature is increased (56).
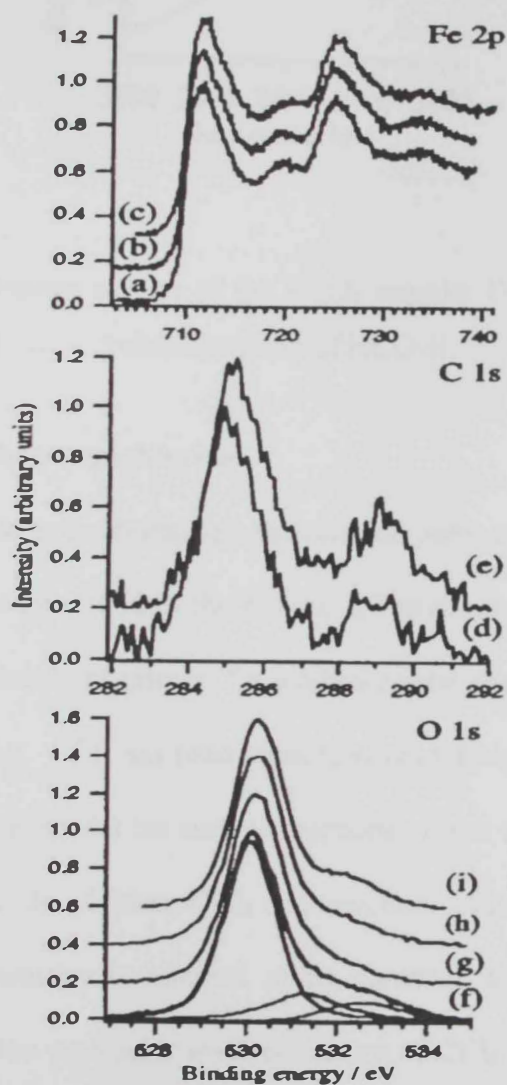
Figure 1-9: XPS data obtained on the Fe_2O_3 catalyst calcined at 723 K: Fe 2p spectra (a) before and after chemisorption of HCO_2H at (b) RT and (c) 773 K; C 1s spectra after chemisorption of HCO_2H at (d) RT and (e) 773 K; O 1s spectra of the sample as calcined (the results of the fitting procedure are also shown) (f), and of the sample (g) before chemisorption (but after the cleaning procedure) and after chemisorption of HCO_2H at (h) RT and (i) 773 K.
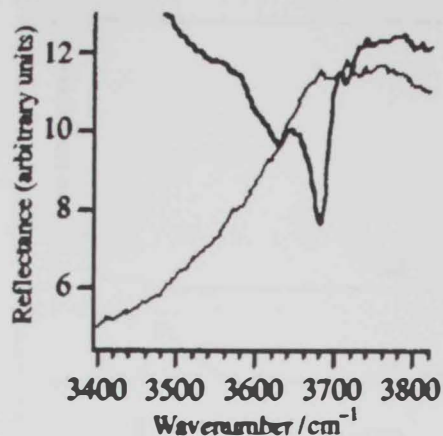
Figure 1-10: FTIR reflectance spectra of the Fe_2O_3 sample: O-H stretching region obtained before (_____) and after (.........) chemisorption of HCO_2H.

1.3.8 Reaction with Carbon tetrachloride

There is a growing interest in understanding the reaction paths and reactive sites of iron-oxide surfaces at the molecular level within the context of environmental applications (86). For example, a particular molecule of interest for environmental studies on iron oxide surfaces is carbon tetrachloride (CCl_4). CCl_4 has been considerably investigated in the literature (87, 88) and therefore can be used to model the surface reactions of iron oxides with various chemicals containing the C–Cl bond. In addition, CCl_4 is a common contaminant in a variety of natural settings (89), and its chemistry is relevant to its potential use as a tracer in geophysical investigations. Study of the molecular level chemistry of CCl_4 with iron oxides requires the investigation of well-characterized single-crystal surfaces of iron oxides. Thermogravimetric analysis (TGA) (90), as well as gas chromatographic (GC) and mass spectroscopic (MS) studies of the chemical reactions of CCl_4 with powdered $\alpha\text{-}Fe_2O_3$ (91) indicate that thermal decomposition of CCl_4 in the presence of $\alpha\text{-}Fe_2O_3$ occurs at temperatures above approximately 650 K; however, the reactive surface sites have not been identified (87).
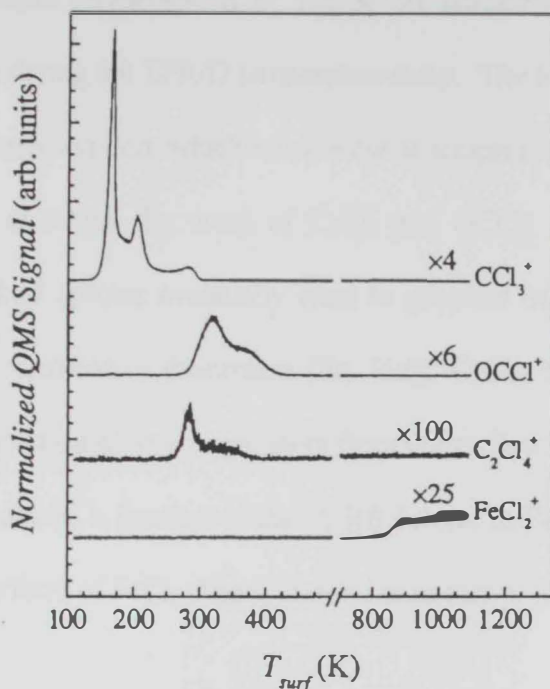
Figure 1-11: TPR/D spectra collected after exposing a freshly sputtered and annealed selvedge surface to 2 L of CCl_4 at an adsorption temperature of approximately 100 K. The temperature ramp rate is 2.5 K/s.

Figure 1-11 shows the TPR/D spectra collected after exposing a freshly sputtered and annealed Fe_3O_4 selvedge surface to 2 L of CCl_4. The spectra are complex and indicate a rich surface chemistry corresponding to the variety of binding sites expected for this surface (92, 93). Six separate desorption features are clearly observed. The CCl_4 desorption spectrum consists of three well-resolved desorption waves. The overall surface chemistry can be expressed by the following schematic chemical equations:

$$CCl_4(g) \xrightarrow{100K} CCl_4(ad) \longrightarrow CCl_4(g) \tag{5}$$

$$CCl_4(g) \xrightarrow{100K} CCl_2(ad) + 2Cl(ad)$$

$$\xrightarrow{\Delta} CCl_4(g) \tag{6a}$$

$$\xrightarrow{\Delta} \tfrac{1}{2}\, C_2Cl_4(g) + 2Cl(ad) \tag{6b}$$

$$\xrightarrow{\Delta, \text{lattic O}} OCCl_2(g) + 2Cl(ad) \tag{6c}$$

27
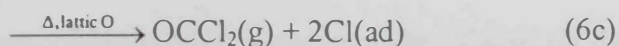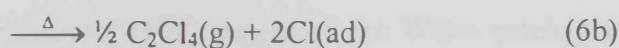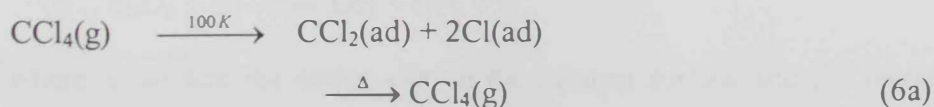
Eq. (5) describes a simple physisorption at 100 K on unreactive surface sites, followed by desorption upon heating during the TPR/D temperature ramp. The left hand side of Eqs. (6a)–(6c) describes dissociative chemisorption, which must occur at temperatures below 250 K, since this is the lowest temperature at which the onset of C_2Cl_4 and $OCCl_2$ desorption can be measured. Dissociatively chemisorbed species eventually react to generate one of three possible products: CCl_4 is produced by recombinative desorption (Eq. (6a)), C_2Cl_4, by associative desorption (eq. (2b)), and $OCCl_2$, by extraction of an oxygen atom from the surface lattice (Eq. (6c)). Though not shown in the above equations, a fraction of the Cl left behind in Eqs. (6b) and (6c) is ultimately observed to desorb in the form of $FeCl_2$ at temperatures in excess of 820 K (87).

1.3.9 Reaction with hydrogen peroxide

Hydrogen peroxide has been found to be useful in wastewater treatment (94,95) and in soil remediation (96,97). It is a powerful oxidant for contaminants working either alone or in conjunction with a catalyst (98). The most common homogeneous catalyst is Fe^{2+}. When combined with H_2O_2, it is well known as Fenton's reagent (98); heterogeneous catalysts involve metal oxides, and supported metal oxides (99). Recently, the application using iron oxide catalyst has been studied extensively (96, 99–102). Goethite, hematite, semicrystalline, and ferrihydrite have been used as catalysts to treat the organic contaminants (58,63,64).

In earlier work (100, 103, 104), the catalytic decomposition of hydrogen peroxide with metals or metal oxides has been described by the Weiss mechanism, in which the major reaction is:

$$H_2O_2 + S \longrightarrow \cdot OH + OH^- + S^+ \qquad (7)$$
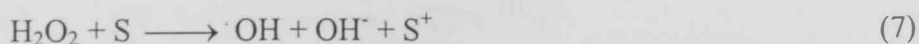
where S denotes the active site on the catalyst surface and SC represents the oxidized site. Recently (1998), Lin and Gurol (105) suggested the Weiss mechanism cannot appropriately explain the decomposition of H_2O_2 by granular goethite. Based on the surface complexation

28

of iron oxide, they proposed another reaction mechanism which is similar to the Fenton-like reaction of Fe_3C/H_2O_2 system (106). The H_2O_2 decomposition rate (R_H) can be expressed as given in eq. (8) according to the new reaction mechanism proposed in Table 1-5:

$$R_H = \frac{KS_T[H_2O_2]}{1+K_H[H_2O_2]} \tag{8}$$

where $k = 2k_1k_2k_3/k'$, $K_H = k_1(k_3 + k_{2a})/k'$, $k' = k_3(k_{1a} + k_2) + k_{1a}k_{2a}$; S_T is the total concentration of the surface sites, and $[H_2O_2]$ represents the H_2O_2 concentration in the batch reactor. This equation resembles the classic Langmuir–Hinshelwood equation (L–H equation) (107) in heterogeneous catalysis, where k and K_H correspond to the rate constant and equilibrium binding constant (101). The kinetic model has been verified at pH 7 between 1.1 and 11 mM of $[H_2O_2]$. When $K_H[H_2O_2] \ll$ 1, Eq. (8) can be reduced to a second-order kinetic expression verified by Lin and Gurol (105):

$$R_H = kS_T[H_2O_2] \tag{5}$$

Table 1-5: Proposed mechanism for decomposition of H_2O_2 on goethite (105).
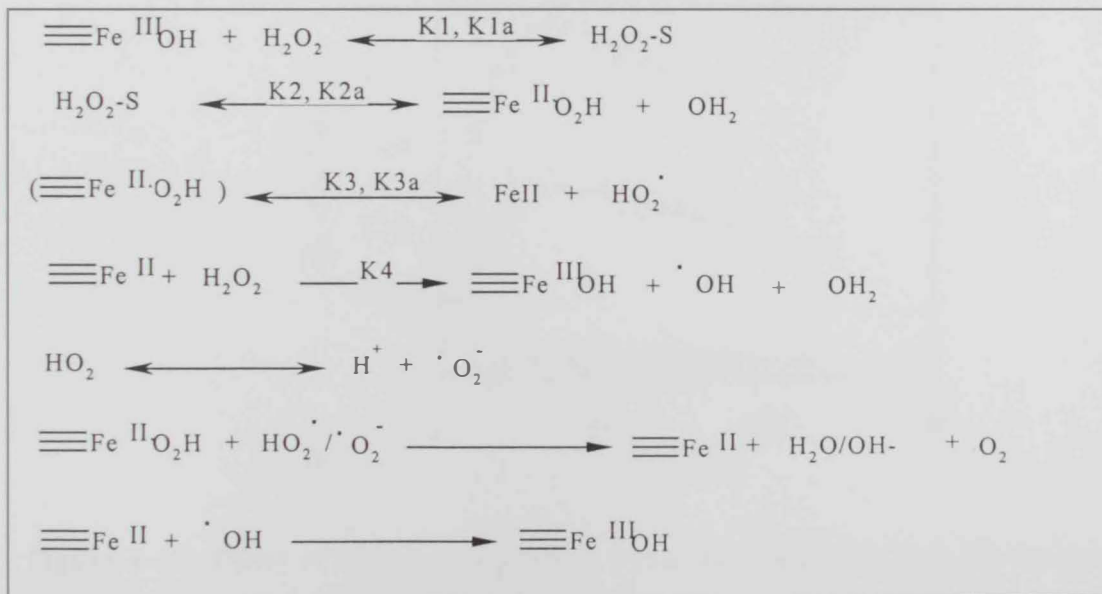
Chou and Huang (108) have proposed the following conclusions:

1. The decomposition rate of H_2O_2 is proportional to both C_H and concentration of the catalyst at

low C_H, but decays at high C_H, which can be interpreted using the modified Langmuir–Hinshelwood equation by incorporating the substrate inhibition model (see Figure 1-12,13) (108).

(a)

(b)
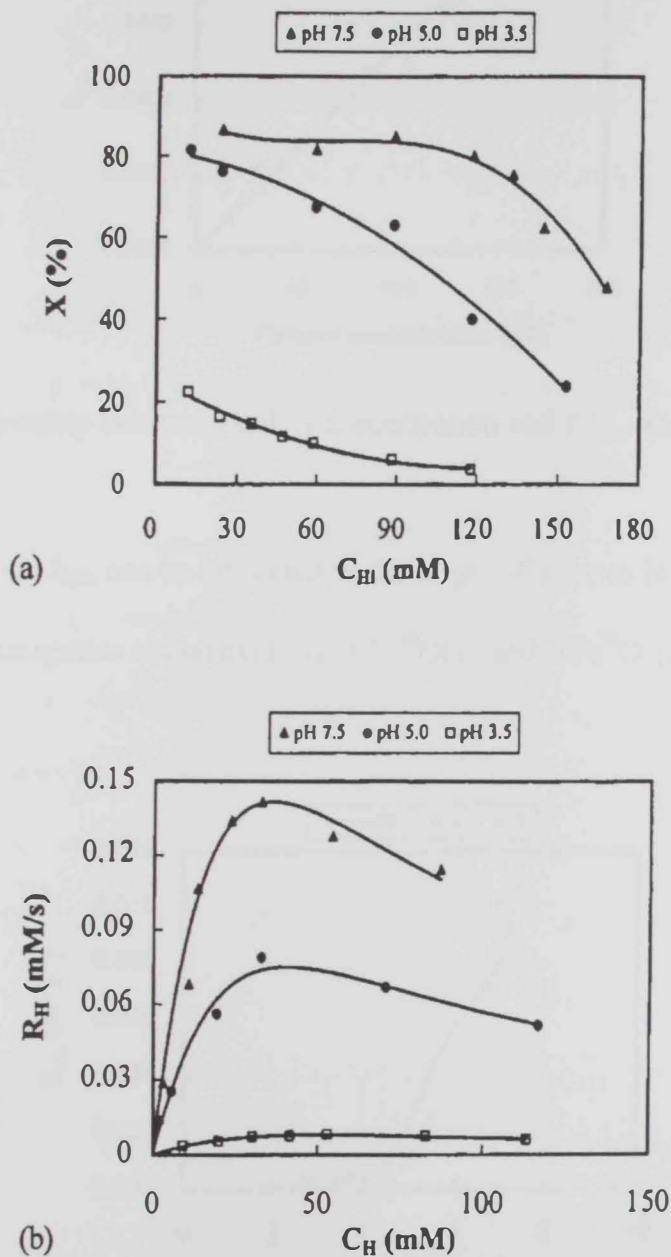
Figure 1-12: Effect of H_2O_2 concentration on (a) the conversion and (b) the decomposition rate of H_2O_2. $\iota = 11.8$ min, m = 167 g/l, m denotes the catalyst concentration.
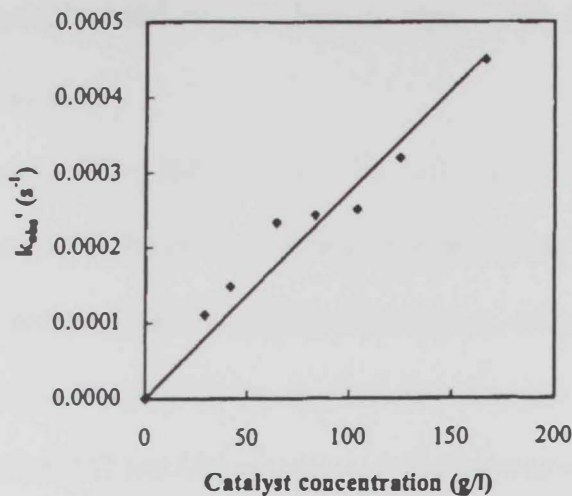
Figure 1-13: Relationship between catalyst concentration and K'_{obs}. $C_{Hi} = 24.4$ mM, $m = 167$ g/l, pH = 4.8.

2. The effect of pH on k_{obs} can be attributed to the large differences in reaction rates between H_2O_2 and three surface species of iron oxide, *i.e.* $\equiv Fe^{III}OH_2^+$ and $\equiv Fe^{III}O^-$ (see Figure 1-14) (108).
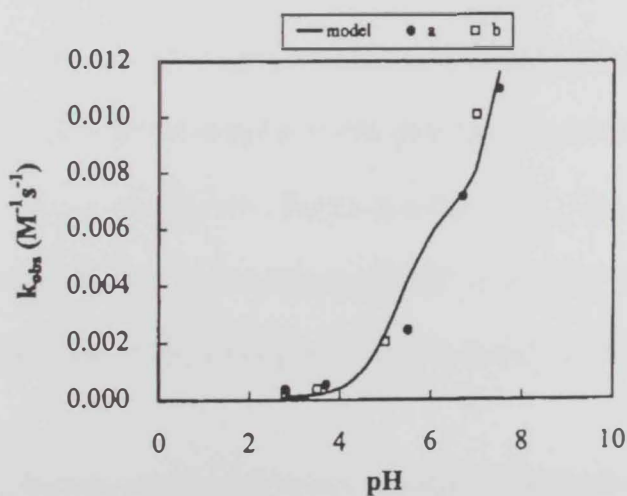
Figure 1-14: Model fitting for H_2O_2 decomposition at different pH values. The solid line represents the model prediction.

1.4 Reactivity of complicated molecules on iron oxide powder

1.4.1 Water-gas shift reaction

The water-gas shift reaction, $CO + H_2O = CO_2 + H_2$, has been used to produce hydrogen from synthesis gas stream generated by the steam reforming of hydrocarbons (109). The reaction has also been applicable to the catalytic reactions of the hydrocarbon oxidation and the auto exhaust combustion. The isotopic exchange study on the catalytic water-gas shift reaction shows that the carbon atom transfer between CO and CO_2 and the oxygen atom transfer among CO, CO_2 and H_2O occurs during the reaction (110, 111). The study has indicated the reaction to be reversible, which make feasible its application in converting CO_2 to CO. Many investigators have reported that metals and metal oxides are effective catalysts for the water-gas shift reaction (112). Among the metal oxide catalysts tested so far, Fe_3O_4/Cr_2O_3 and Cu/ZnO systems are known to be the most active catalysts for the reaction. An Fe_3O_4/Cr_2O_3 catalyst, considered as a high temperature catalyst, is prepared in the form of ferric oxide and then some chromium oxides are added to prevent the thermal sintering of the catalyst in the operation. Iron oxide-based catalysts are still widely studied in the catalytic reactions such as the water-gas shift reaction, the oxidation of hydrocarbons, the conversion of CO_2 to CO, or the Fischer-Tropsch reaction (113, 114). The Au/Fe_2O_3 catalyst exhibits a high catalytic activity even at low temperature (383-633 K) in the water-gas shift reaction; this result attracts much attention in developing the iron oxide-based catalyst (109).

1.4.2 Adsorption and decomposition of dimethyl methyl phosphonate on metal oxides

Within the last few years important studies of the fundamentals of the interactions between organophosphonate compounds and metal oxide surfaces have been carried out (115-135). Dimethyl methylphosphonate (DMMP), Figure 1-15, is a widely used model compound for the simulation of the interactions of phosphonate esters with surfaces. Phosphonate esters occur widely

32

in the spectrum of toxic man-made chemicals, being used as pesticides and chemical warfare agents.

$$\text{H}_3\text{C}-\overset{\overset{\displaystyle O}{\|}}{\underset{\text{OMe}}{\text{P}}}-\text{OMe}$$
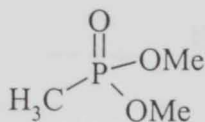
Figure 1-15: Dimethyl Methylphosphonate (DMMP).

The interactions of phosphonate esters with metal oxide surfaces are important for the study of the fate and transport of pesticides in soils and in the development of catalytic agents for the destruction of chemical warfare agents and for the protection of personnel (136).

The decomposition behavior of DMMP on metal oxides can be most easily examined with infrared spectroscopy by studying the methyl stretching modes. The decomposition proceeds on alumina, magnesia, and lanthana *via* very similar paths (136). The first step is coordination on the surface through the P=O bond to acidic surface sites. Subsequently, stepwise loss of the two methoxy groups is observed, with the evolution of methanol from the surface. In the case of magnesia, evidence is seen for the formation of a surface methoxy group which is lost when oxygen is added at 300 °C. Evidence has been found for the formation of surface methoxy groups on both magnesia and lanthana. The integrity of the P-CH$_3$ bond is maintained even on heating to 300-400 °C in oxygen (136).

On iron oxide, the interaction of the surface with DMMP appears to proceed in a different fashion. The complex formed between the surface and the PdO bond is much stronger, since the P=O vibration appears to shift to 1077 cm^{-1} at 100 °C, compared to a shift to 1172 cm^{-1} at 100 °C on lanthana. Additionally, there is indication of the formation of a second type of complex, one involving the nucleophilic attack of a surface OH group at the phosphorus atom of DMMP (136) (Figure 1-16).

33
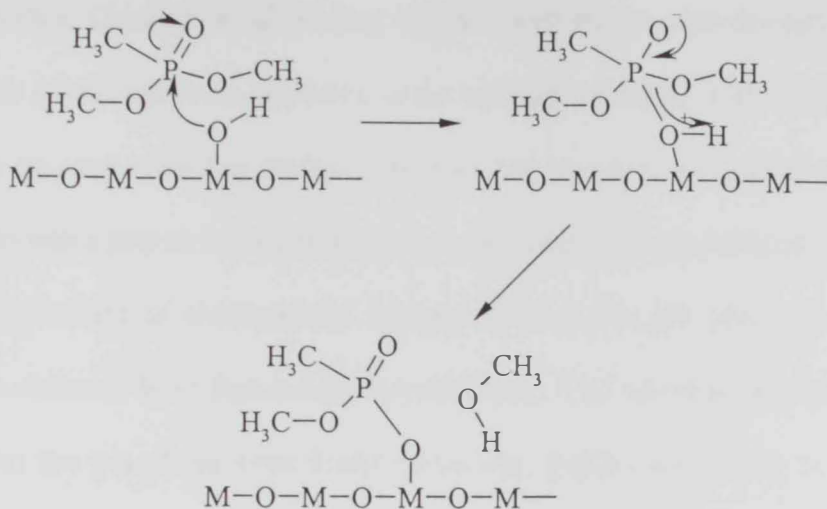
Figure 1-16: Nucleophilic attack of the surface on DMMP.

However, even at 100 °C, no elimination of a significant fraction of the methyl groups is indicated by a loss of intensity, unlike on magnesia or lanthana surfaces, whereby at 100 °C, one methoxy group had already been eliminated. Decomposition takes place on the iron oxide surface at 100 °C and even more strongly by 200 °C, as indicated by the loss of intensity in the methyl stretching region and the formation of the surface methoxy groups; however, there is no apparent selectivity for either the methoxy groups or the phosphorus-bound methyl group. On iron oxide, all the carbon containing species appear to be eliminated from the surface by 300 °C. The oxidation of the P-CH$_3$ bond of DMMP on iron oxide is made possible by the participation of the Fe$^{(III)}$/Fe$^{(II)}$ couple (136).

1.4.3 Adsorption of chlorophenols

The presence and widespread use of chlorinated aromatic solvents, chemical cleaning agents, biocides, preservatives and pesticides in the environment represents a serious problem because of their toxicity, persistence and accumulation potential in plants and animal tissues (137,138). Soluble chlorinated organic compounds have recently shown their extended potential to enter the food chain (139). Due to their low and inefficient bio-degradability these compounds are found in

natural water bodies. Chlorination of drinking waters (disinfection) under day light irradiation leads to the formation of chlorophenols especially in the presence of humic acid (140). Environmental photochemistry on semiconducting surfaces has been also shown to be determined by the surface adsorbed species which play an important role in scavenging the photogenerated charges (141-148).

The mechanism of chlorophenol adsorption from the gas phase on dry oxide was observed to be different from that in aqueous solutions. The adsorbed species produced upon absorption from the gas phase were found to be very stable and heating to 120 °C did not promote desorption of these species. The observations for gas phase adsorption and from the aqueous solutions can be represented schematically (Figure 1-17):
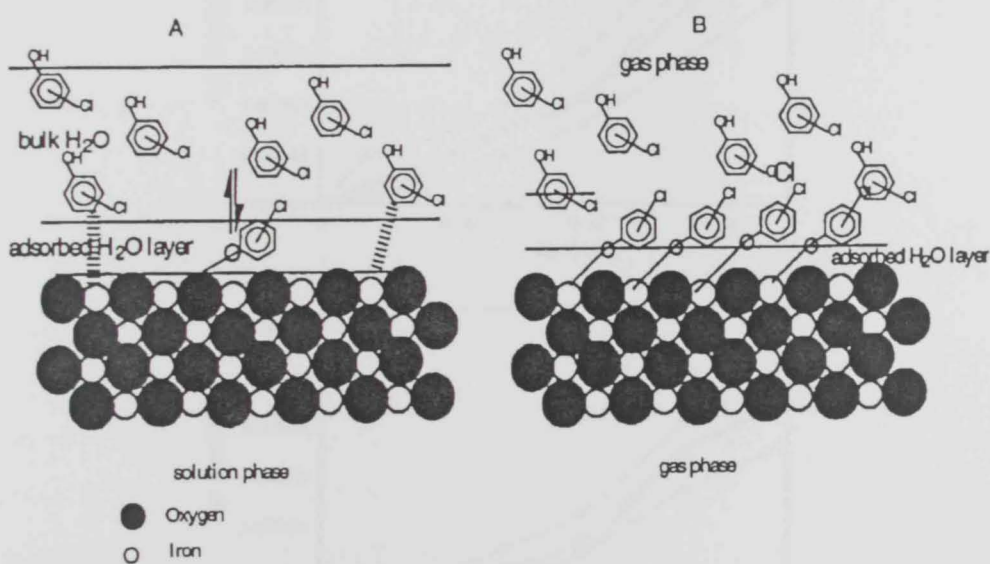
Figure 1-17: Adsorption of chlorophenol compounds in solution and gas phase.

This scheme shows chlorophenol (CP) in equilibrium with the adsorbed water layer on the oxide surface and the bulk water (141). In this model, only a few chlorophenol molecules can reach the oxide surface and form the surface complex. The gas phase adsorption of chlorophenols is not limited by the chlorophenol dissolution in water, and therefore, a higher surface adsorption is observed (141).

35

Figure 1-18 (a) and (b) show adsorption isotherms in aqueous solution for 2-CP, 2,3-DCP, 2,4-DCP and 2,4,6-TCP on α-Fe$_2$O$_3$ and α-FeOOH. Mono-, di- and trichlorophenols exhibit similar adsorption properties on both iron oxides. The amounts adsorbed show the progression: 2-CP > 2, 3-DCP > 2, 4-DCP > 2,4,6-TCP. As described before (141), the higher adsorption of 2-CP is due to the higher solubility of 2-CP and its lower hydrophobic character. However, in these studies the adsorption results could not be fitted by a Langmuir or Freundlich adsorption isotherms.
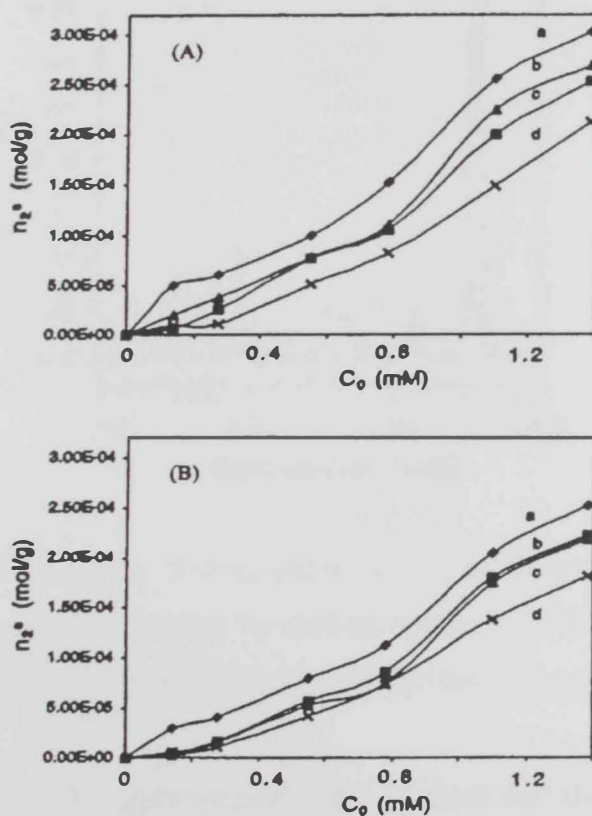
Figure 1-18: (a) Adsorption isotherm of: (a) 2-CP, (b) 2,3-DCP, (c) 2,4-DCP, (d) 2,4,6TCP on hematite. (b) Adsorption isotherm of: (a) 2-CP, (b) 2,3-DCP, (c) 2,4-DCP, (d) 2,4,6-TCP on goethite.

This suggests the simultaneous presence of both chemical and physical interaction taking place between the adsorbate and adsorbent (149-151).

1.4.4 Reaction with Pyridine

The IR spectrum of the α-Fe_2O_3 exposed to pyridine at RT and heated at 373 K for 10 min is reported in Figure 1-16. The intensity of the py-L_s^a peaks decreases more than that of the py-B_s^a, thus suggesting that the bond between pyridine and the L_s^a is weaker than the bond between pyridine and the B_s^a. The spectra obtained after exposure of the α-Fe_2O_3 powder to pyridine at 373 K are shown in figure 1-19 (56).
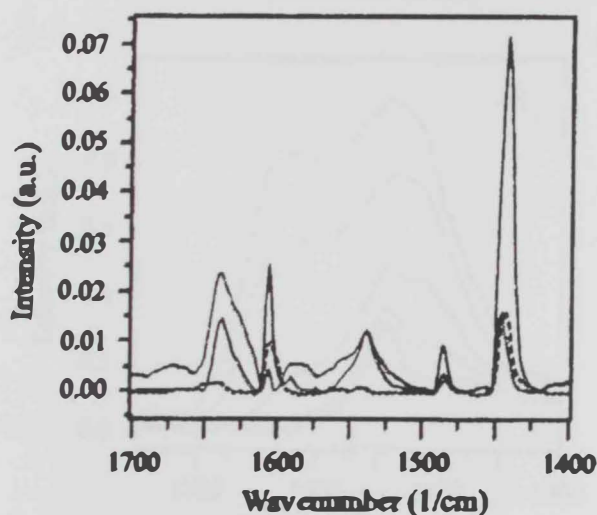
Figure 1-19: IR spectra obtained after the exposure of the α-Fe_2O_3 (hematite) powder to the pyridine + N_2 mixture at RT (___), and after heating the obtained system at 373 K (....); IR spectra obtained after the exposure of the α-Fe_2O_3 (hematite) powder to the pyridine + N_2 mixture at 473 K.

It can be seen that the py-L_s^a/B_s^a peaks intensity ratio increases with the temperature of exposure (from 1.7 at RT to 4.7 at 373 K) suggesting that the treatment at 373 K causes the decrease of the B_s^a, probably because of the condensation of adjacent OH groups(56). This result is consistent with the behaviour observed for the α-Fe_2O_3 powder heated at increasing temperatures. The heating treatment of the hematite powder causes the intensity decrease of the peaks attributed to the H-bonded hydroxyl groups centred around 3663 and 3622 cm^{-1} (Figure 1-20) (56).

37
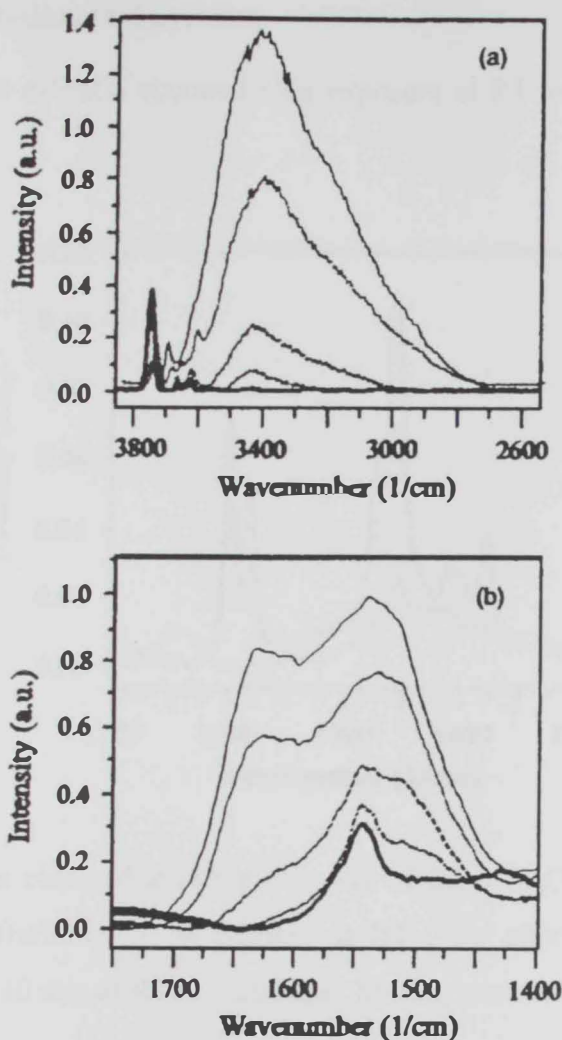
Figure 1-20: IR spectra obtained for the α-Fe$_2$O$_3$ (hematite) powder before the heating treatment (___) and after the heating treatment at 323K (…), 373 K (---), 423 K (-.-.-), 473 K (—); (a) region between 2600 and 3800 cm^{-1}, (b) 1400 and 1750 cm^{-1}.

The chemisorption of pyridine was also carried out under HV conditions and followed by means of XPS and QMS. The presence of pyridine on the iron oxide surface was never revealed by XPS (at exposure temperatures between RT and 473 K) (56). This may indicate that the interaction between pyridine and hematite surface is not strong enough to withstand the vacuum conditions. The vacuum conditions also cause the condensation of the weakly bonded OH groups and the decrease of the Brönsted acidity (56).

1.4.5 Reaction with 2,6-dimethyl pyridine

The IR spectrum of the α-Fe$_2$O$_3$ obtained after exposure at RT to a lutidine + N$_2$ mixture is shown in Figure 1-21.
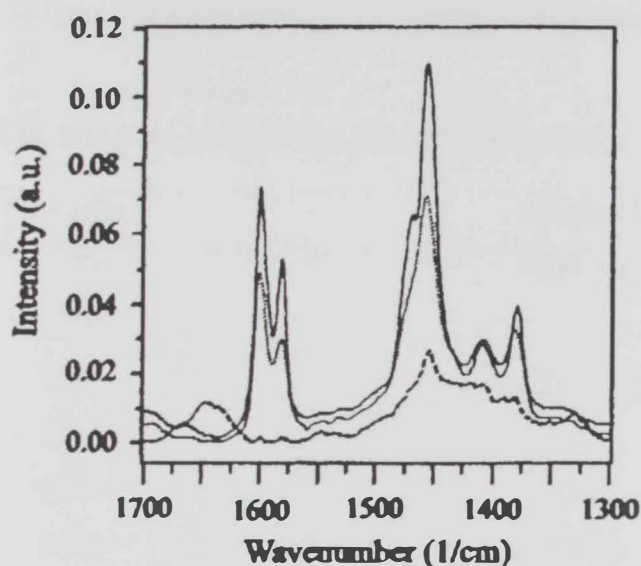
Figure 1-21: IR spectra obtained after the exposure of the α-Fe$_2$O$_3$ (hematite) powder to the 2,6-dimethyl pyridine (lutidine) + N$_2$ mixture at RT (—), after exposure of the obtained system to a N$_2$ flow for 10 min at RT (⁻⁻⁻) and after heating treatment to 373K (- - -).

The spectrum shows the presence of several peaks centered around 1602, 1583, 1470 and 1458 cm^{-1}. Lutidine is a probe molecule more specific than pyridine with respect to the B$_s^a$ when adsorption is perpendicular to the planar surfaces. This characteristic relies on the steric hindrance of the probe molecule as well as on its higher basicity (pKa = 6.7 for lutidine and 5.2 for pyridine) (152). Once again, the IR peaks observed after exposure to the lutidine are compatible with the presence of a liquid layer of lutidine and analogous to the pyridine case, the IR spectrum obtained after the N$_2$ treatment (Figure 1-21), clearly shows that liquid-like lutidine is easily removed (56).

IR peaks observed after the N$_2$ exposure, (Table 1-6 and Figure 1-21), are centred around 1603, 1580 and 1455–1457 cm^{-1} and suggest the presence of 2,6-dimethyl pyridine co-ordinated to

the surface acid sites. The IR spectrum of the α-Fe_2O_3 exposed to lutidine at RT and heated at

373K (for 10 min) is shown in Figure 1-21. Examination of the spectrum shows the presence of

the 2,6-dimethyl pyridinium ion as indicated by the two peaks centred around 1645 and 1455–

1457 cm^{-1} (153). The existence of the pyridinium ions confirms the presence of exposed B_s^a.

Table 1-6: FTIR data (cm^{-1}) of pyridine adsorbed on hematite.

Py/Fe$_2$O$_3$ [a]	Pyridine [b]
1639	1583 (vs.)
1606	
1591	1572 (m)
1574	
1541	
1483	1482 (s)
1443	1441 (vs)

a) 56, (b) 153)

In contrast, the heating treatment causes the condensation of the OH groups and then the

abrupt decrease of the Brönsted acid sites as confirmed by the IR spectrum obtained after the

exposure of the Fe$_2$O$_3$ powder at the 2,6-dimethyl pyridine at 473 K: in actual fact, no traces

of lutidine bonded to the oxide surface are evident at this temperature (56).

1.4.6 Dehydrogenation of ethylbenzene

The dehydrogenation of ethylbenzene is a large scale industrial reaction that is carried out at

870 K over iron oxide catalysts in the presence of steam (154). As it is possible to prepare

epitaxial iron oxide films of different stoichiometry on Pt (111) single crystal (155), ideal

model catalysts for this reaction are available. In addition, recently an ordered potassium-

promoted film was prepared (156). This is of special interest as potassium is the main

promoter for industrial catalysts and increases the conversion rate by about one order of magnitude (157).
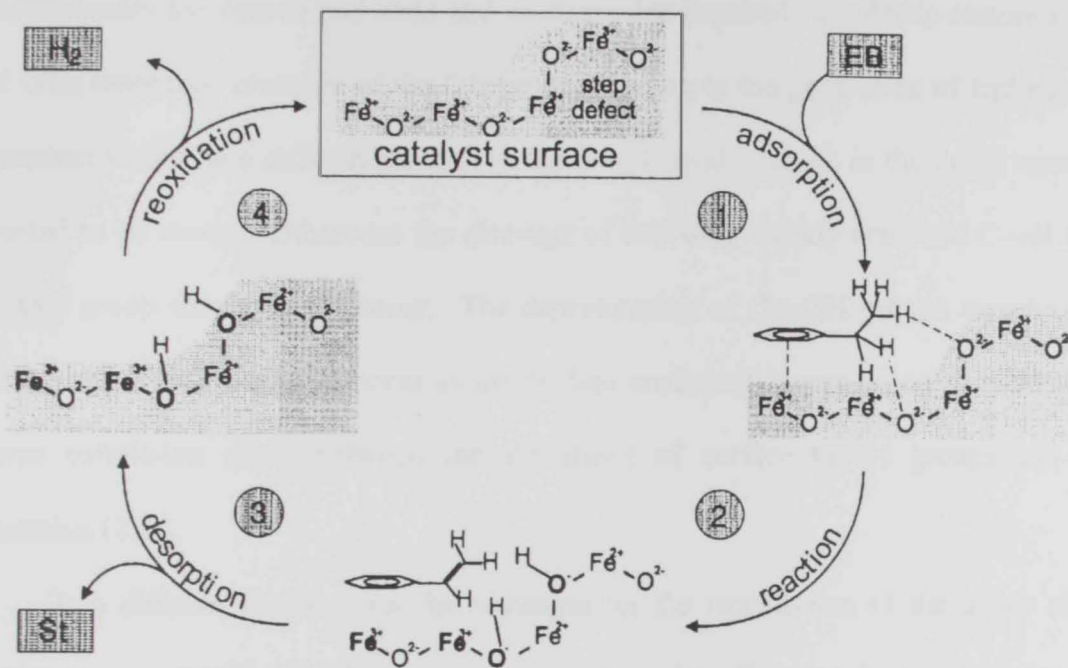
Figure 1-22: Reaction scheme for the dehydrogenation of EB on defective $\alpha-Fe_2O_3$ (0001) model catalysts.

This scheme (Figure 1-22) reveals that the active site is a rather complex ensemble and can be envisaged as a difficult *in situ* rearrangement of the catalysts surface microstructure and may account for the induction time observed in the high pressure reaction experiment (158). At the oxygen site of the defect, the elementary step of dehydrogenation of ethyl to an ethylene group takes place. In addition to this hydrogen abstraction there is also the transition of two electrons from the ethyl carbon atoms to the catalyst thus reducing the iron atoms adjacent to the receiving oxygen atoms. It is assumed that the iron atom which is required for the fixation of the EB molecule is not reduced in its valence as then the interaction with the aromatic ring would be strengthened resulting in a site blocking. Even though it is not known how the electron transfer occurs, a reduction of the Fe^{3+} ions

41

near the oxygen anions receiving the hydrogen seems to be reasonable (158). After desorption of the product molecule a reduced catalyst with the two OH groups and two Fe^{2+} site is evident. This represents the deactivated state and reactions are required in order to restore the active site. The homolytic cleavage of the OH groups leading to the generation of hydrogen as the by-product would be a difficult reaction as the O—H bond strength in the deactivated state is expected to be strong. Otherwise the cleavage of two only weakly activated C—H bonds in the ethyl group would hardly occur. The deprotonation of the OH groups may be the rate-limiting step in the overall process as the surface analytical investigation showed that clear inverse correlation exists between the abundance of surface O—H groups and the EB conversion (158).

Two different situations can be envisaged for the regeneration of the active site. One situation assumes that the O—H groups are cleaved homolytically using the two electrons stored at the two OH adjacent iron atoms thus producing one molecule of dihydrogen. Such reactions are also discussed in other areas of C—H activation catalysis where the formation of a cyclic metal hydride state is envisaged which reacts with the neighboring proton from the second O—H group (158).

The chemisorption of ethylbenzene, styrene and water occurs *via* interaction with acidic iron atoms exposed on the defect free surfaces of Fe_3O_4 (111) and $\alpha-Fe_3O_4$ (0001), whereas physisorption without chemical interaction takes place on the FeO (111) surface exposing no iron atoms. The heterolytic dissociation of water on Fe_3O_4 (111) can be considered as an acid-base reaction, which is facilitated by neighboring Lewis acidic iron and Brönsted basic oxygen sites. These sites are located on the surface in a distance that fits to the geometry of the water molecule, so that they can adsorb the resulting OH^- and OH^+ species after activation and heterolytic dissociation of the molecule. EB and St chemisorb molecularly onto the same adsorption site with their phenylrings oriented parallel to the surface planes,

42

where their HOMO π-electron orbitals couple to empty Fe $3d$ orbitals of exposed iron sites. This interaction can also be considered as an acid-base reaction between the soft Lewis bases EB and St and Lewis acidic surface iron site, where the chemisorption strength is related to the electronic structures or acid-base characters of the reactant molecules and oxide surface sites. No defect-related adsorption states with higher binding energies exist (Figure 1-23) (159).
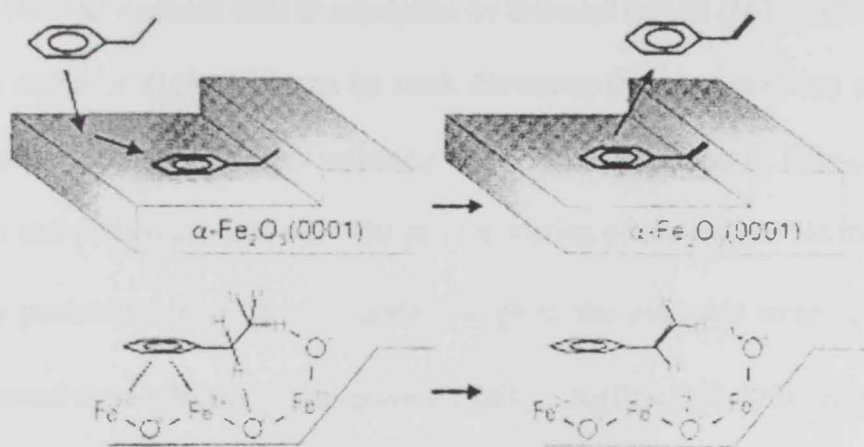
Figure 1-23: Mechanism proposed for the styrene synthesis reaction on α–Fe_2O_3 (0001) model catalyst films. Ethylbenzene adsorbs at Fe^{3+} sites exposed on regular terraces with the phenyl ring oriented parallel to the surface. At catalytically active surface defects like steps, the upward titled ethyl group meets a favorable geometry for coupling to Brönsted basic oxygen sites that deprotonate two C-H groups, simultaneously two electrons are transferred to the catalyst *via* the π–electron system of the phenyl ring.

1.4.7 Arsenic adsorption onto iron oxides

Arsenic is a toxic trace element occurring in natural waters in a variety of forms including soluble, particulate, and organicbound, but mainly as inorganic trivalent As(III) and pentavalent As(V) oxidation states. In many parts of the world, groundwater is polluted with arsenic. This pollution can be caused by human activities (mining, pesticides *etc.*) but usually, the main source of arsenic is geogenic (160). Epidemiological studies have demonstrated a significant increase in the risks of

lung, skin, bladder, liver, and other cancers associated with high levels of arsenic in drinking water. It has also been shown that arsenic interferes with some hormones by altering downstream receptor function (161, 162). Consequently, in the case of arsenic, the European standard level in drinking water has been lowered to 10 µg/L (Directive 98/83/CE) and similar reductions in arsenic levels have been adopted elsewhere, including the United States (160). To remove arsenic from groundwater, classical methods such as adsorption by activated carbon (163), membrane processes (164), or ion exchange (165, 166) can be used. However, the most common arsenic removal method is coupled coagulation and softening (167), removing arsenic through processes of chemisorption and particulate removal. The prior oxidation of the trivalent form of arsenic into the less toxic pentavalent form is an important stage in the treatment since arsenate (AsO_4^{3-}, As(V)) is removed more effectively than arsenite (AsO_3^{3-}, As(III)) (168-170). But, this method is too costly in terms of investment and running costs to be applied in plants of low flows (<10 m^3/h) in sparsely inhabited zones (*e.g.*, the center of France or some areas around the world where major environmental problems with arsenic have been identified (171)). Therefore, it is essential that methods that allow those installations to supply drinkable water at low cost should be developed.

Clays or modified clays are used worldwide as adsorptive media for heavy metals (172, 173), bacteria (174), or organic contaminants (175). Experiments have shown that clay functionalization can be optimized by matching clay structure with a suitable reactive (176).

Arsenic adsorption was carried out on simple materials such as goethite and amorphous iron hydroxide, and more complex matrices such as clay pillared with titanium(IV), iron(III), and aluminum(III) (177). These matrices were synthesized from a bentonite whose montmorillonitic fraction was pillared according to optimized parameters. These sorbents were characterized by various methods: XRD, FTIR, BET, DTA/TGA, surface acidity and zetametry. Elimination of

arsenite and arsenate as a function of pH was studied. Arsenate elimination was favored at acidic pH, whereas optimal arsenite elimination was obtained at 4<pH<9 (177). For pH values above 10, the pillared clays were damaged and elimination decreased. Equilibrium time and adsorption isotherms were also determined for arsenite and arsenate at each matrix autoequilibrium pH. Amorphous iron hydroxide had the highest adsorption capacities both towards arsenate and arsenite (177). Adsorption capacities of goethite and iron- and titanium-pillared clays toward arsenate were similar, but those toward arsenite were different. Desorption experiments from the various matrices were carried out. Iron- and titanium-pillared clays showed a desorption capacity above 95% and around 40% respectively, but no desorption rate could be obtained for iron (hydr)oxides as they were damaged during the process (177).

1.5 Support effects on iron oxide catalyst

1.5.1 Catalytic reduction of SO_2 over supported transition-metal oxide catalysts

Since the 1930s, various commercial flue gas desulfurization (FGD) processes, including throwaway, adsorption, absorption, and catalytic reduction, have been developed. These technologies have recently attracted increasing attention as the regulations for the emission of SO_x have become more stringent, and can now deliver desulfurization rates above 90% (178-180). Among the FGD processes, the throwaway method has the drawback of requiring subsequent waste disposal (181-184). Meanwhile, with both adsorption and absorption it is necessary to devise a process to treat SO_2 released from the sorption process. This leaves catalytic reduction, in which SO_2 is reduced to elemental sulfur, as the method of choice. This method has the advantages of feasible recovery of sulfur and no waste disposal problem. Reducing agents for the catalytic reduction of SO_2 include carbonaceous material, CH_4, CO and H_2. By using coke as a reducing agent, Lepsoe (185) obtained 80% conversion of SO_2 at 850 °C. Salis and Berk (186)

45

and Mulligan and Berk (187) reported only slightly higher conversion rates, using CH_4 as a reducing agent, over activated alumina or transition-metal sulfide catalysts, whilst Zhu *et al*. (180) obtained complete conversion of SO_2 over ceria-based catalysts at 750 °C, also using CH_4. Other reports (188-198) indicate that when using CO as a reducing agent, lower reaction temperatures (320–800°C) can be used. Another intensively investigated reducing agent, H_2, has also been shown to effectively reduce SO_2 to elemental sulfur (179, 199-206).

The results shown in Figures 1-25 and 1-26 also exhibit that the Fe_2O_3/CeO_2 catalyst possesses excellent durability, while the activity of Fe_2O_3/γ-Al_2O_3 declines appreciably with time. Inhibition of Fe_2O_3/γ-Al_2O_3 may be caused by the stronger adsorption of SO_2 (197).
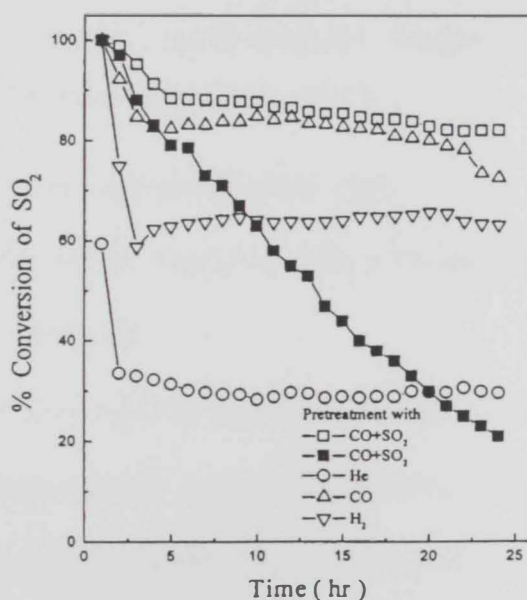
Figure 1-25: Effect of pretreatment on the conversion of SO_2. Catalyst: Fe_2O_3/CeO_2 (hollow symbols) or Fe_2O_3/γ-Al_2O_3 (solid symbols). Weight of catalyst: 0.25g. Feed: 1000 ppm SO_2, 3000 ppm CO. Reaction temperature: 300 °C.

Figure 1-26: Effect of pretreatment on the yield of elemental sulfur. Catalyst: Fe_2O_3/CeO_2 (hollow symbols) or $Fe_2O_3/\gamma-Al_2O_3$ (solid symbols). Weight of catalyst: 0.25g. Feed: 1000 ppm SO_2, 3000 ppm CO. Reaction temperature: 300 °C.

The following conclusions were inferred from this work:

1. With $\gamma-Al_2O_3$ as the support, $Fe_2O_3/\gamma-Al_2O_3$ is the most active catalyst of those tested for the reduction of SO_2 (197).

2. Presulfidization of the catalyst is necessary. For the catalytic reduction of SO_2, if the catalyst is pretreated with $CO + SO_2$ a higher stability is obtained and higher activity than those catalysts pretreated with CO, H_2 or He (197).

3. CO can adsorb onto and reduce the Fe_2O_3/CeO_2 catalyst most effectively, while the adsorption of SO_2 somewhat causes the inhibition of $Fe_2O_3/\gamma-Al_2O_3$. This explains why Fe_2O_3/CeO_2 has higher activity and stability than $Fe_2O_3/\gamma-Al_2O_3$ (197).

1.5.2 Chlorocarbon destruction by supported iron oxide catalyst

Although the reactions of chlorocarbons with metal oxides to yield carbon oxides and metal chlorides are often thermodynamically favorable (207), liquid-solid or gas-solid reactions are

47

involved, and usually stoichiometric reactions are only observed on the surface of the metal oxide. Kinetic parameters involving ion (Cl^-/O^{2-}) migration inhibit complete reaction. Therefore, the use of ultrahigh surface area metal oxides allows reasonably high capacities for such chlorocarbon or chlorofluorocarbon destructive adsorption processes (207-209).

$$2\,MgO + CCl_4 \longrightarrow 2\,MgCl_2 + CO_2 \qquad\qquad \Delta H_{rxn} = -334 \text{ kJ}$$

$$2\,MgO + CF_2Cl_2 \longrightarrow MgCl_2 + MgF_2 + CO_2 \qquad \Delta H_{rxn} = -485 \text{ kJ}$$

However, when nanoscale particles of MgO or CaO are used, the path length for migration of ions from bulk to surface is small. Indeed, Klabunde *et al* (210) found that nanoparticles of MgO could be partially or almost fully oxygen-18 exchanged with $H_2^{18}O$ depending on the reaction temperature (in the range of 300-700 °C) (211). Since the amount of iron present was very small, iron was found to play a catalytic role, which could be attributed to Cl^-/O^{2-} exchange catalysis (212,213). When CCl_4 attacks the surface of Fe_2O_3, dissociative adsorption occurs, probably with the intermediacy of chemisorbed CCl_2. At this point, $COCl_2$ may form as an intermediate that goes on to react in a similar mode to produce CO_2 and more $FeCl_x$ (210). The $FeCl_x$ formed quickly exchanges Cl^- with O^{2-} in such a way that Cl^- is driven into the bulk of the small particle, whereas O^{2-} comes to the surface:

$$
\begin{array}{ccc}
\begin{array}{c}
\text{O Fe O Fe} \\
\text{MgO MgO} \\[6pt]
[Fe_2O_3](MgO)_3
\end{array}
&
\xrightarrow[\;-\,O^{2-}\;]{2\,Cl^-}
\;
\begin{array}{c}
\overset{\displaystyle Cl\;\;Cl}{\diagup\;\diagdown} \\
\text{O Fe O Fe} \\
\text{MgO MgO} \\[6pt]
[Fe_2O_2Cl_2](MgO)_3
\end{array}
&
\longrightarrow
\;
\begin{array}{c}
\text{O Fe O Fe} \\
\text{MgCl MgO} \\
\text{Cl} \\[6pt]
[Fe_2O_3](MgO)_2(MgCl_2)
\end{array}
\end{array}
$$
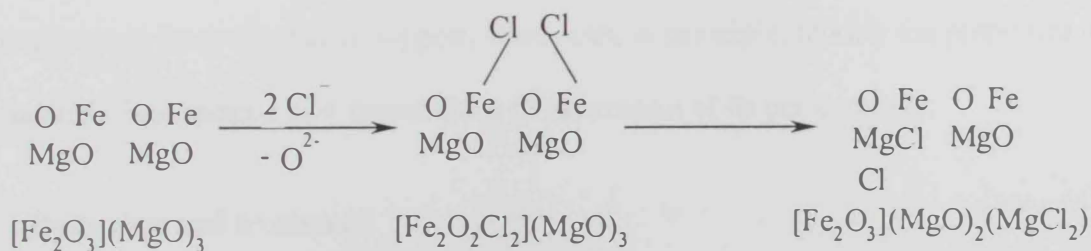
In the presence of Fe_2O_3 the mechanism of this chlorocarbon decomposition process change (214-218).

1.6 Methods of preparation of nanoscale iron oxides and supported iron oxide

Nanoscale particles have received considerable attention in view of the potential for new materials and unique properties. The novel properties and the numerous applications of

nanophase materials, especially ceramic powders, have encouraged many researchers to invent

and explore the methods, both chemical and physical, by which such materials can be prepared.

1.6.1   Physical/Aerosol methods

Several physical aerosol methods have been reported for the synthesis of nanosize particles of ceramic

materials. These include gas condensation techniques (219-226), spray pyrolysis (327-334), thermal

decomposition of metal-organic precursors in flame reactors (280-283) and other aerosol processes.

1.6.2 Chemical methods

1.6.2.1 Sol-gel method

The role of sol-gel processing, as well as the role of chemistry in general, in materials

fabrication has been growing rapidly. The development of sol-gel processing of materials, and

especially of ceramics, has been described in several books and reviews (239-253).

1.6.2.1.1 Study of nanoparticle support interactions in a Fe_2O_3-SiO_2 nanocomposite prepared by a sol-gel method

The synthesis of nanocomposites has gained acceptance in several fields of application of

nanomaterials (254-258).   The main reason is that the preparation of nanocomposites

represents an effective solution to the tendency of nanopowders to aggregate(259). Additional

advantages come from the matrix support, which can, in principle, modify the properties of the

nanomaterial, thus opening new possibilities to the control of its performance.

1.6.2.2 Hydrothermal treatment

1.6.2.2.1 Preparation of hematite nanocrystals

Hematite nanocrystals modified with surface layers of amorphous hydrous iron oxides have

been prepared by hydrothermal conditions in the absence of alkali. The formation temperature

49

was found to be *ca.* 130 °C. When the temperature was lower than 130 °C, no product was formed, while above this temperature, the amount of amorphous hydrous iron oxides at the surfaces of hematite nanocrystals was drastically decreased. The amorphous layers on the hematite nanocrystals obtained at 130 °C were determined to be $Fe_2O_3.1.64H_2O$. The coercivity for the hematite nancrystals with modified layers was 0.534 kOe, which is slightly larger than the values for hematite nanocrystals with few agglomerations (260).

1.6.2.3 Impregnation and drying

The impregnation method is used to prepare catalysts ultrafine particles are deposited on high surface area supports. A solution containing the catalyst component (single or plural) is impregnated into the pore of the support and adhered by the subsequent drying and calcinations. The metal compounds are held by adsorption of metal cations on the basic site on the support (O^{2-} or basic OH^-) or by ion exchange between metal cations and H^+ of acidic OH^- groups. Usually the former is called an impregnation method and the latter is called the ion exchange method (261).

1.6.2.3.1 Synthesis of supported catalysts by impregnation and drying using aqueous chelated metal complexes.

Supported metal and metal oxide catalysts comprise the most important class of heterogeneous catalysts in industry. Therefore, the synthesis of supported catalysts is of utmost scientific and industrial importance. Several reviews on the synthetic methods to prepare supported catalysts have been reported in the literature by Anderson (262), Geus and Van Veen (263), Che (264), and De Jong (265). The methods applied widely involve ion exchange (262), homogeneous deposition precipitation (266, 267), redox chemistry (265) and chemical vapor deposition (265). By far the most commonly used synthetic route involves impregnation of porous support bodies with a solution

of the metal (oxide) precursor followed by evaporation of the solvent. The most attractive feature of this route is its simplicity in the practical execution on both laboratory and industrial scales. The method is often referred to as impregnation and drying. Although the practical execution is seemingly simple, the fundamental phenomena underlying impregnation and drying are extremely complex. More often than not the interaction between the metal precursor and the support is limited, thereby allowing redistribution of the active phase over the support body during drying. Since evaporation of the solvent takes place at the exterior of the support particles, capillary flow of solution to its exterior surface may take place, thereby causing production of so-called eggshell catalysts, often with a poor dispersion of the active phase (268). The pioneering work of Kotter and Riekert (269) has shown that an increase in the viscosity of the impregnation solution suppresses the outward flow of the solution and leads to a more uniform activity profile over the supported bodies. Alternative approaches involve very high or very low drying rates (263), but results are of moderate quality only. Quite unnoticed by the academic catalysis community, an alternative approach to impregnation and drying has been utilized in industrial practice as well as by a few academic groups. The essence of this approach is to use aqueous solutions of multidentate chelated metal complexes.

1.6.2.4 Liquid phase deposition

Liquid-phase deposition (LPD) (270,271) has been developed for the preparation of metal oxide thin films. In this process, it is possible to form thin film metal oxides or hydroxides directly on the substrate which is immersed in the treatment solution for deposition (272).

1.7 Aims and objectives

As stated already in this chapter, chapter 1 (literature review), the use of inorganic solids as heterogeneous catalysts has attracted much attention in recent years in the literature and heterogeneous catalysts themselves are used extensively in industrial applications. Recent studies

51

have shown that one group of inorganic solids, are the metal oxides, which exhibit remarkable catalytic properties, in particular in their role as adsorbents. Information on the structure of a heterogeneous catalyst can sometimes be determined by spectroscopy and related studies of reactive molecules adsorbed on single crystal surfaces. However, these studies are generally carried out in ultra-high vacuum conditions, which are very different from those used in practice. In general, practical heterogeneous catalysts are high surface area materials that may contain several different phases and which operate at 1 atm pressure and higher pressures. The focus in this project is to investigate the different forms of iron oxide in such structures and to examine the relationship between the structure and the reactivity using newly constructed experiments in an effort to ascertain the catalytic behaviour. The aims and objectives of this thesis therefore are as follows:

1. To prepare a series of iron oxides of high surface area for use in environmental catalyis using chemical methods.

2. To characterize the iron oxides using FTIR, XRD *etc*.

3. To examine the role of the iron oxides as adsorbents as environmental catalysts for the decomposition of a selected environmentally important molecule such as CCl_4 using a series of new experiments with varying parameters.

4. To compare the empirical results with recent structural models reported in the literature, to examine the structure-catalytic behaviour relationship of such iron oxides.

This work should contribute further to the understanding of the structure-catalytic behaviour relationship of iron oxides in environmental catalysis from an empirical perspective and in addition the use of the newly synthesized and characterized oxides as potential adsorbents in their practical use as filters in environmental applications.

CHAPTER 2

SYNTHESIS AND CHARACTERIZATION OF THE ADSORBENTS /CATALYSTS

CHAPTER 2: SYNTHESIS AND CHARACTERIZATION OF THE ADSORBENTS/CATALYSTS.

2.1 Introduction

Inorganic materials including noble metals, metal oxides, metal carbides, metal nitrides, and elemental carbon have been of great importance in today's chemical research. This importance stems from the variety of unique properties such materials exhibit, including chemical, physical, mechanical, and magnetic properties, which make them very useful in a wide range of advanced application.

Metal oxides have been of special importance due the important fields of advanced applications they have been employed in, including catalysis, magnetic recording, and advanced materials such as ceramics. It has been well proven that the bulk behavior of materials can be dramatically altered when constituted of nanoscale building blocks especially in chemical applications such as catalysis. When prepared from nanometer-sized particles, large portion of their atoms reside on the surface increasing the reactive sites where reactions can take place on the surface and as a result metal oxides have shown significantly better performance in several applications when fabricated from Nanometer-sized particles.

The synthesis of nanoscale particles has received considerable attention in the literature in view of the potential to prepare further new materials and their related unique properties (273). The novel properties, especially significantly reactive surfaces, and the numerous applications of such nanophase materials has led to a profusion of research in this field, involving new methods of synthesis and the modification of existing methods.

In the first phase of this project, the synthesized pure iron oxides were prepared by a precipitation method (discussed below), while the mixed oxides were prepared by the sol-gel method. This latter process typically involves the hydrolysis of reactive metal precursors (usually alkoxides in an alcoholic solution) resulting in the corresponding hydroxide. Condensation of the

hydroxide molecules by elimination of water leads to the formation of a network structure leading to gelation and resulting in the formation of a dense porous gel. The formed gel is a polymer of a three-dimensional skeleton surrounding interconnected pores (Figure 2-1). Subsequent removal of the solvents and appropriate drying of the gel results in an ultrafine powder of the metal hydroxide. Further heat treatment of the hydroxide leads to the corresponding ultrafine powder of the metal oxides (273).

In contrast, the supported oxides were prepared by the wet impregnation method. The impregnation method is used to prepare catalysts of ultrafine particles that are deposited on high surface area supports. A solution containing the catalyst precursor is impregnated into the pores of the support and adhered by the subsequent drying and calcinations. The metal compounds are held by adsorption of the metal cations on the basic site on the supports (O^{2-} or OH^-) or by ion exchange between the metal cations and H^+ of the acidic groups. Usually the former is called the impregnation method and the latter is called the ion-exchange method (261).
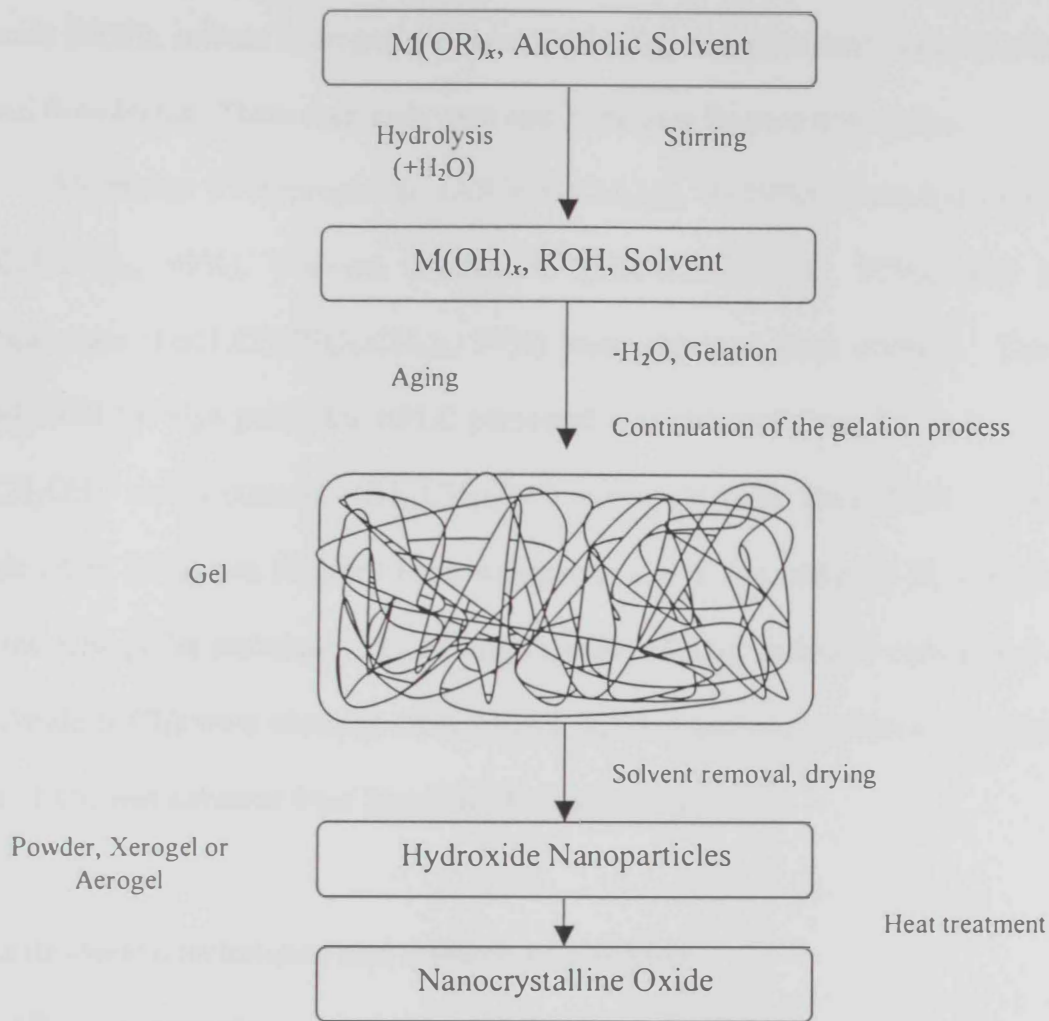
Figure 2-1: A flow chart of a typical sol-gel process for the preparation of nanoscale metal oxide powders.

55

2.2 Experimental section

2.2.1 Materials

Hydrated iron (III) nitrate ($Fe(NO_3)_3.9H_2O$), hydrated iron(II) sulfate ($FeSO_4.7H_2O$), potassium hydroxide (KOH), sodium hydrogen carbonate ($NaHCO_3$) and potassium nitrate (KNO_3) were obtained from Merck. These chemicals were used to prepare the pure iron oxides.

Aluminum tri-*iso*propoxide ($Al(OCH(CH_3)_2)_3$, 99.99%), tetraethyl orthosilicate ($Si(OCH_2CH_3)_4$, 99%), titanium *n*-butoxide ($Ti(O(CH_2)_3CH_3)_4$, 97%), and iron(III) acetylacetonate ($Fe(H_3COCHCOCH_3)_3$, 97%) were obtained from Aldrich. 2-propanol ($(CH_3)_2CHOH$ (of high purity for HPLC purposes) was obtained from J.T. Baker. Ethanol (CH_3CH_2OH) and 1-butanol ($CH_3(CH_2)_3OH$) were obtained from BDH. Potassium bromide (KBr, 99%) was obtained from Aldrich for use in recording FT-IR measurements using the KBr pellet technique. Titanium(IV) oxide (TiO_2), activated carbon and carbon tetrachloride (CCl_4) were obtained from Aldrich for the catalytic reactions. Aluminum(III) oxide (Al_2O_3) was obtained from Sasol North America Inc.

2.2.2 Instruments, techniques and methods of synthesis

2.2.2.1 IR measurements

All samples were investigated by FTIR spectroscopy on a Nicolet FT-IR Magna-IR 560 spectrophotometer (E.S.P) with a flexible configuration enabling a high degree of accuracy and sensitivity over a variety of wavelength ranges. The spectrometer has more than four external beams and can accommodate more than six attachments as detectors, including a microscope and TGA. The system is fully computerized using state-of-the-art software (Omnic, v.5.0), with a user-friendly graphical interface and includes comprehensive spectral libraries. In each experiment, the catalyst was first mixed with KBr (2% sample by wt). The samples were pressed into a disc and loaded into an IR cell. The spectra were

56

recorded at room temperature by accumulating 32 scans at a spectral resolution 4 cm^{-1}, using the empty cell as background over a range of 500 to 4000 cm^{-1}.

2.2.2.2 XRD spectra

A Philips X-ray diffractometer, model PW/1840, with Ni filter, Cu-Kα radiation (λ = 1.542 Å) at 40 kV, 30 mA and scan speed 0.02° s^{-1} was used for running powder X-ray diffraction measurements on all samples. The diffraction peaks between $2\theta = 2°$ and 60° were recorded. The corresponding spacing, d (Å) and the relative intensities ($I/I°$) were calculated and compared with the JCPDS-ICDD card values.

2.2.2.3 Surface area measurements

BET SA measurements were determined using N$_2$ adsorption at 77 K (-196 °C) on a Quantachrome NOVA-1000 volumetric gas sorption instrument. All samples were degassed at 120 °C prior to analysis. The specific surface area was determined from the linear portion of the BET plot (P/P_0 = 0.05-0.30).

2.2.3 Preparation of pure, mixed and supported iron oxides

2.2.3.1 Preparation of pure iron oxides

2.2.3.1.1 Hematite, α-Fe$_2$O$_3$

Hematite was prepared by transformation of ferrihydrite (Fe$_5$HO$_8$.4H$_2$O). In the preparation of hematite, the first step involves the precipitation of ferrihydrite which is then converted into hematite in aqueous suspension by rearrangement and dehydration within the ferrihydrite aggregates. This transformation takes place under weakly acidic to weakly alkaline conditions (2).

In a typical experiment, 40 g (1.0×10^{-1} mol) $Fe(NO_3)_3.9H_2O$ was dissolved in 500 mL twice distilled water, preheated to 90 °C and the precipitation of the ferrihydrite occurred with the addition of 300 mL 1 M KOH preheated to 90 °C. 50 mL of 1 M $NaHCO_3$ was then added (preheated to 90 °C) to the brown, voluminous precipitate and the resultant suspension (pH = 8 - 9) was held in a closed flask at room temperature for 48 hours. The product was then filtered through filter paper and subsequently washed with twice distilled water.

2.2.3.1.2 Magnetite, Fe_3O_4

The method employed here is based on the oxidative hydrolysis of $FeSO_4$ solution in an alkaline medium (274). In a typical experiment, 80 g (5.3×10^{-1} mol) $FeSO_4.7H_2O$ was dissolved in 560 mL deionized water previously flushed with Argon. The glass reaction vessel (1 L) was closed with an air tight plastic lid which had several perforated holes (acting as insertion inlets) and a thermometer (Figure 2-2). The reaction vessel was placed in a water bath at 90 °C. The thermometer was inserted to monitor the temperature and the entire system was purged with Argon. Once the reaction temperature reached 90 °C, 240 mL of an oxygen-free solution containing 6.46 g (6.00×10^{-2} mol) KNO_3 and 44.9 g (8.00×10^{-1} mol) KOH was added dropwise within approximately 5 minutes. After addition of this solution, the reactor was heated for another 30-60 min, cooled overnight and the black resultant precipitate was filtered and washed with twice distilled water.
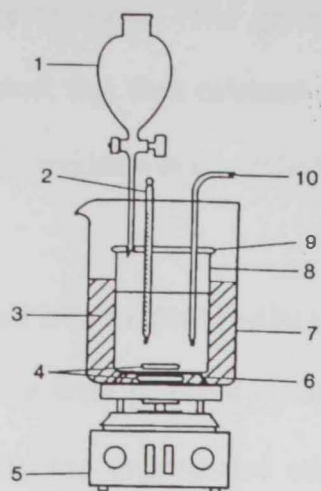
Figure 2-2 Experimental setup for the synthesis of magnetite: 1 Drop funnel, 2 thermometer, 3 water bath at 90 °C, 4 magnet, 5 heater and magnetic stirrer, 6 support for the reaction vessel, 7 external beaker used as a water bath, 8 reaction vessel, 9 plastic lid with inlet holes, 10 purge gas inlet (Argon).

2.2.3.1.3 Maghemite, γ-Fe$_2$O$_3$

Maghemite having the composition of hematite and the structure of magnetite, can be considered as completely oxidized magnetite. Maghemite was prepared by the synthesis of magnetite in a crucible placed in a furnace for 2 hours at 250 °C.

2.2.3.2 Preparation of mixed iron oxides (Fe$_2$O$_3$-Al$_2$O$_3$, Fe$_2$O$_3$-SiO$_2$ and Fe$_2$O$_3$-TiO$_2$)

The mixed oxides were prepared by a one step sol-gel method. In each case, 10 g (5.0 x 10^{-2}) of aluminum tri-*iso*propoxide (or tetraethyl orthosilicate, or titanium butoxide) was first dissolved in 500 mL *iso*propanol (or the corresponding alcohol, ethanol in the case of silicon ethoxide or 1-butanol in the case of titanium butoxide) and stirred thoroughly to ensure complete dissolution of the aluminum tri-*iso*propoxide. An equivalent 3.5 mL of water was then added drop wise into the solution with stirring. At the same time, 0.69 g (1.95×10^{-3} mol) of iron(III) acetylacetonate dissolved in 400 mL *iso*propanol was added dropwise to the mixture and stirred for 7 hours in order for hydrolysis and complete

gelation of the reactant mixture to occur. The gel was then aged for 3 days at room temperature. The resultant product was then calcined at 500 °C for 6 hours in a furnace. The amount of Fe_2O_3 in the mixed oxides was controlled to be 4% by weight (wt).

2.2.3.3 Preparation of supported iron oxides (Fe_2O_3/Al_2O_3, Fe_2O_3/TiO_2 and Fe_2O_3/C)

All supported iron oxides samples were prepared by using the wet impregnation method. Iron(III) nitrate ($Fe(NO_3)_3.9H_2O$) was impregnated onto various supports (Al_2O_3, SiO_2, TiO_2 and activated carbon). For example, in the preparation of Fe_2O_3/Al_2O_3, 1.07 g (2.65×10^{-3} mol) $Fe(NO_3)_3.9H_2O$ was dissolved in 5.6 mL of twice distilled water which was calculated from the total pore volume of the Al_2O_3 sample used. The solution was then added to 5 g (5×10^{-2} mol) of Al_2O_3 with a specific SA of 128 m^2/g and total pore volume of 1.12 mL/g. The impregnated catalyst precursor was then aged for 0.5 hours, dried in air at 125 °C for 2 hours and calcined in a furnace at 500 °C for a further 6 hours. The metal loading was fixed at 4 wt % for all supported iron oxides.

2.3 Results and characterization

2.3.1 Pure iron oxides

Pure samples of hematite, magnetite and maghemite were obtained. The method that was used to prepare hematite (which had a characteristic dark red colour) gave 7.92 g of product with a specific SA of 51.8 m^2/g (2). The sample of prepared magnetite was black in color with a corresponding specific SA of 17.7 m^2/g. In the preparation of maghemite (obtained by heating the magnetite) the temperature was found to be critical since at a higher temperature maghemite can be converted to hematite. The prepared maghemite in this experiment was found to have the same surface area as the precursor (2), *i.e.* 19.9 m^2/g.

60

The heating temperature in the preparation of maghemite is critical because higher temperatures cause the maghemite to transform to hematite.

2.3.1.1 FT-IR spectra

Table 2-1 shows the FT-IR absorption frequencies of the three types of pure iron oxides prepared in these experiments. All three spectra represented in Figure 2-3 have some common structural features. All oxides show a broad band in the range 3417-3422 cm^{-1}, which can be assigned to the asymmetric and symmetric stretching modes of adsorbed water (275). The strong intensity of the bands indicates that a high amount of water is retained in the dried oxides. The peaks in the range 1624-1638 cm^{-1} are associated with the HOH bending mode of water. There is also a common band in all three spectra at 1049 cm^{-1} which is can be assigned to δ Fe-OH.

Hematite shows two well-resolved bands at 547 and 463 cm^{-1}, which can be assigned to the Fe-O vl and v3 modes respectively (276). In comparison, magnetite shows a strong absorption peak at 569 cm^{-1}, whereas maghemite shows some absorption peaks at 694, 637, 557 and 479 cm^{-1} which are typical for maghemite. Finally, there is common band at 1380 cm^{-1} which is indication to Fe-OH bending mode (275).

Table 2-1: IR frequencies (cm^{-1}) of pure iron oxides.

Hematite	Magnetite	Maghemite
3417	3419	3422
1632	1624	1638
-	877	877
547 and 463	569	694, 637, 557 and 479
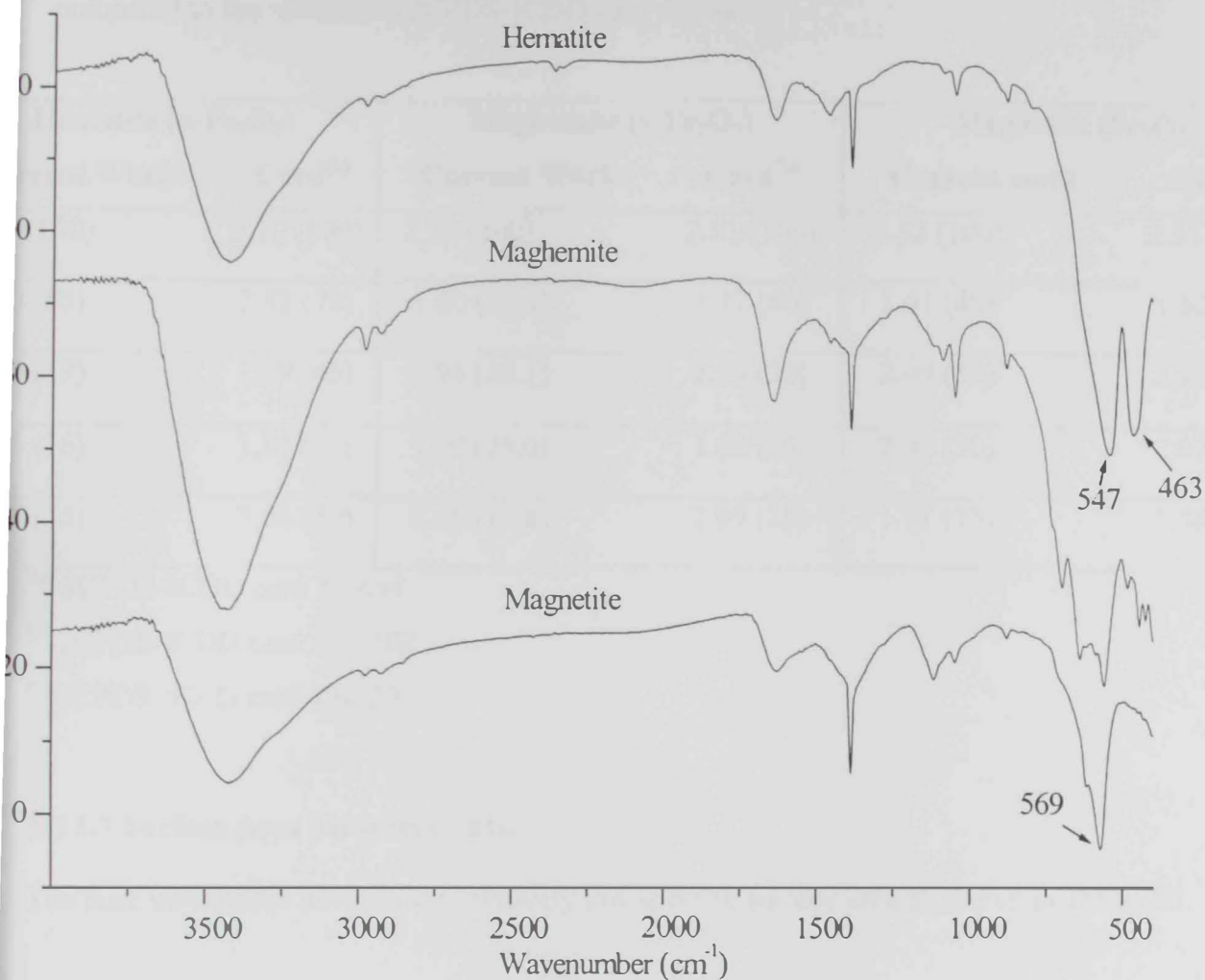
Figure 2-3: FT-IR spectra for hematite, maghemite and magnetite.

2.3.1.2 XRD Measurements

The diffraction patterns obtained for all three iron oxides matched well with the theoretical data of the JCPDS-ICDD card (Table 2-2), with the best correlation seen for hematite and maghemite.

Table 2-2: XRD lines (d-value and intensity of peaks) obtained for maghemite powder compared to the referenced JCPDS-ICDD card values.

Hematite (α-Fe$_2$O$_3$)		Maghemite (γ-Fe$_2$O$_3$)		Magnetite (Fe$_3$O$_4$)	
rrent Work	Card[a]	Current Work	Card[b]	Current work	Card[c]
(100)	2.70 (100)	2.50 (100)	2.51 (100)	2.52 (100)	2.53 (100)
3 (85)	2.52 (70)	1.60 (46.4)	1.47 (40)	1.61 (49)	1.62 (30)
0 (59)	1.69 (45)	2.93 (26.1)	2.95 (30)	2.09 (32)	2.10 (20)
5 (76)	1.84 (40)	1.70 (25.6)	1.60 (20)	2.95 (30)	2.97 (30)
1 (35)	3.68 (30)	2.08 (12.8)	2.09 (15)	1.71 (13)	1.48 (40)

[a] JCPDS-ICDD card 33-664

[b] JCPDS-ICDD card 25-1402

[c] JCPDS-ICDD card 19-629

2.3.1.3 Surface Area Measurements.

The pure iron oxides have shown relatively low specific surface area as shown in Table 2-3.

Table 2-3: Specific surface area of hematite, maghemite and magnetite.

Sample	Surface area (m^2)	Specific Surface area (m^2/g) Current Work	Specific Surface Area (m^2/g) Literature Values[a]
Hematite	18.8	51.8	20-25
Maghemite	14.0	19.9	20
Magnetite	12.6	17.7	4

[a] 2

2.3.2 Mixed oxides

The three types of mixed oxide synthesized by the sol-gel method were also characterized by FT-IR spectroscopy, powder X-ray diffraction and BET SA measurements.

2.3.2.1 FT-IR spectra

All the mixed oxides showed a broad band in the range 3431-3446 cm^{-1} (Figure 2-4) which again can be assigned to the asymmetric and symmetric stretching modes of adsorbed water (275). The broadness of the bands also illustrate that a high amount of water is retained in the dried oxides. The OH bending mode of water is also evident in all three spectra in the range 1633-1635 cm^{-1}. The low intensity peaks observed at 2976 and 2925 cm^{-1} in the IR spectra of mixed iron oxide with alumina and silica represent v C-H which is indicative of the presence of some organic residues that remain adsorbed on the surface after the calcination process. These peaks are not observed in the IR spectrum of Fe_2O_3-TiO_2. The main absorption frequencies are shown in Table 2-4.

Table 2-4: FTIR frequencies incm^{-1} of the mixed iron oxides.

Fe_2O_3-Al_2O_3	Fe_2O_3-SiO_2	Fe_2O_3-TiO_2
3446	3431	3441
2976	2975	-
2926	2925	-
1635	1633	1633
-	1089 and 1051	-
750	769	-
617	-	-
-	-	498
-	461	-

In the IR spectrum of Fe_2O_3-Al_2O_3, two very strong overlapping broad bands are evident at 750 and 617 cm^{-1} inferring the presence of an aluminum-oxygen bond. In comparison, the IR spectrum of Fe_2O_3-SiO_2 shows two bands of medium intensity at 1089 and 1051 cm^{-1} which represent the asymmetric Si-O-Si stretch. The corresponding Si-O-Si symmetric

stretch is observed at 769 cm^{-1} as a low intensity peak, whereas the band at 461 cm^{-1} can be assigned to δ (Si-O-Si), the deformation mode of the silica network. The IR spectrum of Fe$_2$O$_3$-TiO$_2$ shows only one additional (other than v_{sym} and v_{asym} H$_2$O) broad highly intense band centered at 498 cm^{-1}.
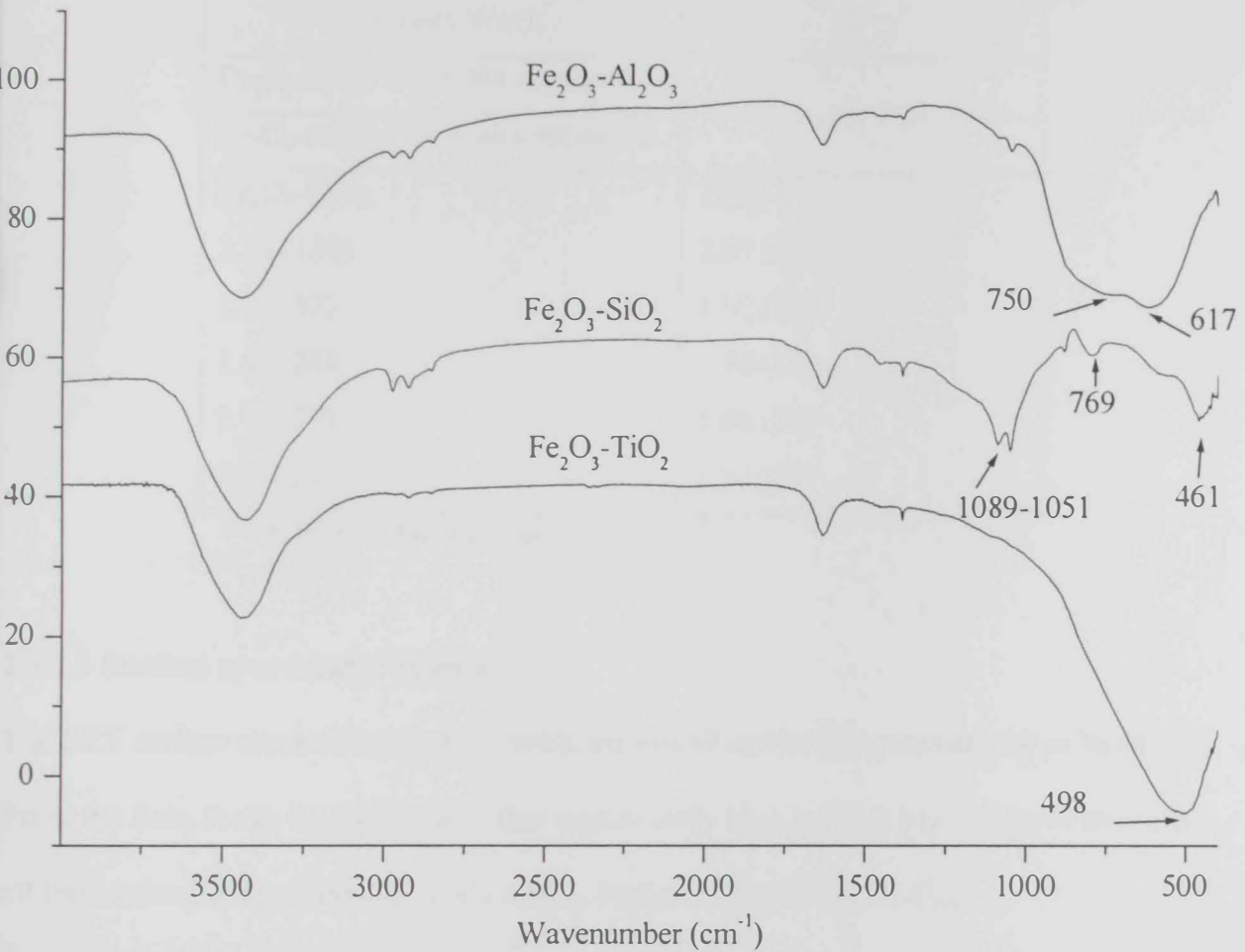
Figure 2-4: FT-IR spectra of three types of mixed oxides.

2.3.2.2 XRD measurements

To detect any chemical or structural changes in the structures under investigation, some selected samples were matched with the relevant the d-plane spacing. The XRD lines of the mixed oxides are represented in Table 2-5. The powder XRD profiles for Fe$_2$O$_3$-SiO$_2$ and Fe$_2$O$_3$-Al$_2$O$_3$ samples showed no diffractions patterns suggesting that these samples are

amorphous powders. The XRD profile for Fe_2O_3-TiO_2 showed d-values at 3.50, 1.88, 1.66,

1.70 and 2.37 respectively as shown in table 2-5.

Table 2-5: XRD lines of all mixed oxides.

Mixed Iron Oxides Current Work	Iron Oxide Mixed With
Fe_2O_3-SiO_2: No peaks appeared	
Fe_2O_3-Al_2O_3: No peaks appeared	
Fe_2O_3-TiO_2	TiO_2: [a]
3.50 (100)	2.07 (100)
1.88 (37)	3.32 (80)
1.66 (28)	1.70 (30)
1.70 (27)	1.66 (30)
2.37 (25)	1.88 (10)

[a] JCPDS-ICDD card 8-117

2.3.2.3 Surface area measurements

The BET surface areas of the Fe_2O_3-containing mixed oxides are summarized in Table 2-6.

From the data, it can be clearly seen that significantly high surface areas were obtained for

all three mixed oxides, namely Fe_2O_3-Al_2O_3, Fe_2O_3-SiO_2 and Fe_2O_3-TiO_2.

Table 2-6: The BET surface area of three types of mixed iron oxides.

Sample	Specific Surface Area (m^2/g)	
	Current Work	Literature Values[a]
Fe_2O_3-Al_2O_3	396	245
Fe_2O_3-SiO_2	376	29
Fe_2O_3-TiO_2	20	104 [a,b]

[a] 262

[b] Calcinide at 500 °C for 6 hr in flowing O_2.

66

Clearly the sol-gel method resulted in materials of very high surface area. These methods results in materials of high surface area. The precursor used appeared to give strong support resulting in high surface area materials.

Specifically, the surface area of Fe_2O_3-Al_2O_3 obtained from aluminum tri-*iso*propoxide was always higher than that obtained from the *sec*-butoxide. In part, this could be attributed to the solvent used in each case. *Sec*-butyl alcohol has a critical temperature of 263 °C as compared to that of 235 °C for 2-propanol. Since in both cases the temperature of drying the gel was 250 °C, more complete removal of the solvent in the case of *iso*propoxide is expected (277).

2.3.3 Supported iron oxides

Three types of supported iron oxide were synthesized by the wet impregnation method. These are Fe_2O_3/Al_2O_3, Fe_2O_3/TiO_2 and Fe_2O_3/C. They were characterized by FT-IR, XRD and SA measurements.

2.3.3.1 FT-IR spectra

All oxides showed the characteristic broad band centered within the range 3431-3477 cm^{-1}, which, as mentioned previously can be assigned to the asymmetric and symmetric stretching modes of adsorbed water (275), Figure 2-5. The relative intensity of the bands indicates that high water content is retained in the dried oxides. The peak at 1630 cm^{-1} seen in all three spectra represents the OH bending mode of water. The very weak intensity peak at 2924 cm^{-1} in all three supported iron oxides spectra is assigned to ν C-H which indicates the presence of some organic residues adsorbed on the surface of the samples. The IR spectra and characteristic absorption frequencies for all three samples are summarized in Table 2-7.

Table 2-7: IR frequencies (cm^{-1}) of the supported iron oxides.

Fe$_2$O$_3$/Al$_2$O$_3$	Fe$_2$O$_3$/TiO$_2$	Fe$_2$O$_3$/C
3477	3432.6	3446.3
2924	2924	2924.81
1631.8	1630.3	1630.3
-	-	1095.4
749.11	-	-
603.4	-	-
-	522.8	469.2

In Fe$_2$O$_3$/Al$_2$O$_3$, the two very strong bands at 749.11 and 603.4 cm^{-1} are attributed to the aluminum-oxygen bond. In the spectrum of Fe$_2$O$_3$/TiO$_2$, one very intense broad band at 522.8 cm^{-1} is observed which can be attributed to the asymmetric stretching band of the Ti-O bond. The IR spectrum of the Fe$_2$O$_3$/C has sharp peaks at 1095 and 469.2 cm^{-1}.
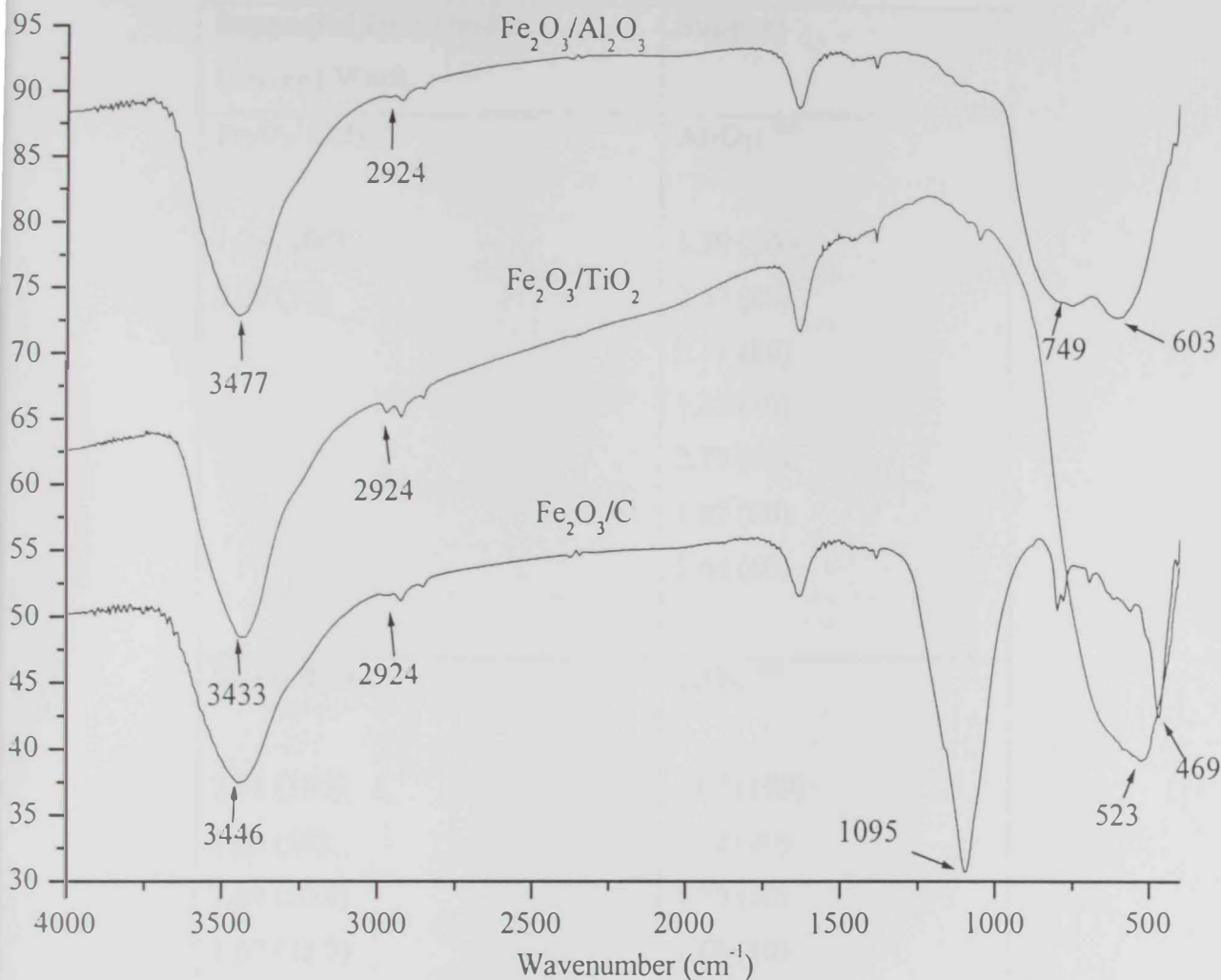
Figure 2-5: FT-IR spectra of the three types of supported iron oxides.

2.3.3.2 XRD measurements

To detect any chemical or structural changes in the materials under investigation, some selected samples were studied by powder XRD and matched with the relevant the *d*-plane spacing. The XRD lines of the mixed oxides are tabulated in Table 2-8.

Table 2-8: XRD lines of all supported iron oxides.

Supported Iron Oxides Current Work	Support
Fe$_2$O$_3$/Al$_2$O$_3$:	Al$_2$O$_3$: [a]
1.98 (100)	1.39 (100)
2.29 (30)	2.57 (80)
	2.11 (80)
	1.43 (80)
	2.79 (60)
	1.87 (60)
	1.64 (60)
Fe$_2$O$_3$/TiO$_2$:	TiO$_2$: [b]
3.51 (100)	2.07 (100)
1.89 (51)	3.32 (80)
1.69 (50.9)	1.70 (30)
1.67 (35.7)	1.66 (30)
3.24 (33.9)	1.88 (10)
2.38 (28.1)	
Fe$_2$O$_3$/C:	C:
3.35 (100)	
1.82 (22.7)	
2.52 (21.2)	
2.46 (15.4)	
4.28 (13.2)	
2.70 (12.4)	

(a) and (b): JCPDS-ICDD cards 4-877 and 8-117 respectively.

2.3.3.3 Surface area analysis

The surface areas of the pure supports and the supported iron oxides are tabulated in Tables 2-9 and 2-10 respectively. Comparisons with the previously published values are shown in Table 2-10. The materials used as supports have been found to have relatively high surface areas.

Table 2-9: Specific surface areas of pure supports.

Supports	Specific Surface Area (m^2/g)
Al_2O_3	128
TiO_2	50
Charcoal	483

Table 2-10: Specific surface area of supported iron oxides.

Supported Iron Oxides	Specific Surface Area (m^2/g) Current Work	Specific Surface area (m^2/g) Literature Values [a]
Fe_2O_3/Al_2O_3	121	213
Fe_2O_3/TiO_2	36	31
Fe_2O_3/C	40	-

[a] 278

From Table 2-10, it can be seen that all three supported iron oxides samples show relatively lower surface areas as compared with previously reported work. This could be due to the fact that commercial materials were used with an average surface area as including supports while previous works involved materials prepared by advanced chemical methods including sol-gel techniques (278). Interestingly, as previous stated, when sol-gel techniques were used to prepare the mixed oxides as discussed in the previous section, much higher specific surface area were obtained.

2.4 Conclusion

Pure iron oxides were prepared by classical methods and gave a slightly low surface area. Mixed iron oxides were prepared by the sol-gel method and yielded high surface area particles. The supported iron oxides were prepared by wet impregnation methods which also gave moderate high surface areas. All these oxides were characterized by FT-IR, XRD and BET. The surface area of hematite and magnetite in this work was greater than the literature values, but maghemite gave approximately the same surface area as that quoted in the literature. In the case of the mixed oxides, the specific surface area of Fe_2O_3-Al_2O_3 was found to be 396 m^2/g which is very high. The Fe_2O_3-SiO_2 system in this work yielded a very high surface area compared to the corresponding literature value, which probably can be attributed to the sol-gel method employed in this work. The supported oxides gave a moderate high surface area, because the support materials used had a low surface area.

CHAPTER 3

REACTIVITY STUDIES
OF CCl$_4$
DECOMPOSITION

CHAPTER 3: REACTIVITY STUDIES OF CCl₄ DECOMPOSITION.

3.1 Introduction

Chlorinated hydrocarbons are widely used chemicals in industry whose corresponding wastes may be classified as hazardous and toxic. The simplest subgroup of the chlorinated hydrocarbon family is composed of the chlorinated methanes, including chloromethane (CH_3Cl), dichloromethane (CH_2Cl_2), trichloromethane ($CHCl_3$) and carbon tetrachloride (CCl_4) (279). These chemicals are generally used as industrial solvents.

The toxicities of alkyl halides, *e.g.* carbon tetrachloride, CCl_4, varies to a great extent depending on the compound in question. Most of these compounds cause depression of the central nervous system, and individual compounds exhibit specific toxic effects (280).

Carbon tetrachloride was used for many years in the U.S.A as a consumer product. However, due to its toxicity, the U.S. Food and Drug Administration (FDA) decided to prohibit its household use in 1970. It is a systemic poison that affects the nervous system when inhaled, and the gastrointestinal tract, liver and kidneys when ingested. The biochemical mechanism involving carbon tetrachloride generates reactive radical species, including,

Unpaired electrons
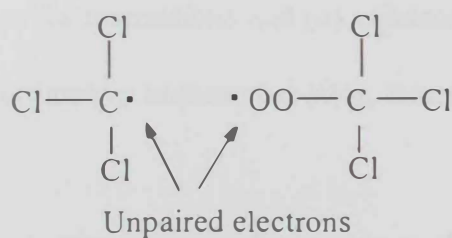
Figure 3-1: Reactive radical species of CCl_4.

which react with biomolecules, such as proteins and DNA. The most damaging of such reactions occurs in the liver as lipid peroxidation, which involves the attack of free radicals

on unsaturated lipid molecules, followed by oxidation of the lipids through a free radical mechanism (280).

As well as minimizing the widespread use of these compounds, it is of vital importance environmentally to establish the appropriate methods for the complete safe destruction of such species (281). The most common method to destroy chlorocarbons is by incineration (282,283). Other methods which are at various stages of development include catalytic decomposition (284-286), reverse burn gasification (287), plasma arc thermal decomposition (282) and the use of genetically engineered microbes (288). The difficulty associated with the incineration of these compounds (289) and their related toxic by-products makes it an inefficient method for disposal purposes. On the other hand, the presence of such compounds in air in low concentration makes it essential to develop new technologies to decompose and remove them from the air.

Adsorption on solid surfaces and heterogeneous catalysis have been amongst the most promising methods developed for the removal of chlorocarbons (290-295). There is a growing interest in the creation of high surface area materials (nanoscale materials), especially metal oxides, and in their applications such as their use as environmental catalysts (296-298). The uniqueness of these materials stems largely from two properties: (i) large exposed surface areas for interactions and (ii) enhanced surface reactivities due to their richness in reactive coordinative unsaturated sites, usually edges, corners and kinks (299).

The objective of this chapter is to develop a new method to decompose CCl_4 at a lower temperature than previously found, to choose the optimum catalyst and to study the effects of varying the temperature on the CCl_4 decomposition. Some suggested possible structural inferences will be explored based on the empirical results obtained via surface area measurements and FT-IR methods of characterization.

3.2 Experimental methods

3.2.1 Materials and reagents

Carbon tetrachloride (99.9%+ pure) was obtained from Aldrich and used as received. Catalysts were prepared according to the procedures described previously in chapter 2. Deionized distilled water was used in all reactions.

3.2.2 Characterization of reactions products

Gaseous products were studied by FT-IR spectroscopy using a self-constructed IR cell equipped with KBr windows and a finger trap to condense/collect gaseous products (Figure 3-2). Solid samples were studied by XRD before and after each reaction.
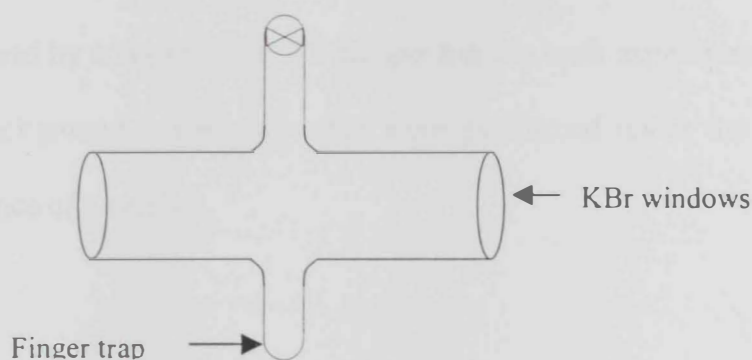
Figure 3-2: IR cell used for gaseous products.

3.2.3 Adsorption and decomposition of CCl₄

The adsorption and chemical degradation of CCl_4 was studied using a closed Schlenk tube reactor equipped with a vacuum line (Figure 3-3). In a typical experiment, for example hematite, a 5.20×10^{-3} mol (0.827 g of hematite) sample was placed in a Schlenk pyrex tube reactor and heated under dynamic vacuum (5.00×10^{-2} torr) to the process temperature at a rate of ≈ 10 deg/min. This was achieved using a cylindrical heater placed around the reactor and monitored by a temperature controller and a k-type thermocouple

75

placed in close proximity to the sample. The desired amounts of CCl_4 (0.10 mL, 9.74×10^{-4} mol) and water (0.10 mL, 5×10^{-3} mol) were then injected through a septum inlet positioned at the top of the reactor where the CCl_4 evaporated immediately in the tube reactor due to low pressure and high temperature. In all experiments, the molar ratio between the catalyst and CCl_4 was 1:5. The reaction was left for 2 hr where the process temperature stabilized to the order of $\pm 1\ ^\circ C$. The gaseous products were collected in a pre-evacuated IR cell. The line between the reactor and IR cell was also pre-evacuated. In all experiments, the pressure inside the IR cell was kept the same prior to transfer of the product. The gaseous products were collected by condensing in the finger trap of the IR cell using a liquid nitrogen bath. The FT-IR spectrum was then recorded for the gaseous products after warming the IR cell trap to room temperature. Quantitative measurements and comparisons were obtained by comparing the FT-IR spectrum in each experiment with those obtained from the background experiments that were performed under the same conditions without the presence of a catalyst.

Vacuum

IR cell

ection septum

Liquid N₂ trap

Furnace
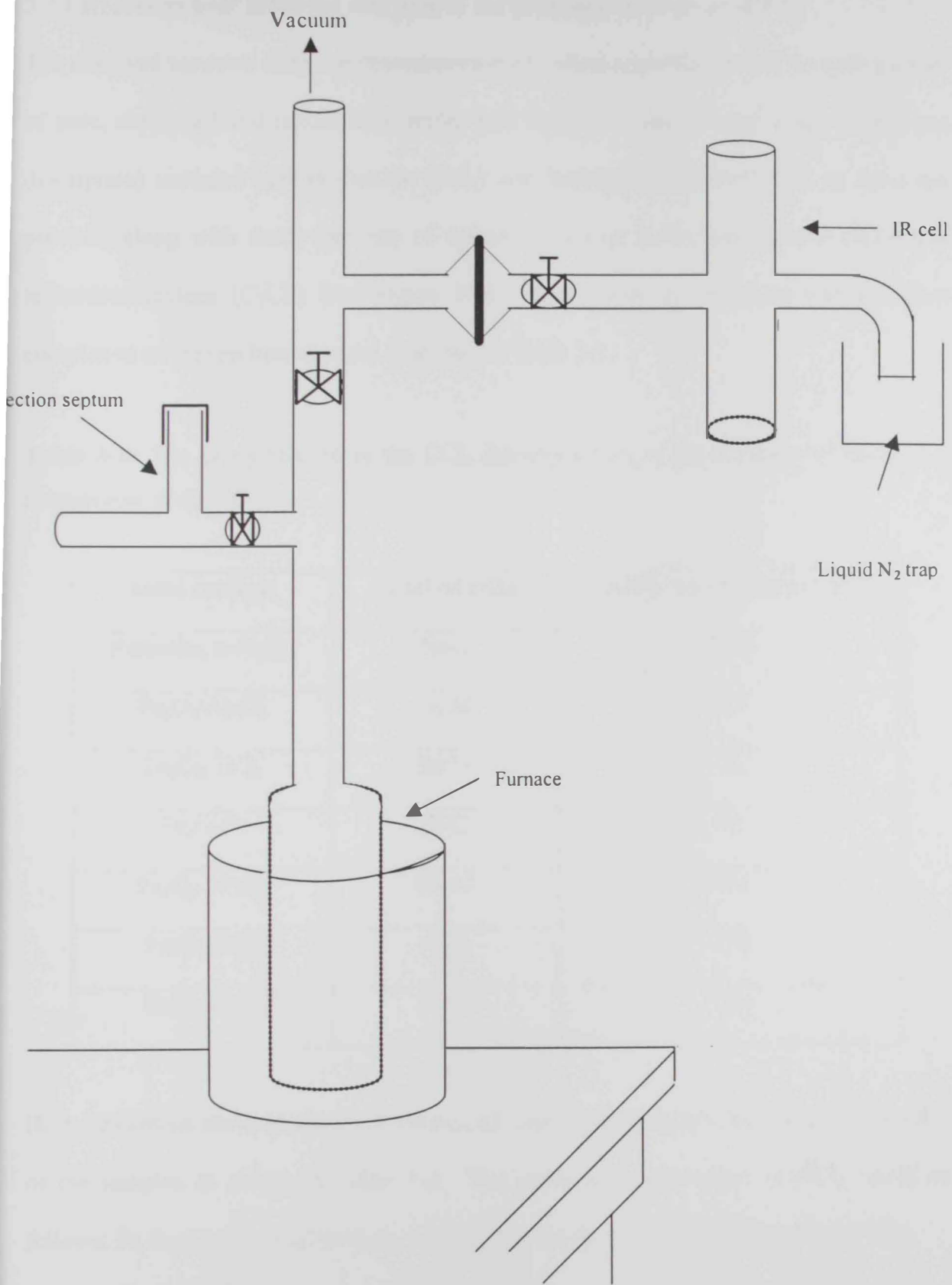
Figure 3-3: Closed reactor system.

3.3 Results

3.3.1 Reactions over different catalysts in the presence of water at 400 °C

The observed products from the decomposition of carbon tetrachloride (CCl_4) over a series of pure, supported and mixed iron oxides (see Table 3-1 and chapter 2 for a complete description) included carbon dioxide (CO_2) and hydrogen chloride (HCl) as the main products along with small amounts of carbon monoxide (CO), phosgene ($COCl_2$) and tetrachloroethylene (C_2Cl_4) (see Figure 3-4). The colour of the solid samples upon completion of the reaction changed as shown in Table 3-2.

Table 3-1: The catalysts used in the CCl_4 decomposition in the presence of water at a temperature of 400 °C.

Solid catalyst	Catalyst code	Specific surface area (m^2/g)
Hematite, α-Fe_2O_3	Hem	51.8
Fe_2O_3/Al_2O_3	Fe/Al	121
Fe_2O_3/TiO_2	Fe/Ti	36
Fe_2O_3/C	Fe/C	40
Fe_2O_3-Al_2O_3	Fe-Al	396
Fe_2O_3-SiO_2	Fe-Si	376
Fe_2O_3-TiO_2	Fe-Ti	20

High percentage decomposition/conversion of carbon tetrachloride was obtained by most of the samples as shown in Table 3-2. The percentage conversion of CCl_4 varied as follows: Fe_2O_3-Al_2O_3 > Fe_2O_3/Al_2O_3 > α-Fe_2O_3 > Fe_2O_3/C > Fe_2O_3-SiO_2 > Fe_2O_3-TiO_2.

As shown in Figures 3-4 and 3-5 respectively, carbon dioxide (CO_2) and hydrogen chloride (HCl) were the major products from this degradation process over all the solid catalysts suggesting almost complete oxidation of CCl_4. Carbon monoxide (CO) was observed with some catalysts in the following order: $Fe_2O_3/C > Fe_2O_3\text{-}SiO_2 > Fe_2O_3/TiO_2 > \alpha\text{-}Fe_2O_3 > Fe_2O_3\text{-}TiO_2$. Phosgene ($COCl_2$) was also observed and its amount varied in the order: $Fe_2O_3/C > Fe_2O_3\text{-}SiO_2 > Fe_2O_3/TiO_2 \approx Fe_2O_3\text{-}TiO_2$. A small amount of tetrachloroethylene (C_2Cl_4) were also observed in all reactions except in the cases of $Fe_2O_3\text{-}Al_2O_3$ and Fe_2O_3/C.

Table 3-2: Percent conversion of CCl_4 and percent weight loss during the reactions in the solid samples.

Solid catalyst	% CCl_4 decomposition	% weight loss during reaction
Hematite, $\alpha\text{-}Fe_2O_3$	96.32	18.72
Fe_2O_3/Al_2O_3	97.55	23.67
Fe_2O_3/TiO_2	25.92	21.87
Fe_2O_3/C	94.54	40.95
$Fe_2O_3\text{-}Al_2O_3$	98.27	22.87
$Fe_2O_3\text{-}SiO_2$	89.17	33.48
$Fe_2O_3\text{-}TiO_2$	73.95	43.99
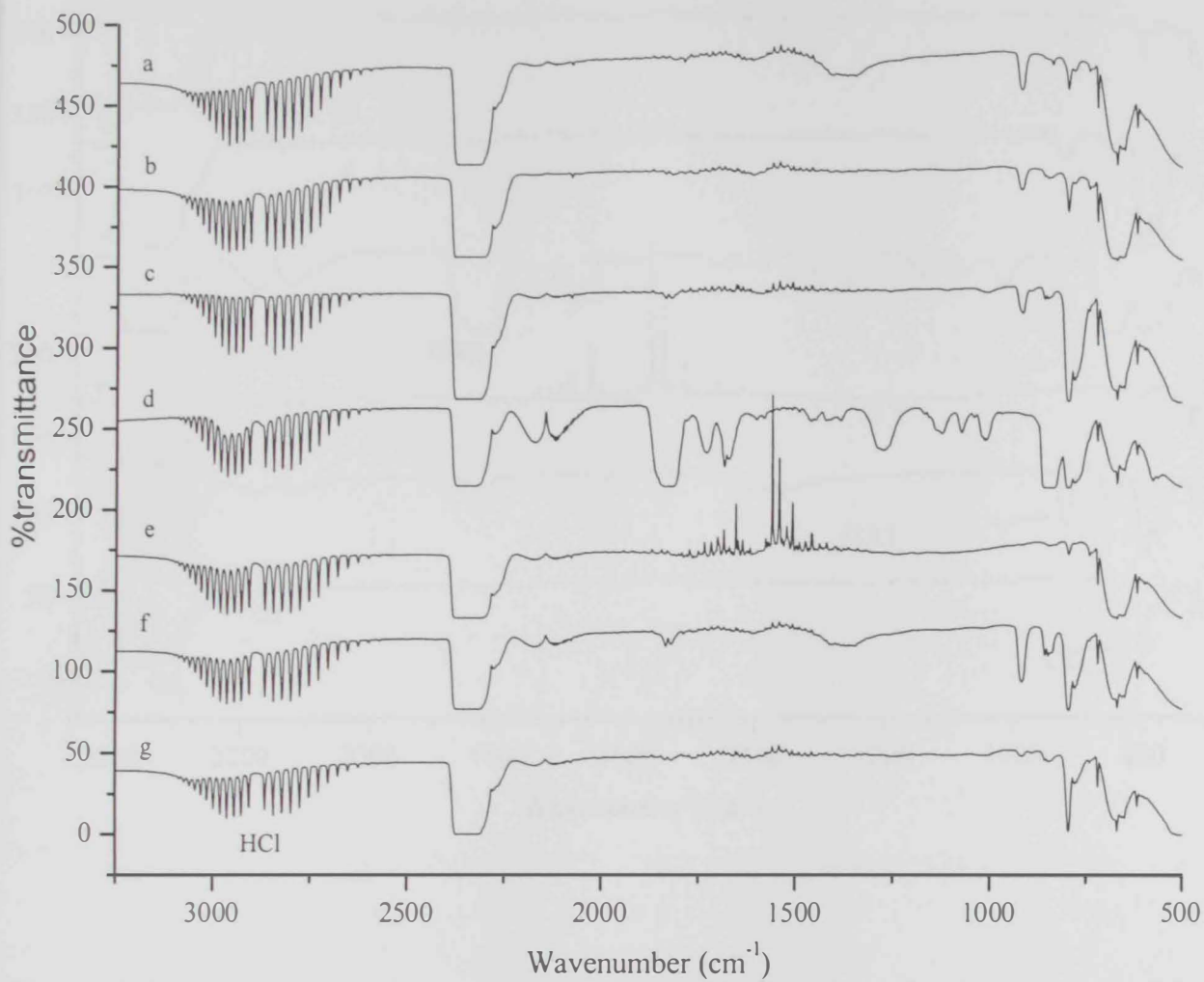
Figure 3-4: FT-IR spectra of the gaseous products obtained from the decomposition of CCl$_4$ by (a) α-Fe$_2$O$_3$, (b) Fe$_2$O$_3$/Al$_2$O$_3$, (c) Fe$_2$O$_3$/TiO$_2$, (d) Fe$_2$O$_3$/C, (e) Fe$_2$O$_3$-Al$_2$O$_3$, (f) Fe$_2$O$_3$-SiO$_2$, (g) Fe$_2$O$_3$-TiO$_2$.
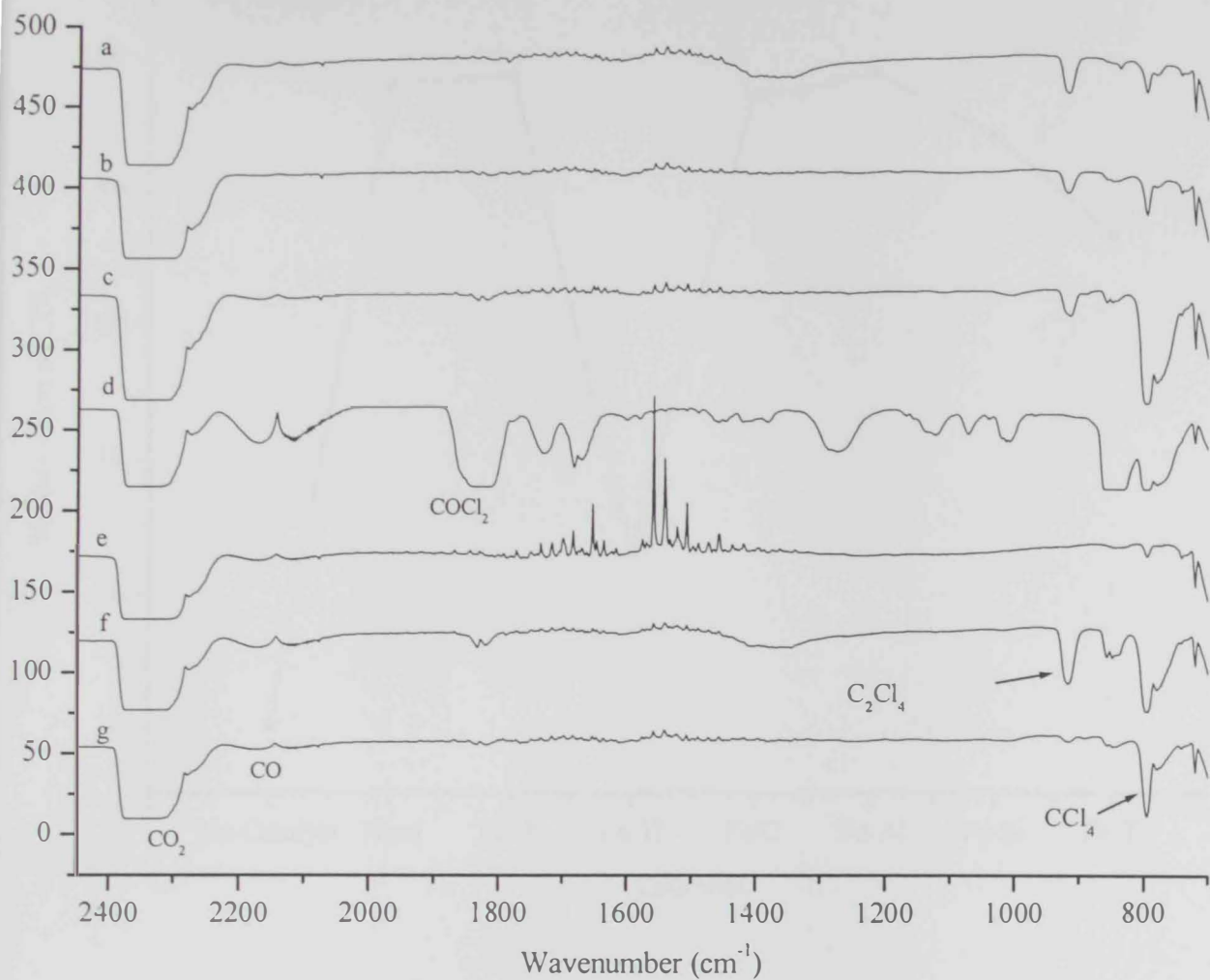
Figure 3-5: FT-IR spectra of the gaseous products obtained from the decomposition of CCl_4 by (a) α-Fe_2O_3, (b) Fe_2O_3/Al_2O_3, (c) Fe_2O_3/TiO_2, (d) Fe_2O_3/C, (e) Fe_2O_3-Al_2O_3, (f) Fe_2O_3-SiO_2, (g) Fe_2O_3-TiO_2 in more precise detail.

As shown in Figure 3-6, the best catalysts used in this process were Fe_2O_3-Al_2O_3 with a 98.27% conversion, Fe_2O_3/Al_2O_3 with a 97.55% conversion and pure α-Fe_2O_3 with a 96.32% conversion. Besides the high percent conversions, these catalysts showed no trace of $COCl_2$ or CO as seen in Figure 3-5.
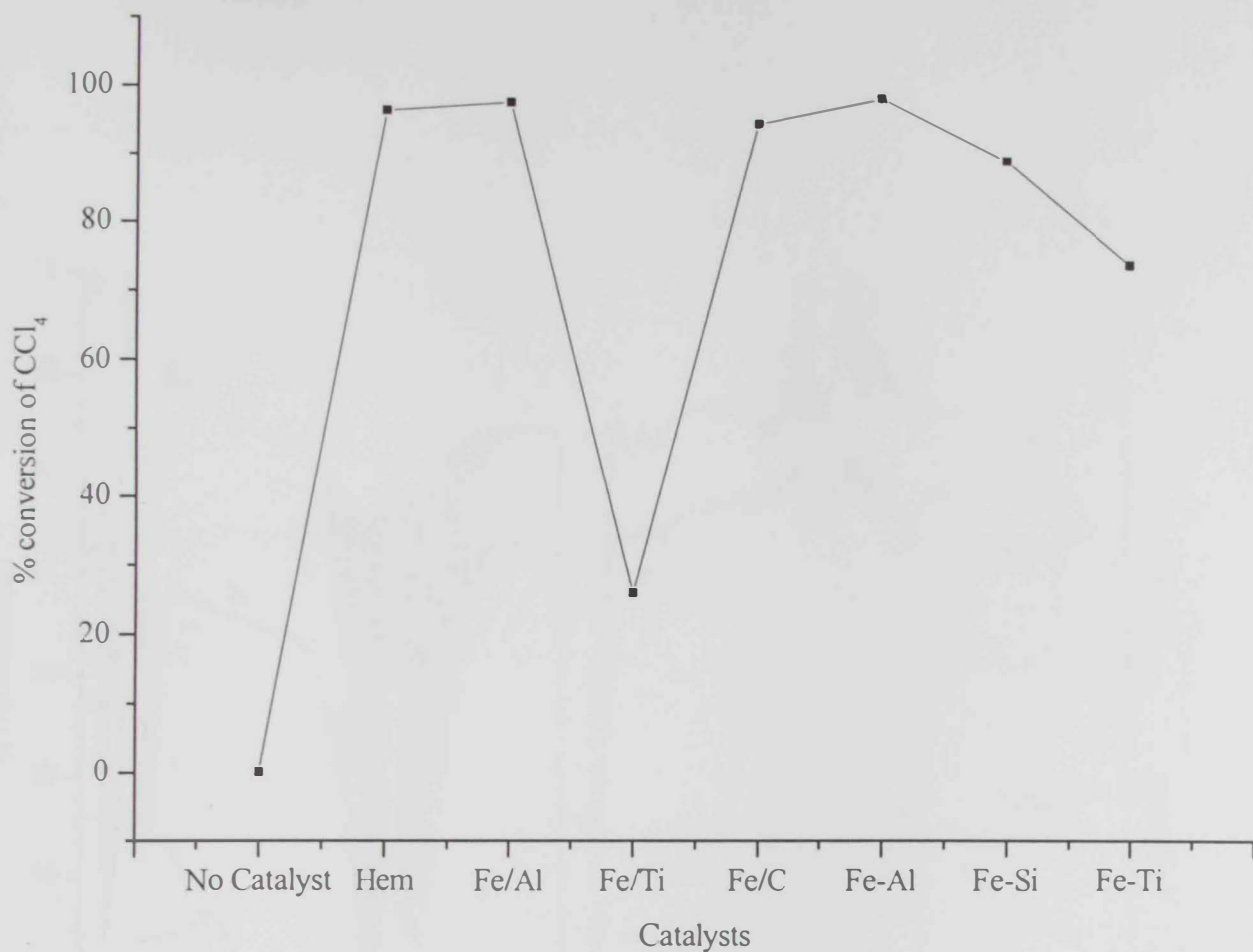
Figure 3-6: Percent decomposition of CCl_4 over the different catalysts in the presence of water at 400 °C.

To investigate the effect of water, the adsorption/decomposition of CCl_4 by Fe_2O_3-Al_2O_3 was then studied in the absence of water at 400 °C, Figure 3-7.

As shown in Figure 3-7, it is clear that the presence of water resulted in almost the complete decomposition of CCl_4 to CO_2 and HCl, while in the absence of water some $COCl_2$ and C_2Cl_4 formed.
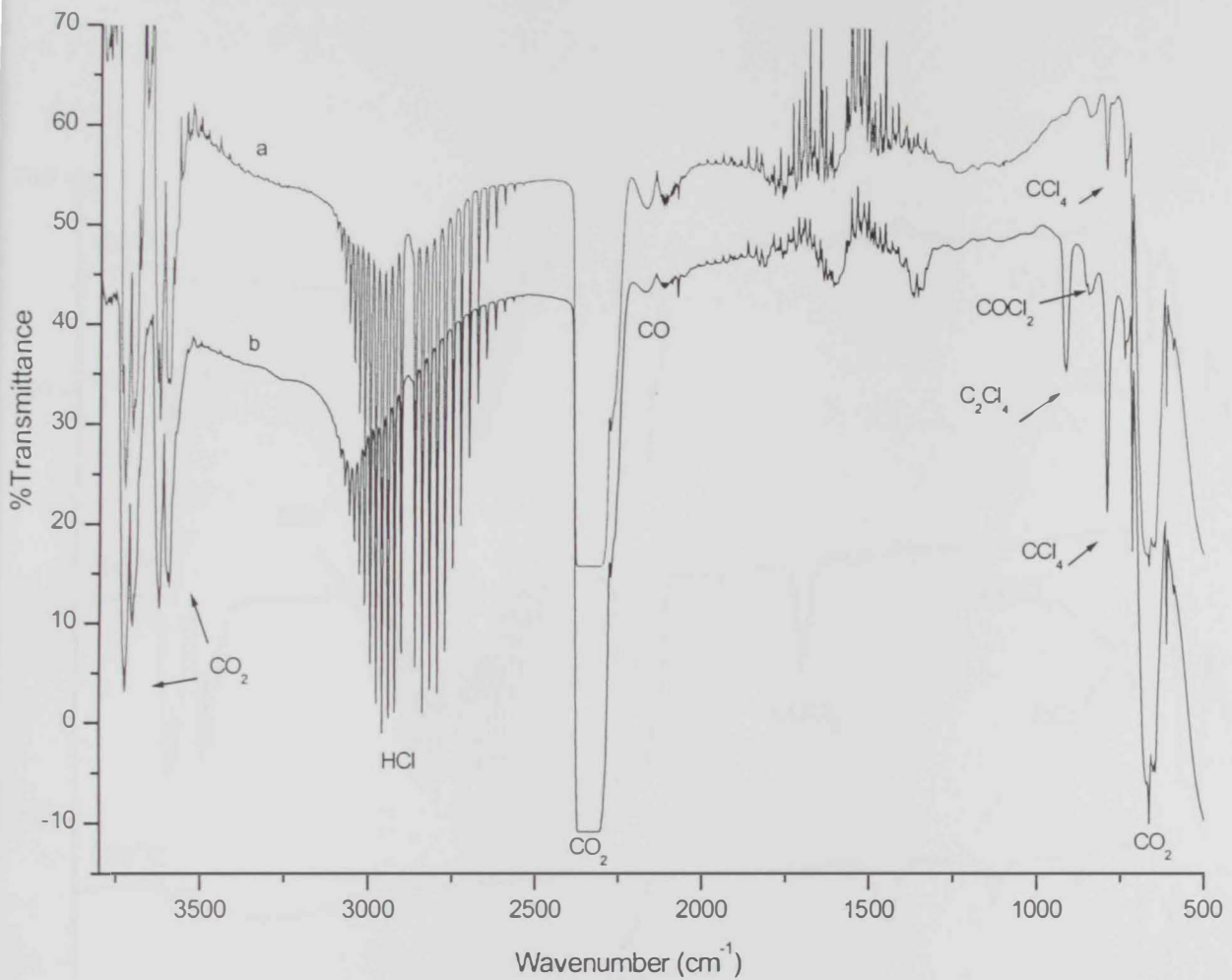
Figure 3-7: FT-IR spectra for the products of CCl_4 decomposition on the Fe_2O_3-Al_2O_3 in (a) the presence and (b) in the absence of water at 400 °C.

3.3.2 Temperature-dependent study on Fe_2O_3/Al_2O_3

To investigate the effect of the temperature, the decomposition of carbon tetrachloride by Fe_2O_3/Al_2O_3 was studied at different temperatures (400, 200 and 100 ^oC) in the presence of water.
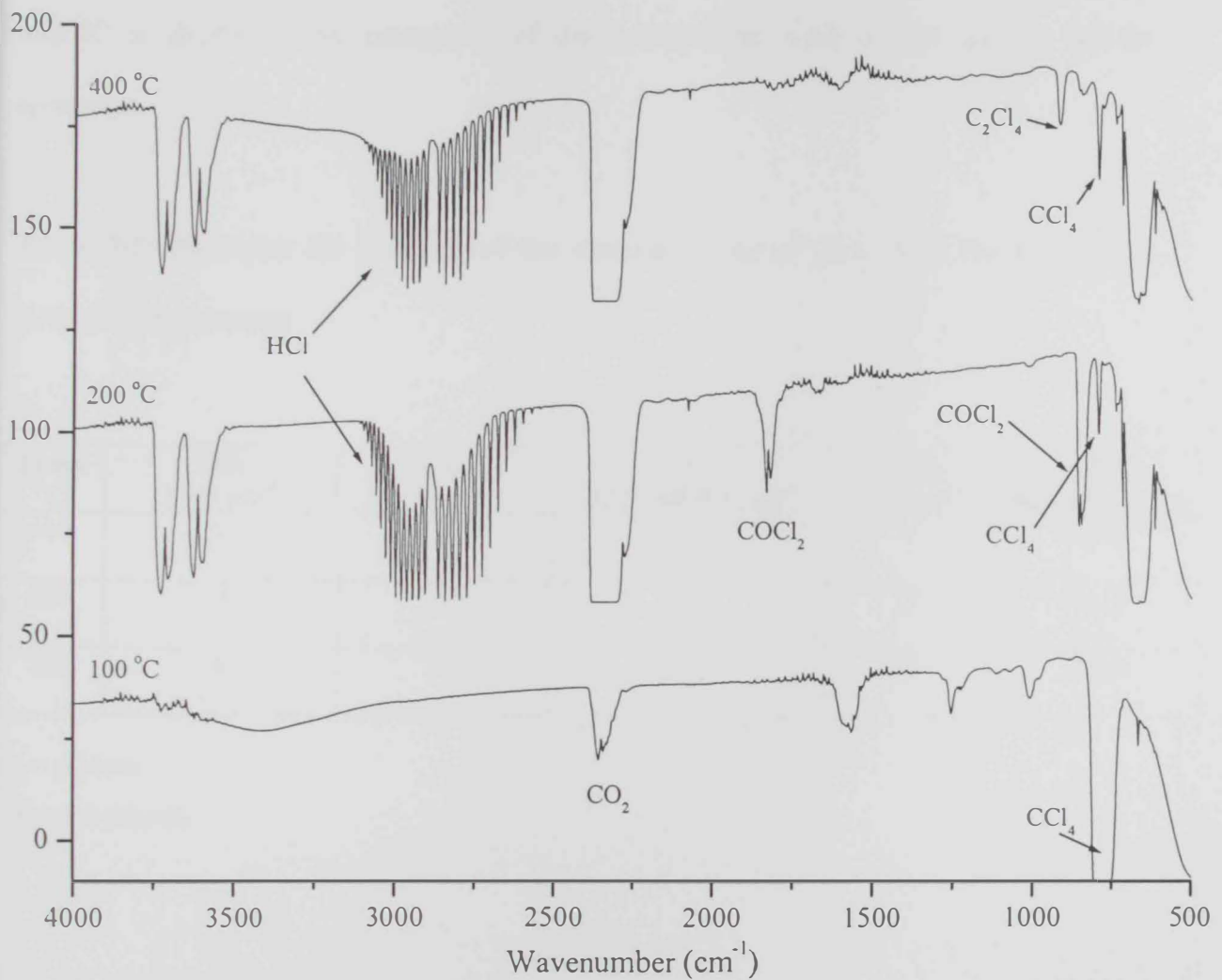
Figure 3-8: FT-IR spectra for the products of the decomposition of CCl_4 over Fe_2O_3/Al_2O_3 at different temperatures in the presence of water.

As shown in Figure 3-8 and Table 3-3, at 100 °C the observed reaction was essentially negligible with only a small amount of CO_2 produced and no evidence of HCl. The reaction initialized at 200 °C where, at this temperature, conversion involving 95.50% CCl_4 decomposition was obtained. At this temperature, $COCl_2$ formed in considerable amounts, while at 400 °C no trace of $COCl_2$ was found and 97.52% CCl_4 decomposition occurred. In addition, C_2Cl_4 was seen not to form at low temperatures and formed only at 400 °C as shown by the emergence of the low-intensity peak at 916 cm^{-1} in the IR spectrum.

Table 3-3: Illustrates the products of the decomposition of CCl_4 over Fe_2O_3/Al_2O_3 at different temperatures.

Temp °C	CO_2 2345 cm^{-1}	CO 2143 cm^{-1}	$COCl_2$ 1816 and 850 cm^{-1}	C_2Cl_4 916 cm^{-1}	%CCl_4 decomposition
400	√	X	X	√	97.52
200	√	X	√	X	95.50
100	√	X	X	X	4.43

√ = present

X = not present

3.3.3 Catalytic decomposition of CCl_4 over different pure iron oxides in the presence of water at 200 °C

The decomposition of carbon tetrachloride was studied over different iron oxides at a temperature of 200 °C. As mentioned in chapter 2, magnetite (Fe_3O_4) converts to maghemite (γ-Fe_2O_3) at 250 °C. For this reason, the reactions were carried out at a temperature less than 250 °C. The aim of this study was to investigate the reactivity of

different pure iron oxides, to compare and contrast them and to study the relationship between the structure and the reactivity of the solid catalysts for the decomposition of CCl_4.

The FT-IR spectra for this study are represented in Figure 3-9. The major product from these reactions was CO_2. The IR spectra of the products obtained from hematite and maghemite were similar. There is a strong and broad band for water centered at 3400 cm^{-1} corresponding to the v_{sym} and v_{asym} bands. The corresponding HOH bend is seen at ≈ 1640 cm^{-1}. It is clear that 200 ^{o}C is too low a temperature to achieve complete conversion of the CCl_4. The percentage of CCl_4 decomposed over hematite and maghemite is 21.34 and 49.22% respectively (see Table 3-4). In the case of magnetite, in addition to seeing evidence for the generation of CO_2 and CO in the spectrum, $COCl_2$ and C_2Cl_4 were also found to be produced as shown by the appearance of peaks at 850 and 916 cm^{-1} respectively. Some HCl was also observed. The percent decomposition of CCl_4 was found to be 35.14%.
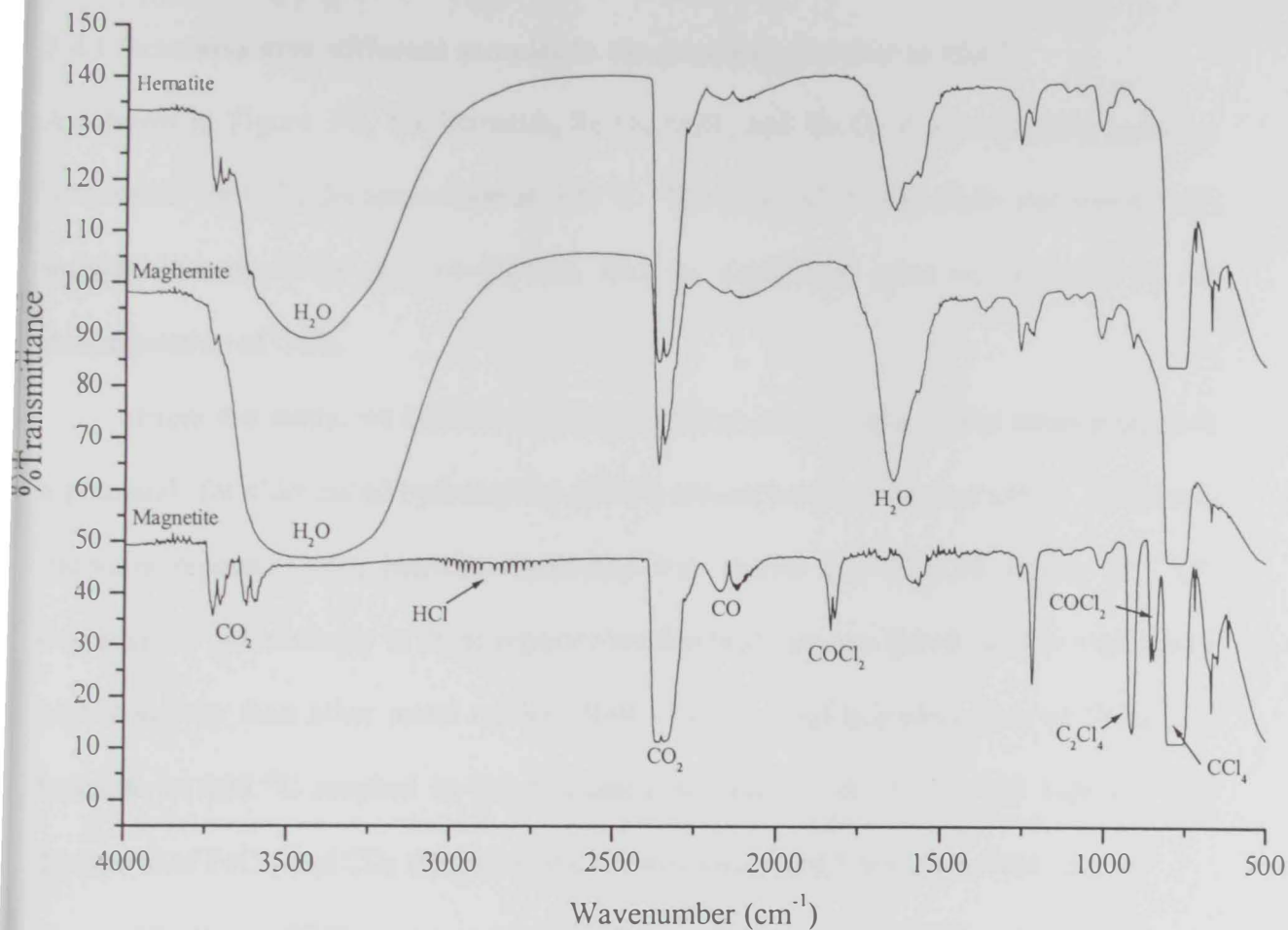
Figure 3-9: FT-IR spectra for the products of the decomposition of CCl₄ over pure iron oxide in the presence of water at 200 °C.

Table 3-4: Adsorption/Decomposition of CCl₄ in the presence of water at 200 °C.

Solid catalyst	% CCl₄ decomposition	% Weight loss
Hematite, α-Fe₂O₃	21.34	7.70
Maghemite, γ-Fe₂O₃	49.22	3.10
Magnetite, Fe₃O₄	35.14	0.45
Fe₂O₃/Al₂O₃	95.48	11.48
Fe₂O₃/C	78.67	17.55

3.4 Discussion

3.4.1 Reactions over different samples in the presence of water at 400 °C

As shown in Figure 3-6, the hematite, Fe_2O_3/Al_2O_3 and $Fe_2O_3-Al_2O_3$ catalysts gave the best results for CCl_4 decomposition at 400 °C. The Fe_2O_3/C, $Fe_2O_3-Si_2O_3$ and $Fe_2O_3-TiO_2$ showed low reactivity and Fe_2O_3/TiO_2 had no significant catalytic potential in the decomposition of CCl_4.

From this study, we believe that iron oxides on a high surface area oxide support is a potential for chlorinated hydrocarbon (CHC) adsorption and decomposition. In several literature reports, (300), hematite (α-Fe_2O_3) was chosen for detailed studies of CHC degradation. Interestingly in those reported studies hematite was found to have a relatively higher activity than other metal oxides (300). The thermal decomposition of CCl_4 over hematite at 400 °C resulted in the formation of $FeCl_3$, CO_2, C_2Cl_4 and $COCl_2$. The formation of $FeCl_3$ and CO_2 represents the thermodynamically favorable reaction:

$$2Fe_2O_{3(s)} + 3CCl_{4(g)} \longrightarrow 4FeCl_{3(s)} + 3CO_{2(g)} \qquad \Delta H = -125.92 \text{ kJ}$$

From the temperature-dependence study, it is clear that $COCl_2$ forms at 200 °C, 300 °C while it disappears at 400 °C. This may indicate that $COCl_2$ is an intermediate product. When the CCl_4 adsorbs on the α-Fe_2O_3 surface, it most likely undergoes dissociative chemisorption to form carbine, CCl_2, a species which then extracts an O^{2-} ion leading to the formation of $COCl_2$ as shown in Figure 3-10 (300). The $COCl_2$ intermediate can further react with the oxide surface to give CO_2 and chloride ions (229). The formation of C_2Cl_4 is a competing side reaction that occurs when two carbine species bond to each other. Since the presence of water results in less $COCl_2$, we believe that water serves as an oxidant, resulting in the incomplete oxidation to CO_2 and enhances the formation of HCl as a result of increased surface OH^- species. As a result, the presence of water is believed to result in incomplete oxidation and regeneration of the oxide catalyst.
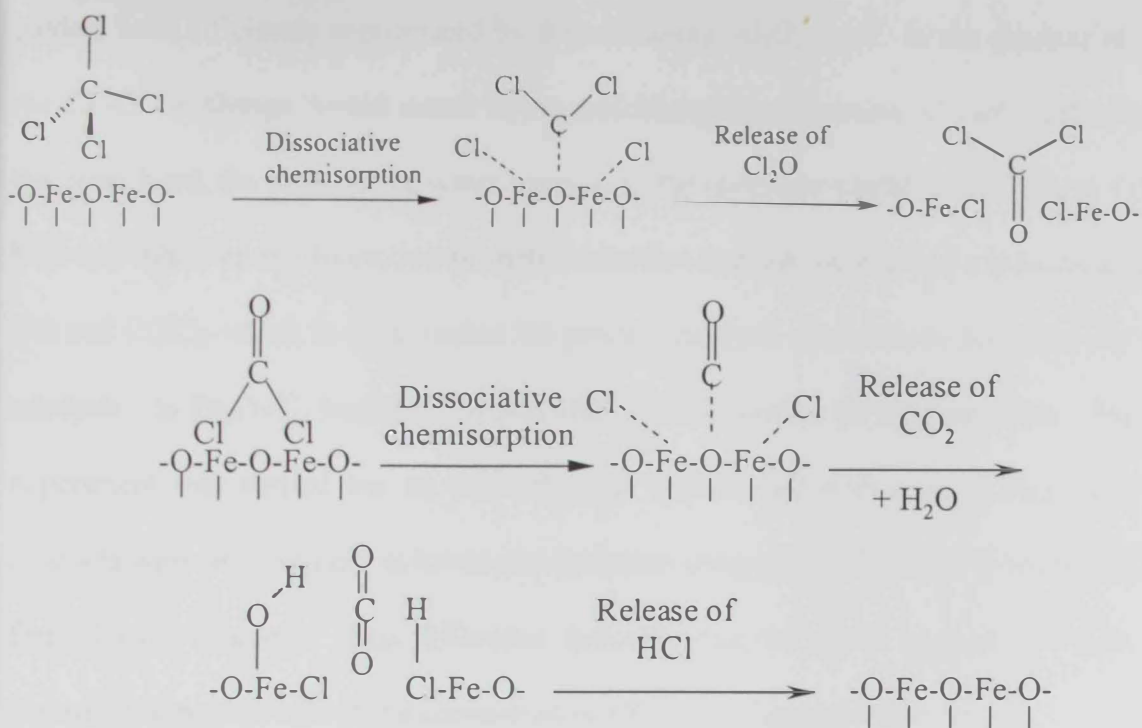
Figure 3-10: Proposed mechanism for the decomposition of CCl_4 over α-Fe_2O_3 (299).

In the case of supported and mixed oxides, with the exception of Fe_2O_3/TiO_2, the percentages of CCl_4 decomposition were very high (see Table 3-2). In Fe_2O_3/Al_2O_3, it seems that the presence of the iron oxide dispersed on alumina catalytically enhanced what can be described as an ion-ion exchange deep into the Al_2O_3 particles resulting in the formation of $AlCl_3$. These results have been interpreted in terms of a series of reaction steps that are all thermodynamically favored, as shown in Figure 3-11. $FeCl_3$ forms first, followed by $FeCl_3/Al_2O_3$ undergoing O^{2-}-Cl^- exchange to give $Fe_2O_3/AlCl_3$. Further adsorption of CCl_4 causes $FeCl_3$ to reform, and this mobile $FeCl_3$ seeks out more Al_2O_3, perhaps at fissures or edges/corners of the Al_2O_3 nanoparticles. Repetition of these steps leads to complete consumption of the Al_2O_3 to form $AlCl_3$ in the absence of water, such that this solid gas reaction becomes stoichiometric. This is a true catalytic effect of Fe_2O_3 since it has been shown that even after the extensive CCl_4 reaction, Fe_2O_3 was present,

having been efficiently regenerated by the remaining Al_2O_3 core. In the absence of water, the Cl^--O^{2-} exchange would result in the stoichiometric formation of metal chloride. On the other hand, the presence of water resulted in the complete oxidation of CCl_4 to CO_2 and HCl and inhibited the formation of metal chlorides and the incomplete oxidation products, CO and $COCl_2$ which in turns makes the process catalytic and extends the reactivity of the catalysts. In Fe_2O_3/C, besides CO_2 and HCl, $COCl_2$ formed in large amounts. The same experiment was carried out on pure charcoal (not coated with iron oxide). The same products were observed but at lower concentration compared to Fe_2O_3/C besides C_2Cl_4 that formed over charcoal. This difference indicates that the small amount of Fe_2O_3 (4%) played an important role in the conversion of CCl_4 (see Figure 3-12).

$$3CCl_4 + 2Fe_2O_3 \longrightarrow 4FeCl_3 + 3CO_2$$
$$\Delta H^o = -304 \text{ kJ}$$

$$2FeCl_3 + Al_2O_3 \longrightarrow Fe_2O_3 + 2AlCl_3$$
$$\Delta H^o = -189 \text{ kJ}$$
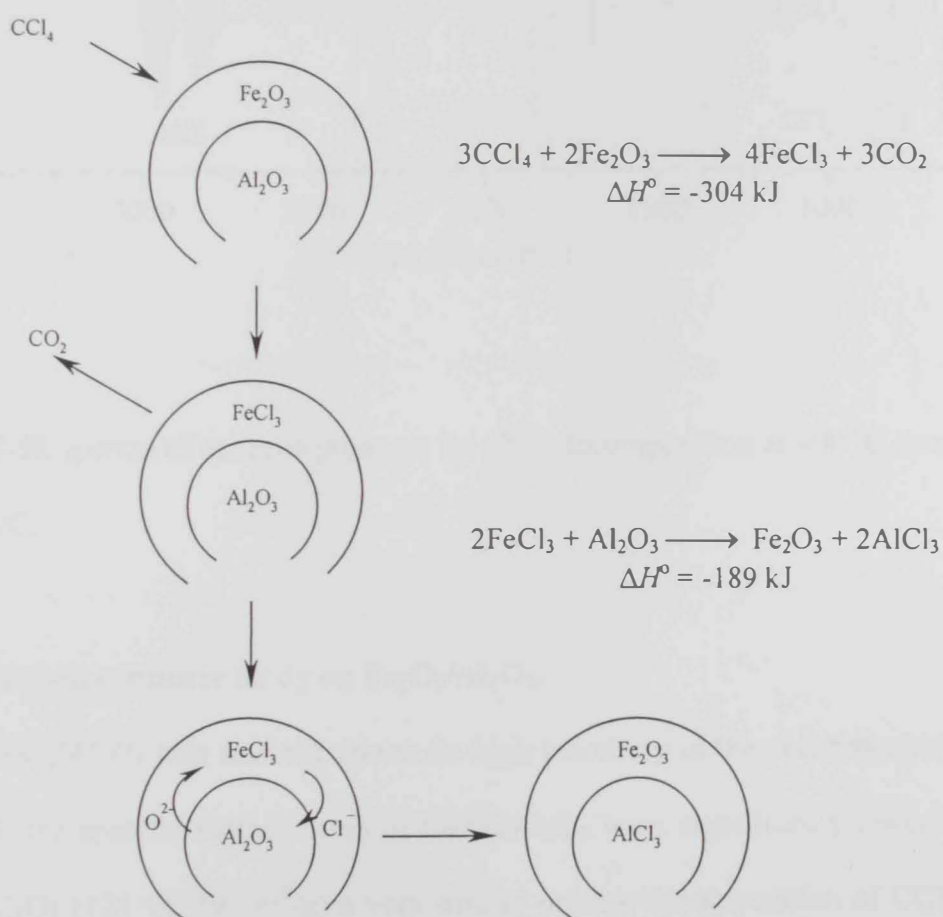
Figure 3-11: Reaction steps of Fe_2O_3/Al_2O_3 with gaseous CCl_4 in the absence of water.
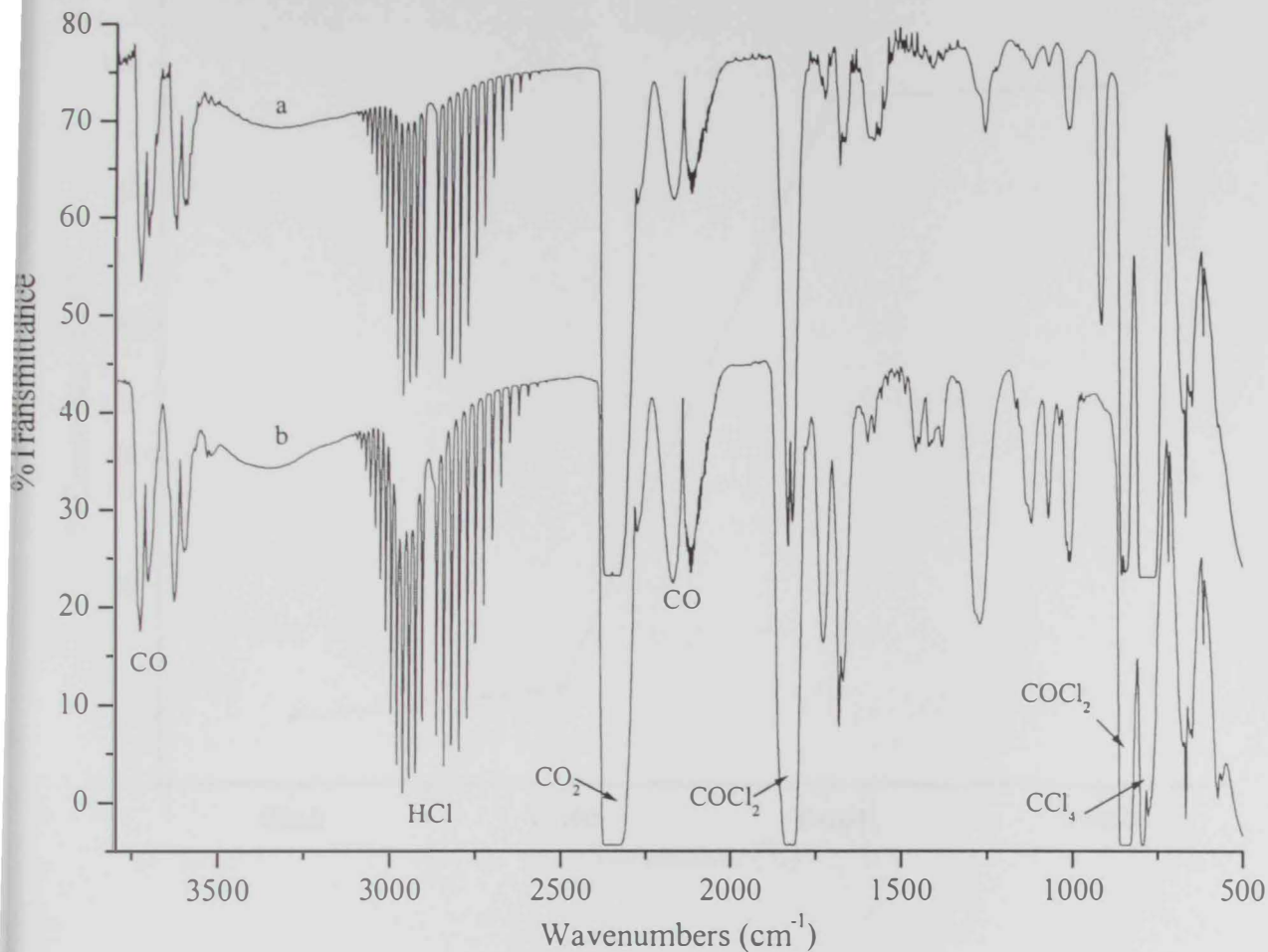
Figure 3-12: FT-IR spectra of gaseous products for CCl$_4$ decomposition at 400 °C over (a) C and (b) Fe$_2$O$_3$/C.

3.4.2 Temperature-dependence study on Fe$_2$O$_3$/Al$_2$O$_3$.

In this study, Fe$_2$O$_3$/Al$_2$O$_3$ was selected due to its high reactivity in the decomposition of CCl$_4$. Although the specific surface areas of Fe$_2$O$_3$/Al$_2$O$_3$ were significantly lower than that of Fe$_2$O$_3$-Al$_2$O$_3$ (121 vs. 396 m^2/g) a very similar percent decomposition of CCl$_4$ by Fe$_2$O$_3$/Al$_2$O$_3$ and Fe$_2$O$_3$-Al$_2$O$_3$ was found at 97.55 and 98.27% respectively.
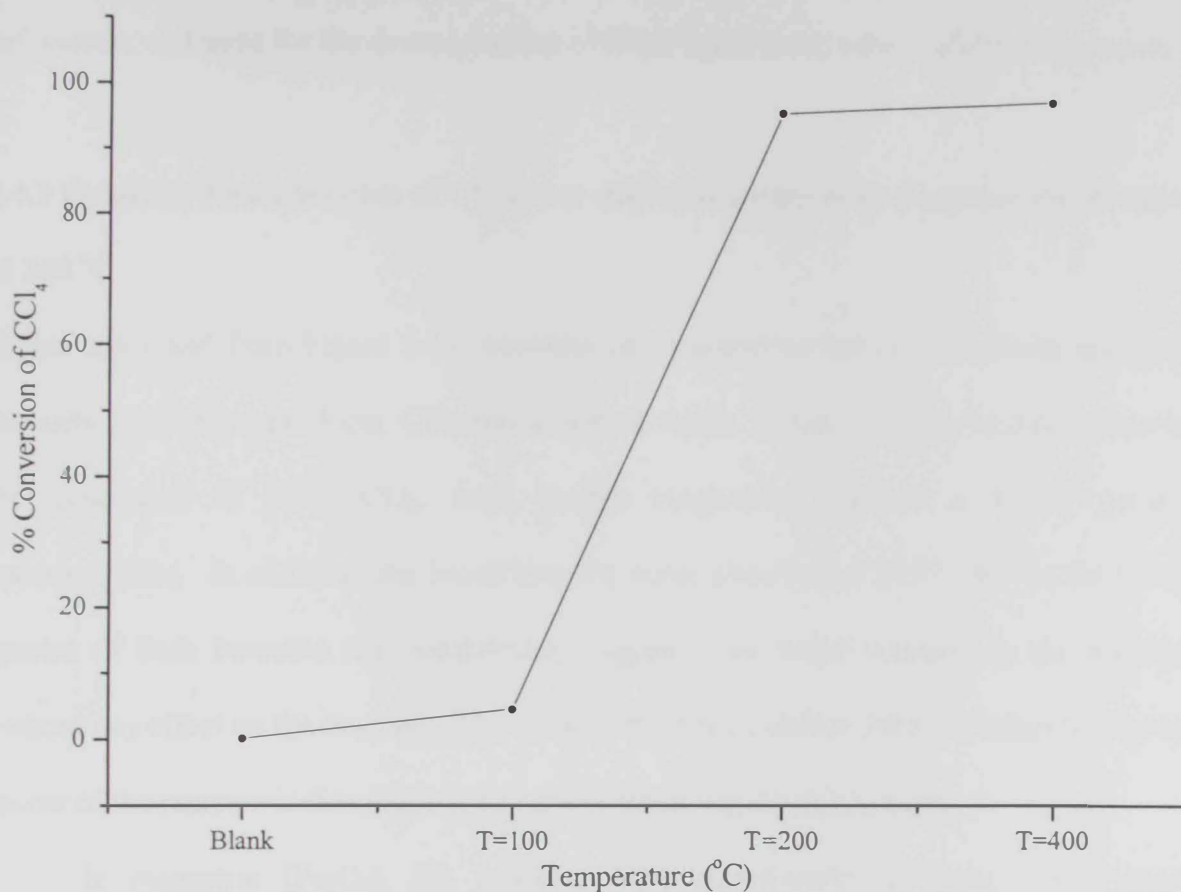
Figure 3-13: Shows the relation between the temperature and the percent CCl_4 decomposed for the Fe_2O_3/Al_2O_3 system.

As shown in Figure 3-13, the Fe_2O_3/Al_2O_3 catalyst showed high reactivity towards CCl_4 at a temperature higher than 200 °C. According to the literature, CCl_4 begins to decompose thermally between 452-552 °C (activation energy = 130 kJ mol^{-1}) (403). However, in this experiment, it was found that CCl_4 starts to decompose at 200 °C in the presence of the catalytic supported oxide, Fe_2O_3/Al_2O_3. These new results indicate clear evidence for the potential to employ such a catalytic system for the low temperature oxidation/decomposition of CCl_4 and other CHC's. This suggests that this new method is a

much easier and simpler method, which could be adopted in industry at a later stage with refinement, and used for the decomposition of CHC's and many other volatile compounds.

3.4.3 Catalytic decomposition of CCl_4 over different catalysts in the presence of water at 200 °C

In this study and from Figure 3-14, hematite and maghemite behaved similarly and gave the same qualitative products, CO_2 and adsorbed water. Quantitatively, hematite showed the generation of more CO_2, even though maghemite showed a higher percent decomposition. In addition, the broad band of water observed at 3447 cm^{-1} in the FT-IR spectra of both hematite and maghemite, suggests that water remains in the medium without any effect on the reaction. The color of the solid catalyst did not change during the course of the reaction indicating that no carbon formed in these reactions.

In magnetite (Fe_3O_4), the products were significantly different. The major observed products were CO_2, $COCl_2$, C_2Cl_4 and small traces of CO and HCl. This different behavior may indicate a different mechanism of the reaction due to different structures.

It is evident from the FT-IR spectra requested in Figure 3-14, magnetite exhibited a good reactivity toward CCl_4 which can be compared to the behavior of mixed oxide catalysts at higher temperature (400 °C). This behavior could be attributed to the rich content in oxygen ions (Fe_3O_4) compared to hematite and maghemite. The presence of large absorption bands for gaseous water in the case of hematite and maghemite indicate that they do not adsorb much water to allow for the reaction with CCl_4. In contrast, the absence of water bands in the case of magnetite indicates that it adsorbs well on magnetite allowing for some reaction with CCl_4, which is supported by the formation of products

93

such as CO_2, C_2Cl_4, $COCl_2$ and HCl. The fact that the reactivity was still low even when water adsorbs may indicate that water only physical adsorbs on the surface of magnetite.
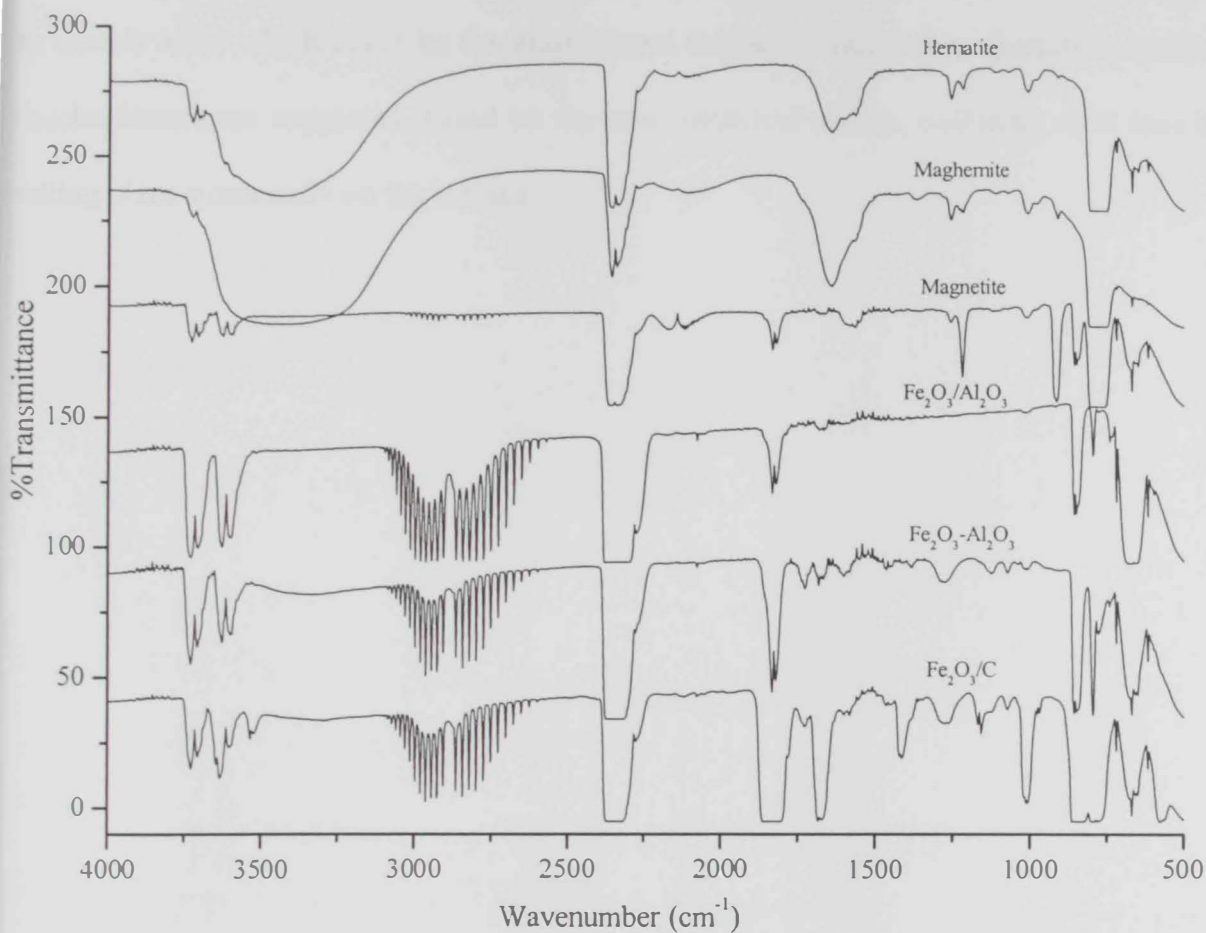
Figure 3-14: FT-IR spectra for the products formed during the decomposition of CCl_4 over solid catalysts in the presence of water at 200 °C.

3.5 Conclusion

In this chapter, a new simpler and easier technique was developed for the decomposition of carbon tetrachloride, using iron oxides, by using a closed reactor system. The optimum catalyst was found to be Fe_2O_3/Al_2O_3 with a high surface area. Small amouns of CCl_4 decomposed at 100 °C which then increased as the temperature increased progressively

with a concomitant decrease in the amount of $COCl_2$. In this work, binary systems have generally shown higher reactivity, especially the Fe_2O_3/Al_2O_3 system than pure iron oxides. Among the pure iron oxides magnetite showed the highest reactivity and an ability to adsorb water which could be the main reason behind its reactivity. Tentative reaction mechanisms were suggested, based on the new empirical results, outlining what may be taking place structurally on the surface.

CHAPTER 4

STRUCTURE-REACTIVITY CORRELATIONS

CHAPTER 4: STRUCTURE-REACTIVITY CORRELATIONS

4.1 Introduction

The purpose of this chapter is to examine firstly some of the characteristics of metal oxides in general, including both main-group and transition metal oxides. The second section of this chapter then looks at structural models, only recently reported (2002) in the literature, specifically in relation to iron oxides and the role of carbon tetrachloride on the surface, which has been the example chosen for this work. These new models are examined in relation to structure-reactivity correlations, based on advanced structural techniques, such as temperature programmed reaction/desorption (TPR/D) studies, Auger electron spectroscopic (AES) measurements *etc.*, facilities which were not accessible in the scope of this project at UAE University. The new empirical results of the experiments carried out in this thesis (for the decomposition of CCl_4 on iron oxides) are then compared with these models to determine if any fit (if at all) is possible based on these models.

Solid acid catalysts have been used for many years in petroleum chemistry and organic syntheses. More recently, several types of solid bases have been discovered and used in heterogeneous catalysis (301,302). Oxides occupy an important place among catalysts, due to the wide range of their structural and electronic properties. This is true for simple oxides such as Al_2O_3, TiO_2, ZrO_2, V_2O_5 or MoO_3 respectively, or more complex oxides such as natural clay minerals, bentonite, heter-poly-anions and zeolites, and mixed oxides such as SiO_2-Al_2O_3, TiO_2-MoO_3, *etc.*

One of the basic questions underlying many studies in the acid-base context is: 'which are the specific properties of the reactants which determine the strength of an acid-base reaction?'. As far as oxides are concerned, depending upon the field of research, various physical parameters have been proposed: the electronegativity of the cation; the ionic radius of the cation and the formal charge; the oxygen partial charge; and the surface

site coordination. The link with the surface acidity relies, in most cases, upon either very qualitative or empirical models (303).

4.2 Acid base properties

4.2.1 Cationic formal charge and ionic radius

In his compilation of the oxide isoelectric points, Parks (304) showed a correlation between the IEPS value and the characteristics of the cation: its formal ionic charge Q_M and its ionic radius r_M. As a function of Q_M, Parks was able to classify oxides according to decreasing IEPS:

M_2O	$Q_M = +1$	$11.5 <$ IEPS
MO	$Q_M = +2$	$8.50 <$ IEPS < 12.5
M_2O_3	$Q_M = +3$	$6.50 <$ IEPS < 10.4
MO_2	$Q_M = +4$	$0.50 <$ IEPS < 7.50
M_2O_5	$Q_M = +5$	IEPS < 0.50
MO_3	$Q_M = +6$	IEPS < 0.50

The basic oxides involve cations with the lowest formal charge. They are alkaline or alkaline-earth oxides. The cations in the acidic oxides have the highest formal charges: +5 or +6. The IEPS values display a saturation value close to zero, because of the water leveling effect. Water, which is the solvent in IEPS measurements, does not allow one to study species more acidic than H_3O^+, such as the M_2O_5 and MO_3 oxides. Parks established that IEPS values are approximately linear decreasing functions of the ratio Q_M/r_M. Yet, the dependence on r_M implied by this relation is not systematically obeyed. There are oxides

which exist of a given cationic charge, in which the increase of IEPS correlates well with the variation in r_M:

MnO_2	$r_{Mn} = 0.42$ Å	IEPS =	4.2
TiO_2	$r_{Ti} = 0.50$ Å	IEPS =	4.7
SnO_2	$r_{Sn} = 0.58$ Å	IEPS =	7.3

But, in the following series, the trend is not obeyed:

MgO	$r_{Mg} = 0.65$ Å	IEPS =	12.4
CdO	$r_{Cd} = 0.97$ Å	IEPS =	10.4
HgO	$r_{Hg} = 1.10$ Å	IEPS =	7.3

Similarly, in the context of heterogeneous catalysis, the average CO_2 adsorption energy on oxides (for example) was shown to increase, which reveals an increasing basic character, when the ratio Q_M/r_M decreases (305).

4.2.2 Cation electronegativity and oxygen charge

Another parameter which is often used, when quantifying the acidity of an oxide, is the cationic Mulliken electronegativity. This is defined as minus the first derivative of the atom energy, E, with respect to its electron number N: $\chi_M = -\dfrac{\partial E}{\partial N}$. Its relevance is easily understood since, according to the Lewis' definition, acidity is the ability to accept an electron pair. The acidity is, thus, expected to be higher for cations of higher electronegativity. In a given oxide series, the higher the cation in the periodic table, the stronger the acidity of the oxide. The further to the left of the periodic table the cation is located, the more basic will be the associated oxide.

In oxides, the ionicity of the oxygen-cation bond is strongly correlated with the electronegativity of the cation. As χ_M increases, the oxygen-cation bond becomes more

covalent and the absolute value of the oxygen effective charge, Q_o, decreases. Sanderson (306) has proposed an empirical method to estimate the partial ionic charges in a binary compound, which assumes that the charge transfer equalizes the electronegativities, χ, of the two species. With this argument, he predicted that Q_o decreases in the series: Na_2O, MgO, Al_2O_3, SiO_2 and SnO_2. Tanabe and Fukuda (307), by measuring the CO_2 adsorption energy in the series of alkaline-earth oxides, found that the basicity decreases from BaO to MgO: $BaO > SrO > CaO > MgO$. Basicity, thus, varies monotonically with the oxygen charge which, according to Sanderson, is equal to -0.61, -0.60, -0.57 and -0.50 in this series. This argument was used by Auroux and Gervasini (305), who proved, for a large number of oxides, that the NH_3 adsorption energy decreases when the percentage of ionic character, defined according to Sanderson's scale (308), increases, while the CO_2 adsorption energy increases along the same series. With this same criterion, Vinek et $al.$ (309) explained the results of the oxygen $1s$ core level shifts, quoted associated with a larger oxygen charge.

4.2.3 Hydroxyl groups on the surfaces of oxides

Thiel and Madyes's review (310) gives a good overview of the experimental studies on the dissociation of water at surfaces. Most of these studies have been performed on powders which become hydroxylated more easily than planar surfaces. This effect is associated with the high density of defects on powders. This has been confirmed by several studies of the dissociation of water on planar surfaces with low densities of steps (311-313).

Infra-red absorption and HREELS give access to the values of the OH^- stretching frequencies. When water, acids or bases are dissociated on a surface, several types of OH^- groups are formed. Some hydroxyl groups result from the adsorption of a proton on a surface. Others are pre-formed OH^- groups which adsorb on surface cations (314). The

stretching frequencies depend not only on the type of OH⁻ group but also on the surface site and on the number of bonds formed between the OH⁻ group and the surface (Figure 4-1). Some correlations exist between the stretching frequency shift and the nature of the adsorption site (315-319):

- Higher frequencies are assigned to hydroxyl groups bound to surface cations, and lower frequencies to protons adsorbed on surface oxygens. Both families present many internal splittings on rough surfaces, due to all the possible surface sites, adsorption sites – on bridge, ternary, *etc.*, - and lateral interactions between adsorbed groups.

- On a given compound, lower stretching frequencies characterize less basic oxygens because they reveal weaker O–H bonds. For hydroxyl groups adsorbed on a surface cation, lower frequencies characterize more acidic cations, because a weaker O–H bond is generally associated with a stronger OH-cation bond. This is not always obeyed when different compounds are compared.

- The stretching frequency of hydroxyl groups bound to a single surface cation is lower on more under-coordinated cations. The reverse is true for protons adsorbed on the top of a surface oxygen.

Information on the preferential bonding between adsorbate and surface ions, and on water dissociation may also be obtained by secondary ion mass spectrometry, in the limit of low surface damage. When hydrogen or oxygen isotopes are used to mark water (*e.g.* D_2O or $H_2^{18}O$), the surface oxygens may, in addition, be distinguished from those belonging to the water molecules in the fragments (320).
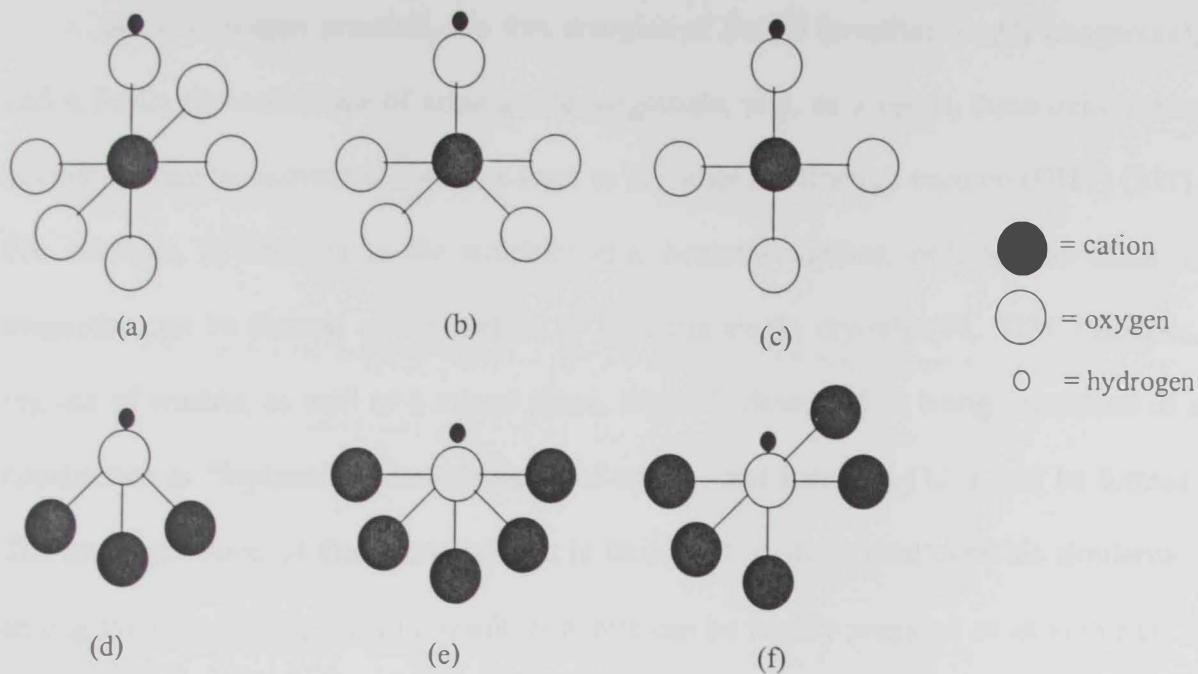
Figure 4-1: Configuration of OH⁻ groups on the surfaces of the oxides: (a), (b), (c) the hydroxyl group is adsorbed on a six-, five- and four-fold coordinated surface cation, respectively; (d), (e), (f) the proton is adsorbed on three- and five-fold coordinated surface oxygen, respectively.

4.3 Surface reactivity of single crystal hematite with CCl₄.

The surface chemistry of iron oxides is important technologically due to its role in catalysis and corrosion. In addition, the iron oxides, magnetite and hematite, are abundant components of the earth's crust and soil, and their chemistry is relevant to environmental research and concerns such as the hydrogeology of aquifers and the remediation of groundwater contamination. For this reason, a molecular-level understanding of the surface chemistry of iron oxides will have an impact in a number of different areas. From a fundamental surface chemical perspective, hematite single crystal surfaces are of great interest because they can be reduced by varying degrees so as to produce a variety of surface reconstructions and, therefore, various surface sites. Consequently, they allow for the study of the dependence of the surface chemistry upon the termination (oxygen *versus* iron), surface stoichiometry, arrangement of surface iron atoms and oxidation state.

At low oxygen pressure, the free energies of $Fe_{1-x}O$ (wustite), Fe_3O_4 (magnetite), and α-Fe_2O_3 (hematite) are of comparable magnitude, and, as a result, these oxides may coexist or may be converted from one form to the other in ultrahigh vacuum (UHV) (321). For example, in addition to the stoichiometric hematite surface, ordered thin films of magnetite can be formed at the surface of hematite single crystals (94, 322). Likewise, regions of wustite, as well as a mixed phase, which is described as being comprised of a coexistence or "biphase" of nanodomains of wustite and hematite (323), can be formed. The interconversion of these terminations is facilitated by the crystallographic similarities among the iron oxides, and as a result, hematite can be readily prepared so as to present a rich variety of iron oxide terminations for chemical study in the well-controlled ultrahigh vacuum ambient.

The difference in the reactivities of these surfaces is dramatic and clearly supports the observation that dissociative adsorption of CCl_4 upon iron oxide is strongly dependent on the nature of the surface. Where CCl_4 dissociation is facile at room temperature on the magnetite termination (Fe_3O_4, Figure 4-2b), it does not appear to occur on the biphase surface, which is comprised of nanodomains of wustite ($Fe_{1-x}O$, Figure 4-2a) and hematite (α-Fe_2O_3, Figure 4-2c).

Significantly, there is a clear and reproducible distinction between the Fe_3O_4 and $Fe_{1-x}O$ surface regions: the wustite ($Fe_{1-x}O$) consistently remains free of chlorine. This result correlates with the AES measurements reported by Camillone III *et al.* indicating the lack of dissociation of CCl_4 on the biphase termination, because it suggests that $Fe_{1-x}O$, which is a component of the biphase termination, does not react with CCl_4.

Figure 4-3 shows the Auger electron spectra collected in the vicinity of the chlorine LMM transition following CCl_4 exposure for the three iron oxide surface phases examined: (a) the magnetite selvedge, (b) the annealed biphase and (c) the as-oxidized biphase. In all three cases the

surfaces were exposed to doses more than sufficient to drive the Cl/O ratio to saturation levels in the magnetite selvedge case. For comparison purposes, the AES resulting from the unexposed magnetite selvedge surface is shown in trace (d) of Figure 4-3.
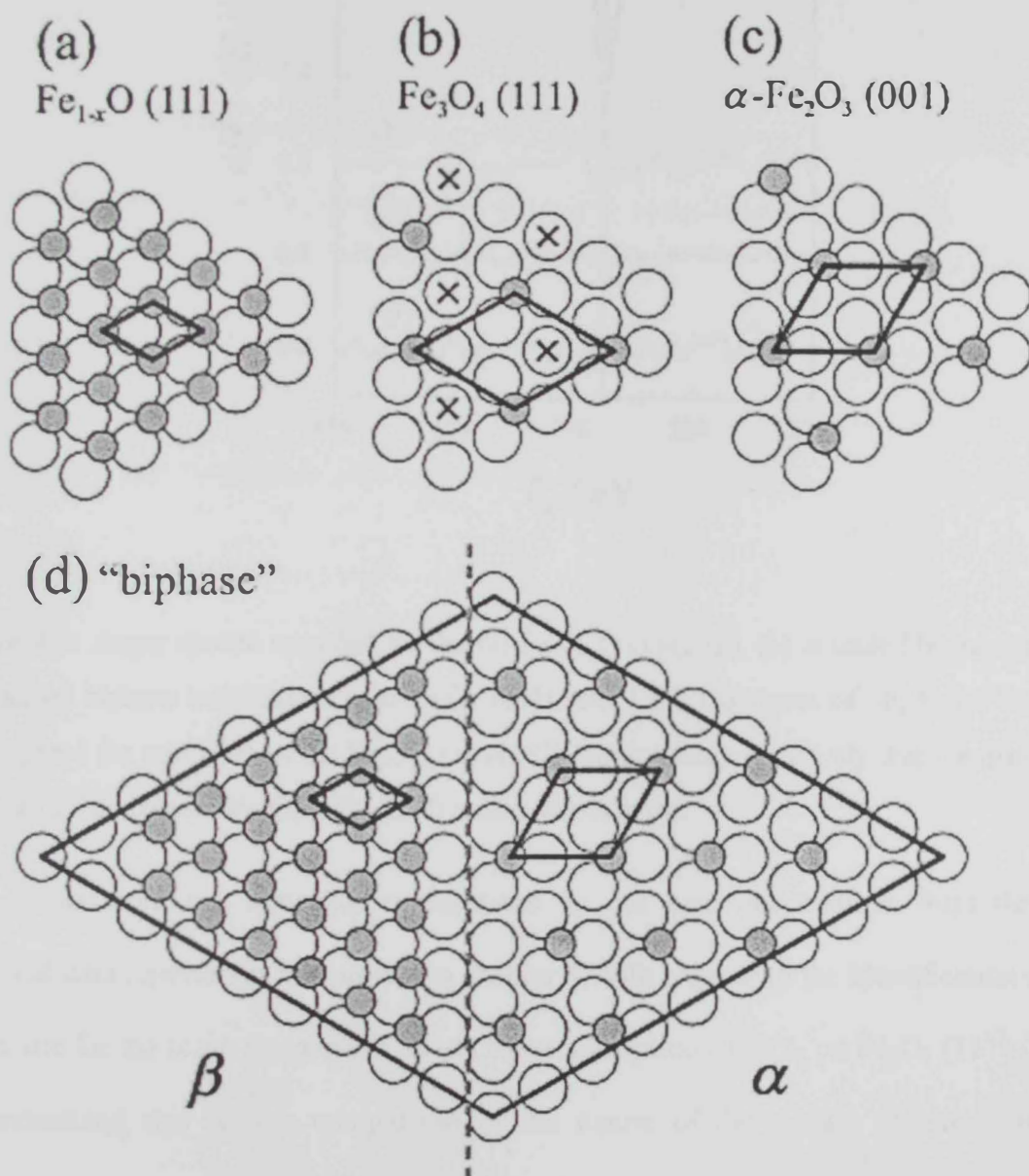
Figure 4-2: (a)–(c), respectively The iron terminations of wustite (Fe$_{1-x}$O(111), a = 3.04 Å), magnetite (Fe$_3$O$_4$(111), with the so-called "mix-trigonal" surface layer, a = 5.92 Å) and hematite (α-Fe$_2$O$_3$ (001) with the single iron surface layer, a = 5.03 Å, (321)). (d) Idealized structural model of the biphase (324) showing regions of α-Fe$_2$O$_3$ (001)-like (α) and Fe$_{1-x}$O(111)-like (β) surface terminations. The large circles represent oxygen atoms and the smaller, darker circles represent iron atoms. The "×" marks the one oxygen atom in all of these surface lattices with a vertical dangling bond.
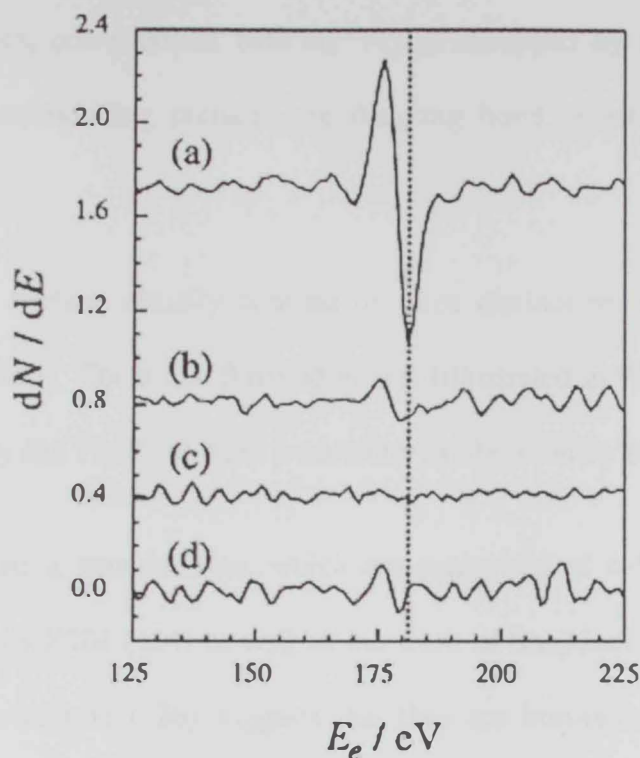
Figure 4-3: Auger spectra recorded for the (a) Fe_3O_4 (111)-(2×2), (b) annealed biphase and (c) as-oxidized biphase terminations of α-Fe_2O_3 (001) after CCl_4 exposures of ~8, 8 and 80 times that required for saturation of the Fe_3O_4 (111)-(2×2) termination, respectively. For comparison, a spectrum for unexposed Fe_3O_4 (111)-(2×2) is also shown in (d).

This work has structural implications on our own observations from the new empirical data reported in this project in chapter 3, with regards to the identification of the active site for the room temperature dissociative adsorption of CCl_4 on Fe_3O_4 (111)-(2×2). To understand this fully a comparison of the nature of the surface structures of the magnetite and biphase terminations must first be made. The magnetite surface is iron-terminated, and there is evidence indicating that it terminates in a 6 Å hexagonal array of surface iron atoms that in the bulk crystal would occupy tetrahedral sites and carry a +3 valence (325). A schematic illustration of the structure proposed by Ritter and Weiss, which is a relaxed version of the so-called mix-trigonal layer, is shown in (Figure 4-2b). It is important for the purposes of this discussion to note that of the four oxygen atoms within

the surface unit mesh, one (marked with an "×") is uncapped by any iron counter ion, leaving, in a covalent-bonding picture, one dangling bond oriented along the surface normal.

The biphase surface actually consists of three distinct regions or nanodomains, referred to as α, β and γ. The α and β nanodomains (illustrated in Figure 4-2d) have been identified as α -Fe_2O_3 and $Fe_{1-x}O$ by their periodicity as observed by STM (324).

Concerning the α nanodomains, which are comprised of α-Fe_2O_3 (001), the 6 Å periodicity observed by STM (324) as well as the work of Shaikhutdinov and Weiss (159) and Scheffler and coworkers (326) suggests that they are iron-terminated. The proposed surface structure is shown in Figure 4-2c, with iron atoms at the surface that in the bulk crystal would occupy octahedral sites and carry a +3 valence. The β nanodomains are considered to be comprised of $Fe_{1-x}O$ (111) because they exhibit an internal periodicity of 3 Å (324). However, as the (111) layers of iron and oxygen in $Fe_{1-x}O$ both have a periodicity of 3 Å, the termination of these regions remains undetermined. Nevertheless, though the possibility cannot be ruled out that they are oxygen-terminated, it is likely that both the α and β nanodomains are iron-terminated, given that the biphase is prepared under conditions which are reducing when compared to the more oxidizing ambients required to generate oxygen terminations (327).

Three qualitatively distinct categories of iron oxide surfaces were identified: (1) the $Fe_{1-x}O$ surface, terminated entirely by iron (or oxygen) atoms and, therefore, presenting only one type of dangling bond to the vacuum, (2) the α-Fe_2O_3 surface, terminated by iron-capped oxygen triads and presenting iron and oxygen dangling bonds oriented away from the surface normal, and (3) the Fe_3O_4 surface, terminated by iron and presenting the same dangling bonds in addition to the vertical dangling bond that in the bulk binds the oxygen

to a tetrahedrally coordinated Fe^{3+}. The importance of the simple experimental observation—that dissociative adsorption resulting in the accumulation of chlorine at the surface occurs on the magnetite and not on the biphase termination (and therefore not on either category 1 or category 2 surfaces)—is that it implies that the presence of both the iron cation and the oxygen atom with the vertically directed dangling bond (as found in category 3) are necessary for the reaction to occur. A suggested mechanism consistent with this implication is that the positively charged iron surface ions act to polarize the chlorine atoms, stabilizing the formation of negatively-charged chloride ions, while the dangling bond associated with the oxygen marked "×" acts as a stabilizing site for the resultant CCl_2 and in effect supplies the electron density required for heterolytic cleavage of the C–Cl bonds to produce Cl^- from CCl_4. This cleavage could occur in a concerted fashion or stepwise through a CCl_3 intermediate (327).

The appeal of this model for the CCl_4–Fe_3O_4 (111) reaction is that it predicts no reaction for either of the iron or oxygen terminations of both $Fe_{1-x}O$ (111) and α-Fe_2O_3 (001). In the case of oxygen termination, the important polarizing influence of the iron cations is absent, and there are no "acceptor" sites for nascent chloride anions. For the case of iron termination, the iron cations are not easily oxidized, and electron density of the oxygen atoms is required in order for the net reaction to occur:

$$CCl_{4(g)} + 2e^- \longrightarrow :CCl_2 + 2Cl^- \qquad \text{Eq. 4-1}$$

Interestingly, despite the close similarity between the magnetite (Fe_3O_4) and hematite (α-Fe_2O_3) terminations (Figure 4-2b and c), the absence of a properly oriented oxygen dangling bond to act as a nucleophile appears to hinder the reaction of the (001) face of hematite with CCl_4. Another contributing factor may be the availability of the electrons of the uppermost oxygen atoms. By counting electrons as they would be

distributed in a covalent crystal, it has been found that in magnetite, the dangling bond of oxygen marked "×" in Figure 4-2b would contain 0.75 electrons, whereas the oxygen atoms in the hematite surface illustrated in Figure 4-2c would contain 0.5. Thus, it would be expected that the magnetite oxygen atoms are more capable of supplying the requisite electron density. This conclusion draws further support from the observation that around the edges of the sample, weak LEED patterns were observed consistent with a (3×3) structure (recently reported by Ketteler *et al.* (321)). Weak chlorine features in the Auger spectra were also reported. Two of the proposed structures for the (3×3) surface possess iron cations and uncapped oxygen anions (321).

As described above, in this case, the presence or absence of iron cations is highlighted; in their absence there is no polarizing influence to drive heterolytic C–Cl bond cleavage and no stabilizing site for nascent chloride ions.

The mechanism for the dissociative adsorption of CCl_4 on magnetite must be different than on pure iron. In the case of zero valent iron (Fe^0) the production of iron chlorides (89) implies that oxidation of iron occurs. The net reaction can be described as electron transfer to Cl resulting in the formation of $FeCl_2$ and an adsorbed diradical :CCl_2 surface species (328). Therefore, it is apparent that the reaction involves electron transfer from Fe^0 to the CCl_4, which dissociates as described in Eq. 4-1. In the case of the iron oxide–CCl_4 interaction, though the end result for CCl_4 is the same, the iron can no longer be thought of as the electron donor, since the Fe_3O_4 (111)-(2×2) surface is considered to be terminated by oxidized iron (Fe^{3+}) (325). Even if the surface iron atoms exist in a less oxidized state due to surface relaxation-related charge transfer, their tendency to be further oxidized is *greatly* decreased compared to Fe^0. Due to the presence of dangling iron bonds, it is expected that the addition of chloride anions to the iron-terminated surface

107

would be energetically favorable, as they would tend to satisfy the dangling coordination sites. However, the question remains: what is the source of electrons required for the transformation of CCl_4 to $:CCl_2 + 2Cl^-$ and what is the surface site which provides the electron density to stabilize hypothetically a doubly positively charged CCl_2 species? It has been proposed that the uncapped oxygen atoms in the Fe_3O_4 (111)-(2×2) provides the requisite electron density (329).

The above-proposed mechanism accounts only for the surface reaction leading to a surface [Cl]/[O] ratio of 0.5 on Fe_3O_4(1 1 1)-(2×2). However, two factors would certainly contribute to propagation of the reaction to higher chlorine coverges. First, it is quite likely that the reaction described by Eq. 4-3c is exothermic, given that two bonds are broken and three are formed. Therefore, the chloride ions may be ejected from the initial reaction site as has been observed on TiO_2 (110) (329), freeing up the iron cation for reaction with another CCl_4. In addition, disruption of the lattice due to the desorption of phosgene ($OCCl_2$) might result in the creation of reactive defect sites.

$$CCl_{4(g)} \xrightarrow{100K} CCl_{4(ad)} \xrightarrow{\Delta} CCl_{4(g)} \qquad \text{Eq. 4-2}$$

$$CCl_{4(g)} \xrightarrow{100K} CCl_{2(ad)} + 2Cl_{(ad)} \xrightarrow{\Delta} CCl_{4(g)} \qquad \text{Eq. 4-3a}$$

$$\xrightarrow{\Delta} \frac{1}{2} C_2Cl_{4(g)} + 2Cl_{(ad)} \qquad \text{Eq. 4-3b}$$

$$\xrightarrow{\Delta,lattic-O} OCCl_{2(g)} + 2Cl_{(ad)} \qquad \text{Eq. 4-3c}$$

$$2Cl_{(ad)} \xrightarrow{\Delta,lattice-Fe} FeCl_{2(g)} \qquad \text{Eq. 4-4}$$
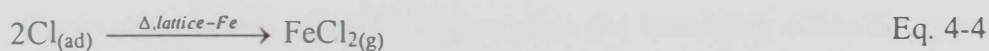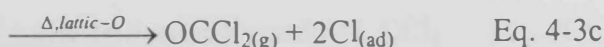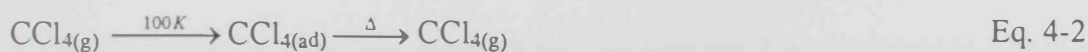
4.4 CCl_4 chemistry on the magnetite selvedge of single-crystal hematite: competitive surface reactions

Another recent interesting structural study undertaken by Adib and co-workers in 2002, involved temperature programmed reaction/desorption (TPR/D) studies to characterize the surface chemistry which occurs between CCl_4 and the Fe_3O_4 (111) selvedge of single crystal α-Fe_2O_3 (0001). Six separate desorption events were clearly observed and four desorbing species were identified: CCl_4, $OCCl_2$, C_2Cl_4 and $FeCl_2$. Adib (330) proposed that $OCCl_2$, CCl_4 and C_2Cl_4 are produced in reactions involving the same precursor, CCl_2. Three reaction paths compete for the CCl_2 precursor: oxygen atom abstraction (for $OCCl_2$), molecular recombinative desorption (for CCl_4) and associative desorption (for C_2Cl_4). During the TPR/D temperature ramp, the branching ratio was shown to depend upon the temperature and the availability of the reactive sites. The data obtained is consistent with a rich site-dependent chemistry (330).

In particular, it was observed that several surface mechanisms responsible for recombinative desorption of CCl_4, associative desorption of C_2Cl_4 and desorption of $OCCl_2$ following oxygen abstraction, compete for the same reaction precursor at a limited number of reaction sites. Based on this observation, it is suggested that CCl_4 dissociatively adsorbs, at temperatures no greater than 250 K, on Fe_3O_4 (111) to form CCl_2 and Cl. These precursors then react to form the desorbing reaction products CCl_4, C_2Cl_4, $OCCl_2$ and $FeCl_2$. Their observations strongly suggest that the branching ratios for recombinative desorption, associative desorption, and lattice-oxygen abstraction depend upon the availability of species reaction sites. Some aspects of the kinetics of desorption of the products from the surface can be elucidated from analysis of the coverage dependence of the evolution of these products. Ultimately, scanning tunneling microscopy (STM) can be used to further investigate the assertion that the surface chemistry of CCl_4 on the Fe_3O_4

(111)-(2×2) surface depends sensitively upon the structure of the surface and the presence or absence of species adsorption sites (330).

4.5 Structure-reactivity relationship

The knowledge of atomic surface structures is the first step towards a deeper understanding of the physical and chemical surface properties of solids. In the case of compound materials with ionic bonding character such as metal oxides, the atomic structures of polar surface orientations can deviate strongly from their corresponding bulk truncations. This is predicted by many theoretical studies, but only a few experimental surface structure determinations exist so far. The (111) surfaces of oxides with the rocksalt structure such as NiO and MgO become stabilized by severe reconstructions (331–333); other surfaces do not reconstruct but become stabilized by strong interlayer relaxions in their surface regions.

The surface structure of Fe_3O_4 (111) films grown epitaxially onto Pt(111) substrates was determined in a previously LEED analysis (334,335). A strongly relaxed bulk termination of Fe_3O_4(111) exposing 1/4 monolayer of iron cations over a hexagonal close-packed oxygen layer was obtained as a best fit structure. On iron oxide single crystal samples prepared under similar conditions two diVerent coexisting Fe_3O_4(111) surface terminations were observed with STM, and two models that diVer from the surface structure model discussed above were proposed for these terminations (336). Magnetite, Fe_3O_4, crystallizes in the cubic inverse close-packed fcc sublattice with Fe^{2+} and Fe^{3+} spinel structure where the oxygen anions form cations located in the interstitial sites (337,338). Two diVerent cation sites exist: the first is tetrahedrally coordinated to oxygen and occupied only by Fe^{3+} ions, and the second is octahedrally coordinated to oxygen and occupied by equal numbers of Fe^{2+} and Fe^{3+} ions (Figure 4-4).
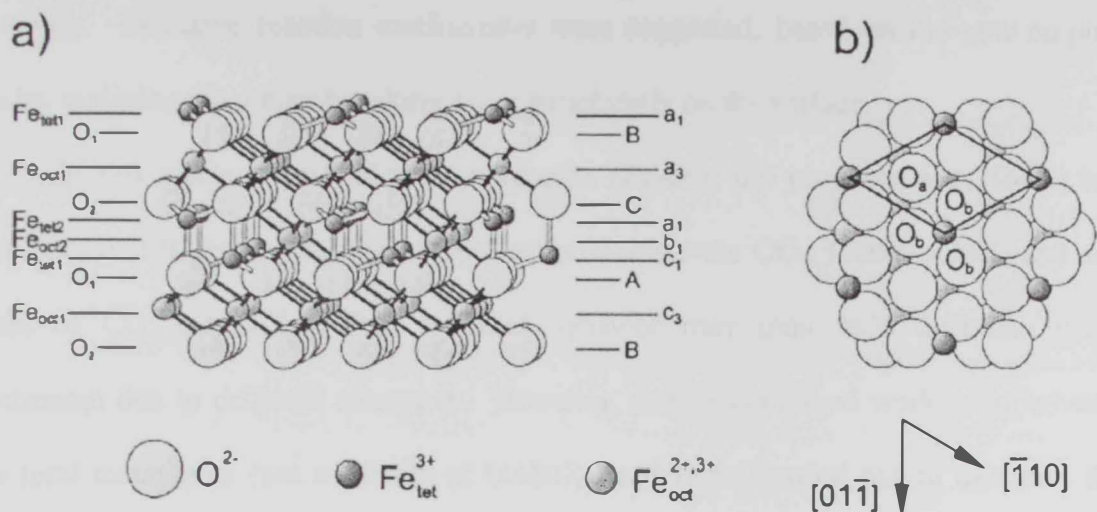
Figure 4-4: Perspective side view (a) and top view (b) of the Fe_3O_4 structure exposing a (111) surface plane without interlayer relaxations. The top view is drawn with the full ionic radii, the side view with ionic radii reduced by a factor of 0.5. Two types of notation for the layer stacking along the [111] direction are given on the left and right side of (a). In the top view in (b) the Fe_3O_4 (111)-(1×1) surface unit cell with a lattice constant of 5.94 is indicated, as well as the symmetrically inequivalent oxygen atoms Oa and Ob respectively.

The Fe_3O_4 (111) surface represents a polar surface termination that should be unstable considering the electrostatic surface energy within simple ionic models. It is concluded that the ionic bond character is reduced at the surface and bonding becomes more covalent there. The large interlayer relaxations induce a strongly modified electron density of states at the surface, which can reduce or completely compensate the excess surface charge of the polar Fe_3O_4 (111) surface. This must represent the mechanism stabilizing the polar surface termination found in this analysis. The dominant contribution of the surface electron density tet1 of states is created by Fe $3d$ states of the Fe cations in the topmost layer, which are imaged as protrusions in the atomic resolution STM images (339).

In chapters 2 and 3 respectively, among the pure iron oxides magnetite showed the highest reactivity and an ability to adsorb water which could be the reason behind its

reactivity. Tentative reaction mechanisms were suggested, based on the new empirical results, outlining what may be taking place structurally on the surface.

In this study, specifically for magnetite (Fe_3O_4), the products were found to be significantly different. The major observed products were CO_2, $COCl_2$, C_2Cl_4 and small traces of CO and HCl. This different behavior may indicate a different reaction mechanism due to different structures. However, further continued work using advanced structural techniques (not available at UAEU) need to be carried out to ascertain these observations.

It is clear from the FT-IR spectra represented in Figure 3-14/Figure 4-5 that magnetite exhibited a good reactivity toward CCl_4 which can be compared to the behavior of mixed oxide catalysts at a higher temperature (400 °C). This behavior could be attributed to the rich content in oxygen ions (Fe_3O_4) compared to hematite and maghemite. The presence of large absorption bands for gaseous water in the case of hematite and maghemite indicate that they do not adsorb much water to allow for is reaction with CCl_4. In contrast, the absence of water bands in the case of magnetite indicates that water absorbs well on magnetite allowing for some reaction with CCl_4, which is supported by the formation of products such as CO_2, C_2Cl_4, $COCl_2$ and HCl. The fact that the reactivity was still low even when water adsorbs may indicate that water only physical adsorbs on the surface of magnetite.
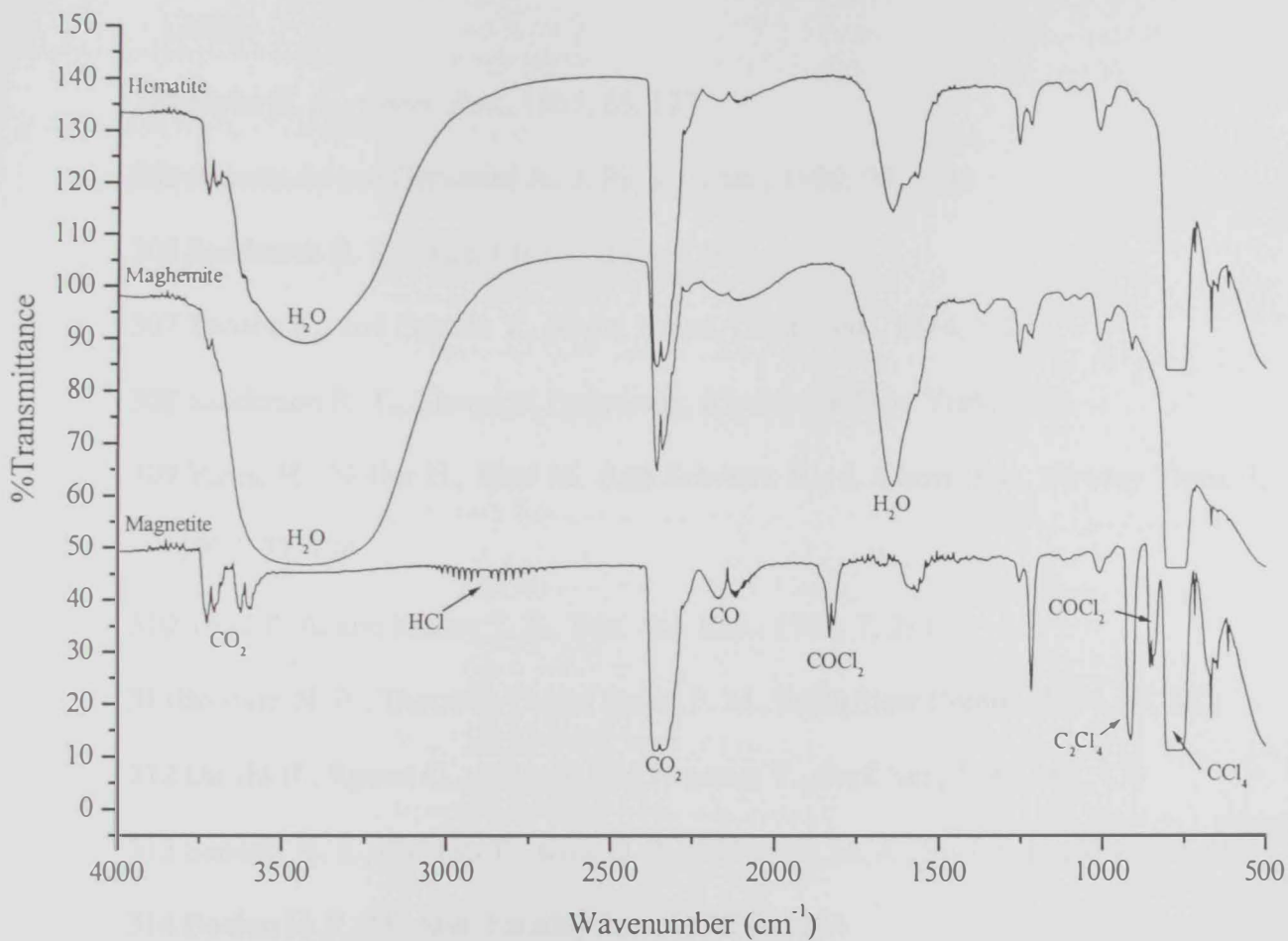
Figure 4-5: FT-IR spectra for the products of the decomposition of CCl_4 over pure iron oxide in the presence of water at 200 °C.

References

301 Tanabe K., Solid *acids and bases*, academic press: New York, 1970.

302 Tanabe K., *Catalysis, science and technology*, New York, 1981

303 Claudine N., Physics and chemistry at oxide surfaces, Cambridge University Press, 1996.

304 Parks G. A., *Chem. Rev.*, 1965, 65, 177

305 Auroux A. and Gervasini A., J. Phys. Chem., 1990, 94, 6371

306 Sanderson R. T, Inorg. Chem., 1964, 3, 925

307 Tanabe K., and Fukuda Y., React. Kunet. Catal. Lett., 1974, 1, 21

308 Sanderson R. T., Chemical Periodicity, Rheinhold: New York, 1960

309 Vinek H., Noller H., Ebel M. And Schwarx K., J. Chem. Soc. Faraday Trans. I, 1977, 73, 734

310 Thiel P. A. and Madey T. E., Surf. Sci. Rep., 1987, 7, 211

311 Brookes N. B., Thornton G. and Quinn F. M., Solid State Comm., 1987, 64, 383

312 Onishi H., Egawa C., Aruga T. and Iwasawa Y., Surf. Sci., 1987, 191, 479

313 Sanders H. E., Gardner P., King D. A and Morris M. A., Surf. Sci., 1994, 304, 159.

314 Boehm H. P., Discuss. Faraday Soc., 1971, 52, 264

315 Coluccia S., Lavagnino S. and Marchese L., Mater. Chem. Phys., 1988, 18, 445

316 Shido T., Asakura K. and Iwasawa Y., J. Chem. Soc. Faraday Trans. I, 1989, 85, 441.

317 Morrow B. A., Stud. Surf. Sci. Catal. A, 1990, 57, 161

318 Knozinger E., Jacob K. H. and Hofmman P., J. Chem. Soc. Faraday Trans., 1993a, 89, 1101

319 Knozinger E., Jacob K. H., Singh S. and Hofmman P., Surf. Sci., 1993b, 290, 388

320 Bourgeois S., Jomard F. and Oerdereua M., Surf. Sci., 1992, 279, 349.

321 Ketteler G., Weiss W., Ranke W. and Shlögl R., *Phys. Chem. Chem. Phys.* 3 (2001), 1114

322 Fellows R. A., Lennie A. R., Raza H., Pang C. L., Thornton G. and Vaughan D. J., *Surf. Sci.* 445 (2000), p. 11

323 Condon N. G, Leibsle F. M, Lennie A. R., Murray B. W., Vaughan D. J. and Thornton G., *Phys. Rev. Lett.* 75 (1995), 1961

324 Condon N. G., Leibsle F. M., Lennie A. R., Murray P. W., Parker T. M., Vaughan D. J. and Thornton G., *Surf. Sci.* 397 (1998), 278.

325 Ritter M. and Weiss W., *Surf. Sci.* 432 (1999), p. 81

326 Wang X. G-, Weiss W., Shaikhutdinov Sh.K, Ritter M., Petersen M., Wagner F., Schög R. and Scheffler M., *Phys. Rev. Lett.,* 81 (1998), 1038.

327 Shaikhutdinov Sh.K and Weiss W., *Surf. Sci.* 432 (1999), L627.

328 Smentkowski V. S., Cheng C. C and Yates J. T, Jr., *Surf. Sci.,* 215 (1989), L279

329 Camillone N., Adib K., Fitts J.P., Rim K.T., Flynn G.W., Joyce S.A., Osgood R.M., Surf. Sci., 511 (2002) 267-282

330 Adib. K, Camillone. N, Fitts. J.P, Rim. K.T, Flynn G.W, Joyce S.A, Osgood R.M, Surf. Sci., 497 (2002) 127–138.

331 Wolf. D, Phys. Rev. Lett. 68 (1992) 3315.

332 Rohr. F, Wirth. K, Libuda. J, Cappus. D, Ba¨umer. M, Freund. H.-J, Surf. Sci. 315 (1994) L977.

333 Pojani. A, Finocchi. F, Goniakowski. J, Noguera. C, Surf. Sci. 387 (1997) 354.

334 Weiss. W, Barbieri. A, Van Hove. M. A, Somorjai. G. A, Phys. Rev. Lett. 71 (1993) 1848.

335 Barbieri. A, Weiss. W, Van Hove. M.A, Somorjai. G.A, Surf. Sci. 302 (1994) 259.

336 Lennie. A.R, Condon. N.A, Leibsle. F.M, Murray. P.W, Thornton. G, Vaughan. D.J, Phys. Rev. B 53 (1996) 10 244.

337 WyckoV. R.W.G, Crystal Structures, 2nd ed., Vol. I, Interscience, New York, 1982.

338 Cornell. R.M, Schwertmann. U, The Iron Oxides, VCH, Weinheim, 1996.

339 Ritter. M, Weiss. W, Surface Science 432 (1999) 81–94

CHAPTER 5

CONCLUSION

CHAPTER 5: CONCLUSION

The main objective of the various reactions and experiments carried out in this project was not only to develop the best technique for the decomposition of CCl_4 but equally to study the relationships between the structure and the reactivity of all types of iron oxides toward CCl_4.

In the first part of this work, a series of pure iron oxides were prepared by classical methods and gave a slightly low surface area. Mixed iron oxides were also prepared by the sol-gel method but yielded high surface area particles. The supported iron oxides were prepared by wet impregnation methods which also gave moderate high surface areas. All these oxides were characterized by FT-IR, XRD and surface area measurements. The surface areas of hematite and magnetite in this work were found to have higher values than those previously reported in the literature, but maghemite gave approximately the same surface area as the quoted values in the literature. In contrast, in the case of the mixed oxides, the specific surface area of $Fe_2O_3-Al_2O_3$ was found to be 396 m^2/g which was found to be very high. The sol-gel method appeared to enhance the process yielding fine particles with a high surface area. The $Fe_2O_3-SiO_2$ system (prepared by the sol-gel method) in this work gave a very high surface area compared to the corresponding value previously reported in the literature. The supported iron oxides gave a moderate high surface area, which can be attributed to the fact that the support materials used themselves had a low surface area.

In the second part of this project, a new simpler and easier technique was developed for the decomposition of carbon tetrachloride, CCl_4, using a closed reactor system. The optimum catalyst was found to be Fe_2O_3/Al_2O_3 with a related high surface area of 121 m^2/g. This system showed a high percentage conversion of CCl_4 (97.55%) in the presence of water at a temperature of 400 ^oC. The presence of water in the

decomposition of CCl_4 over Fe_2O_3-Al_2O_3 resulted in the almost complete decomposition of CCl_4 to CO_2 and HCl while in the absence of water the conversion of CCl_4, $COCl_2$ and C_2Cl_4 was considerably less. The fact that water does not react with CCl_4 under the current experimental conditions in the presence of any adsorbent and its great role in the enhancement of the reactivity in the presence of an adsorbent allows us to believe that CCl_4 is catalytically decomposed through oxidation by adsorbed water molecules and surface hydroxyl groups. Some mechanisms were discussed in relation to this system. In addition, some catalysts were used to decompose CCl_4 at a lower temperature (α-Fe_2O_3, γ-Fe_2O_3, Fe_3O_4, Fe_2O_3/Al_2O_3 and Fe_2O_3/C). Interestingly, these systems showed different products due to different reaction mechanisms.

There are some limitations that can be identified in the technique used in this work. For example, the reactor used was a closed reactor system, which is not a pulsed system and prohibits the study of the kinetics and the amount of products generated with respect to time. In relation to this work, the results can be further improved by using a flow reactor. With such a reactor, the experimental work would be easier to carry out in the laboratory. In addition, the length of time would be considerably reduced to carry out each experiment compared to the closed reactor system. Each reaction in a closed reactor system needs 2 hours at least, which does not count the time consumed in the pre-preparation of the system and the related cleaning of the equipment.

In addition, the various characterization techniques used in this project were limited to FT-IR and XRD due to the lack of advanced structural techniques not available at UAEU. No other techniques were available in the scope of this project here to study the structure of the materials, such as XPS, LEED, AES *etc*. Furthermore, the amount of products generated in the various reactions could not be measured quantitatively; in this work the area under the curve of the respective FT-IR spectra of the results was depended

on for this. Facilities such as mass spectrometry and gas chromatography, which are available at UAEU could not be used either as such facilities need to be directly connected to the reactor systems (in line with the system developed).

However, the despite the limitations, the results do suggest that this work may pave the way for the future development of a newer and simpler technique for the treatment of carbon tetrachloride, which has huge implications environmentally, if fully exploited and developed at a later stage. Interestingly, no such facilities exist in the United Arab Emirates for the decomposition of carbon tetrachloride.

REFERENCES

REFRENCES

1. Stipp. S. L, *Chem. Geolg.*, 190 (2002) 321-337.

2. Cornell. R. M. and Schwertmann. U., *The Iron Oxides: Structure, Properties, Reactions, Occurrence and Uses*. VCH Publishers, Basel, 1996.

3. Stumm. W. and Morgan. J. J., Aquatic Chemistry: *An Introduction Emphasizing Chemical Equilibria in Natural Waters*, Wiley-Interscience, Toronto, 1981.

4. Ford. R. G., Kemner. K. M. and Bertsch. P. M., *Geochim. Cosmochim. Acta* 63 (1999) 39– 48.

5. Manceau. A., Schlegel. M. L., Musso. M., Sole. V. A., Gauthi. C., Petit. P.E. and Trolard. F., *Geochim. Cosmochim. Acta* 64 (2000) 3643– 3661.

6. Alcacio. T. E., Hesterberg. D., Chou. J. W., Martin. J. D., Beauchemin. S. and Sayers. D. E., *Geochim. Cosmochim. Acta* 65 (2001) 1355–1566.

7. Randall. R. S., Sherman. D. M. and Ragnarsdottir. K. V., *Geochim. Cosmochim. Acta* 65 (2001) 1015– 1023.

8. Ding. M., de Jong. B. H. W. S., Roosendaal. S. J. and Vredenberg. A., *Geochim. Cosmochim. Acta* 65 (2000) 1209– 1219.

9. Russel. J. D., Parfitt. R. L., Fraser, A. R. and Farmer, V. C., *Nature* 248 (1974) 220– 221.

10. Persson. P., Nilsson. N. and Sjöberg. S., *J. Colloid Interface Sci.* 177 (1996) 263– 275.

11. Dideriksen. K. and Stipp. S. L. S. (submitted for publication), *Geochim. Cosmochim. Acta*.

12. Piccolo. A., Cellano. G., Arienzo. A. and Mirabella. A., *J. Environ. Sci. Health B* 29 (1994) 1105– 1115.

13. Clausen. L. and Fabricius. I., *Environ. Qual.,* 30 (2001) 858– 869.

14. Zhou. Q. H., Maurice. P. A. and Cabaniss. S. E., *Geochim. Cosmochim. Acta* 65 (2001) 803– 812.

15. O'Melia, C. R., Coagulation and flocculation. In: Weber Jr., W.J. (Ed.), *Physicochemical Processes for Water Quality Control*. Wiley, New York (1972) pp. 61– 109. Chapter 2.

16. Gould. J. P., *Water Resour.* 16 (1982) 871– 877.

17. Astrup. T., Stipp. S. L. S. and Christensen. T. H., *Sci. Technol.* 34 (2000) 4163– 4168.

18. Lundtorp. K., Jensen. D. L., Sørensen. M. A., Mogensen. E. P. B. and Christensen. T. H., *Waste Manage. Res.* 20 (2002) 69– 79.

19. Cantrell. K. J., Kaplan. D. I. and Wietsma. T. W., *J. Hazard. Mater.* 42 (1995) 201–212.

20. Powell. R. M., Puls. R. W., Hightower. S. K. and Sabatini. D. A., *Environ. Sci. Technol.* 29 (1995) 1913– 1922.

21. Taylor. R. M., Schwertmann. U. and Fechter, H., *Clay Min.*, 20 (1985) 147-151.

22. Schwertman. U. and Cornell. R. M., *Iron oxides in the laboratory. Preperation and characterization*, VCH Verlagsgesellschaft mbH, Germany, 1991.

23. Bernal. J. D., Dasgupta. D. R. and Mackay. A. L., *Clay Min. Bull.*, 4 (1959) 15-30.

24. Chukhrov. F. V., Zuyagin. B. B., Gorshkov. A. I., Ermilova. L. P. and Balashova. V. V., *Izvest. Akad. Nauk.* SSSR, 4 (1973) 23-33.

25. Feithnecht. W. and Keller, G., *Z. Anorg. Chem.*, 262 (1950) 61-68.

26. Stampfl. P. P., *Corros. Sci.*, 9 (1969) 185-187.

27. Hansen. H. C. B., *Clay Min.*,24 (1989) 663-669.

28. Murad. E. and Taylor. R. M., *Clay Min.*, 19 (1984) 77-83.

29. Chenavas. J., Joubert. J. C., Capponi. J. J. and Marezio. M., *Solid State Chemistry*, 6 (1973) 1-15.

30. Pernet. M., Chenavas. J. and Joubert. J. C., *Solid State Common*, 13 (1973) 1147-1154.

31. Braun. H. and Gallagher. K . J., *Nature* 240 (1972) 13-14.

32. Howe. A. T. and Gallagher. K. J., *Trans. Farad. Soc.*, 1974, 22-33.

33. Buttner. G., *Bergakademie*, 12 (1961) 780-781.

34. Dezsi. I. and Coey. J. M. D., *Phys. Stat. Sol.*, 15 (1973) 681-685.

35. Towe. K. M. and Bradley, W. F., *J. Colloid Interface Sci.* , 24 (1967) 384-392

36. Russell, J. D., *Clay Min.*, 14 (1979) 190-214.

37. Robi. R. A. and Waldbaum, D. R., *Geol. Surv. Bull. (U.S)* , 1967, 1259.

38. Garrels. R. M. and Christ. C. L., *Solutions, minerals and equilibria.* Harper and Row, Publ., New York, 1965, 450 pp.

39. Mohr. E. C. J., van Baren. F. A. and van Shcuylenborg. J., *Tropical soils.* 3rd ed. Monton-Ichtior, Baru, van Hoeve, The Haugue-Paris-London, 1972, 481 pp.

40. Murad. E., Bowen. L. H., Long. G. L. and Quin. T. G. *Clay Min.* 23 (1988) 161-173.

41. Klabunde. K. J., Stark. J., Koper. O., Mohs. C., Park. D., Decker. S., Jiang. Y., Lagadic. I., and Zhang. D., *J. Phys. Chem.*, (1996) 100, 1213.

42. Klabunde. K. J., Decker. S., Lucas. E., and Koper. O., *in International Symposium on Cluster and Nanostructure Interfaces*, Worl Scientific Pub., New Jersey, Richmond, VA, P. Jena, S. N. Khanna, B. K. Rao (editors) Oct. 1999.

43. Shriver. D. F., Atkins. P. W. and Langforf. C. H., *Inorganic Chemistry*, 2nd edition, W. H. Freeman, New York, 1994.

44. Sachtler. W. M. H., *Ber. Bunsenges.*, (1995) 99, 1295.

45. Henry. C. R., *App. Surf Sci.*, (2000) 164, 252.

46. Puddephatt. R. J., *Met. Clusters. Chem.*, (1999) 2, 605.

47. Trost, B. M., *Angew. Chem.*, Int. Ed. Eng., (1995) 34, 259.

48. Choudary. M., Kantam. M. L. and Santhi. L. P., *Catal. Today*, (2000) 57, 17.

49. Rofer-DePoorter. C.K., *Chem. Rev.* 81 (1981) 447.

50. Kung. H.H., in: *Transition Metal Oxides: Surface Chemistry and Catalysis*, Elsevier, Amsterdam, 1989.

51. Novakova. J., Jiru. P. and Zavadil. V., *J. Catal.* 21 (1971) 143.

52. Rochester. C.H. and Topham. S.A., *J. Chem. Soc., Faraday Trans.* 75 (1979) 1259.

53. Busca. G. and Cotena. N., *Mater. Chem.* 3 (1978) 49.

54. Busca. G. and Lorenzelli. V., *Mater. Chem.* 5 (1980) 213.

55. Busca. G. and Lorenzelli. V., *J. Catal.* 66 (1980) 155.

56. Ferretto. L. and Glisenti. A., *Journal of Molecular Catalysis A: Chemical* 187 (2002) 119–128.

57.   Lorenzelli. V., Busca. G. and Sheppard. N., *J. Catal.* 66 (1980) 28.

58.   Busca. G. and Lorenzelli. V., *Mater. Chem.* 6 (1981) 175.

59.   Busca. G. and Lorenzelli. V., *J. Catal.* 72 (1981) 303.

60.   Busca. G. and Lorenzelli. V., *J. Chem. Soc., Faraday Trans.* 178 (1982) 2911.

61.   Busca. G., *React. Kinet. Catal. Lett.* 20 (1982) 373.

62.   Busca. G. and Rossi. P.F., *Mater. Chem. Phys.* 9 (1983) 561.

63.   Busca. G., Zerlia. T., Lorenzelli. V. and Girelli. A., *J. Catal.* 88 (1984) 125, 131.

64.   Busca. G., Zerlia. T., Lorenzelli. V. and Girelli. A., *React. Kinet. Catal. Lett.* 27 (1985) 429.

65.   Iizuka. H. Ikeda, Terao. T. and Tanabe. K., *Aust. J. Chem.* 35 (1982) 927.

66.   Ishikawa. T., Cai. W.Y., Kandori. K., *Langmuir* 9 (1993) 1125.

67.   Glisenti. A., *J. Chem. Soc., Faraday Trans.* 94 (1998) 3671.

68.   Heinrich. V.E. and Cox. P.A., *The Surface Science of Metal Oxides*, Cambridge University Press, Cambridge, 1994.

69.   Glisenti. A., *J. Mol. Catal. A: Chem.* 153 (2000) 169.

70.   Jin. T., Hattori. H. and Tanabe. K., *Bull. Chem. Soc. Jpn.,* (1983) 56, 3208.

71.   Glisenti. A., Favero. G. and Granozzi. G., *J. Chem. Soc., Faraday Trans.,* 1998, 94(1), 173-182.

72.   Suda. Y., Morimoto. T. and Nagao. M., *Langmuir*, (1987) 3, 99.

73.   Blyholder. G. and Richardson. E.A., *J. Phys. Chem.* 66 (1962) 2597.

74.   Zecchina. A., Scarano. D. and Reller. A., *J. Chem. Soc., Faraday Trans.* 1 84 (1988) 2327.

75.   Batis. H., Harrouch. N. and Ghorbel. A., *J. Soc. Chim. Tunis.* 2 (1985) 51.

76. Zecchina. A., Scarano. D., Bordiga. S., Spoto. G. and Lamberti. C., *Adv. Catal.* 46 (2001) 265.

77. Mackrodt. W. C., Davey. R. J., Black. S. N. and Docherty. R., *J. Cryst. Growth* 80 (1987) 441.

78. Guo. Q., McBreen. P. H. and Møller. P. J., *Surf. Sci.* 423 (1999) 19.

79. Shklover. V., Nazeeruddin. M.-K., Zakeeruddin. S. M., Barbé. C., Kay. A., Haibach. T., Steurer. W., Hermann. R., Nissen. H.-U. and Grätzel. M., *Chem. Mater.* 9 (1997) 430.

80. Gatehouse. B. M., Livingstone. S. E. and Nyholm. R. S., *J. Chem. Soc.* (1958) 3137.

81. Little. L. H., *Infrared Spectra of Adsorbed Species*, Academic Press, San Diego, CA, 1966 (Chapter 3).

82. Morterra. C., Cerrato. G., Bolis. V. and Fubini. B., *Spectrochim. Acta* 49A (1993) 1269.

83. Auroux A. Gervasini, *J. Phys. Chem.* 94 (1990) 6371.

84. Barteau. P. and Delmon. B., *Catal. Today,* (1989) 5, 121.

85. Heiland. G. and Luth. H., *in The Chemical Physics of Solid Surfaces and Heterogeneous Catalysis*, ed. D. P. Woodruff, Elsevier, Amesterdam, (1984) vol. 3.

86. Adib. K. et al., *Surface Science* 497 (2002) 127-138.

87. Dixon-Warren. S.J., Jensen. E.T. and Polanyi. J.C., *J. Chem. Phys.* 98 (1993) 5938.

88. Smentkowski. V.S., Cheng. C.C. and Yates Jr. J.T., *Langmuir* 6 (1990) 147.

89. Haag. W.R. and Yao. C.C.D., *J. Environ. Sci. Tech.* 26 (1992) 1005.

90. Bertoti I.S. Pap, Szekely. T. and Babievskaya. I.Z., *J. Therm. Anal.* 32 (1987) 281.

91. Hooker. P.D. and Klaubunde. K.J., *J. Environ. Sci. Tech.* 28 (1994) 1243.

92. Lennie. A.R., Condon. N.G., Leibsle. F.M., Murray. P.W., Thornton. G. and Vaughan. D.J., *Phys. Rev. B* (1996) 10244.

93. Condon. N.G., Murray. P.W., Leibsle. F.M., Thornton. G., Lennie. A.R. and Vaughan. D.J., *Surf. Sci.* 310 (1994) L609.

94. Huang. C.P., Dong. C. and Tang. Z., *Waste Manage.* 13 (1993) 361.

95. Chou. S., Huang. Y.H., Lee. S.N., Huang. G.H. and Huang. C., *Water Res.* 33 (1999) 751.

96. Watts. R.J., Jones. A.P., Chen. P.H. and Kenny. A., *Water Environ. Res.* 69 (1997) 269.

97. Pardieck. D.L., Bouwer. E.J. and Stone. A.T., *J. Contam. Hydrol.* 9 (1992) 221.

98. Walling. C., *Accounts Chem. Res.* 8 (1975) 125.

99. Valentine. R.L. and Wang. H.C.A., *J. Environ. Eng.* 124 (1998) 31.

100. Al-Hayek. N. and Dore. M., *Water Res.* 24 (1990) 973.

101. Lin. S.S., Ph.D. Dissertation, Drexel University, Philadelphia, (1997).

102. Chou. S. and Huang. C., *Chemosphere* 38 (1999) 2719.

103. Kitajima. N., Fukuzumi. S. and Ono. Y., *J. Phys. Chem.* 82 (1978) 1505.

104. Krutikov. P.G., Cheshun. A.V. and Ragulin. V.V., *J. Appl. Chem. USSR* 57 (1984) 723.

105. Lin. S.S. and Gurol. M.D., *Environ. Sci.* Technol. 32 (1998) 1417.

106. Barb. W.G., Baxendale. J.H. and Hargrave. K.R., *J. Chem. Soc.* 121 (1950) 462.

107. Carberry. J.J., *Chemical and Catalytic Reaction Engineering*, McGraw-Hill, New York, (1976).

108. Chou. S. and Huang. C., *Applied Catalysis A: General* 185 (1999) 237-245.

109. Kim. S.-J. et al., *Applied catalysis A: General* 234 (2002) 35-44.

110. Masuda. M. and Miyahara. K., *Bull. Chem Soc. Jpn.* 47 (1974) 1058.

111. Tinkle. M. and Dumesic. J. A., *J. Catal.* 103 (1987) 65.

112. Vannice. M. A., *in*: J.R. Anderson, M. Boudart (Eds.), *Catalysis Sciences and Technology*, Vol. 3, Springer, new York, (1982) p. 190.

113. Wang. Y. and Davis. B. H., *Appl. Catal. A* 180 (1999) 277.

114. Basinska. A., Jozwiak. W.K., Goralski. J. and Domka. F., *Appl. Catal. A* 190 (2000) 107.

115. Ekerdt. J.G., Klabunde. K.J., Shapley. J.R., White. J.M. and Yates. J. T., *Jr. J. Phys. Chem.* (1988) 92, 6182.

116. Templeton. M.K. and Weinberg. W.H., *J. Am. Chem. Soc.* (1985) 107, 97.

117. Templeton. M.K. and Weinberg. W.H., *J. Am. Chem. Soc.* (1985) 107, 774.

118. Li. Y.-X., Schlup. J.R. and Klabunde. K.J., *Langmuir (*1991) 7, 1394.

119. Lin. S.-T. and Klabunde. K.J., *Langmuir (*1985) 1, 600.

120. Atteya. M. and Klabunde. K.J., *Chem. Mater.* (1991) 3, 182.

121. Li. Y.-X. and Klabunde. K.J., *Langmuir* (1991) 7, 1388.

122. Li. Y.-X., Koper. O., Atteya. M. and Klabunde. K. J., *Chem. Mater.* (1992) 4, 23.

123. Henderson. M.A., Jin. T. and White. J.M., *J. Phys. Chem.* (1986) 90, 4607.

124. Aurian-Blajeni. B. and Boucher. M.M., *Langmuir* (1989) 5, 170.

125. Kuiper. A.E.T. and van Bokhoven, J.J.G.M., *J. Medema, J. Catal.*, (1976) 43, 154.

126. Graven. W.M., Weller. S.W. and Peters. D.L., *I. E. C. Proc. Des. DeV.* (1966) 5, 183.

127. Baier. R.W. and Weller. S.W., *I. E. C. Proc. Des. DeV.* (1967) 6, 380.

128. Tzou, T.Z. and Weller. S.W., *J. Catal.* (1994) 146, 370.

129. Smentkowski. V.S., Hagans. P. and Yates. J. T. Jr., *J. Phys. Chem.* (1988) 92, 6351.

130. Guo. X., Yoshinobu. J. and Yates. J. T. Jr., *J. Phys. Chem.* (1990) 94, 6839.

131. Lee. K.Y., Houalla. M., Hercules. D.M. and Hall. W. K., *J. Catal.* (1994) 145, 223.

132. Palucka. T.P., Eror. N.G. and McNamara. T.A., *Mater. Res. Soc.Symp. Proc.* (1995) 368, 275.

133. Williamson. C.J. and O'Brien. O., *J. Mater. Chem.* (1994) 4, 545.

134. Nadler. M.P., Nissan. R.A. and Hollins. R.A., *Appl. Spectrosc.* (1988) 42, 634.

135. Hedge. R.I. and White. J.M., *J. Phys. Chem.* (1986) 90, 2159.

136. Mitchell. M.B., Sheinker. V.N. and Mintz. E.A., *J. Phys. Chem. B*, (1997) 101, 11192-11203.

137. Hutzinger. O., *The Handbook of Environmental Chemistry*, Springer, Berlin, (1982).

138. Lai. D., *J. Environ. Sci. Health* C2 (1984) 135–140.

139. Riley. P. and Chester. R., *Introduction to Marine Chemistry*, Academic Press, London, (1979).

140. Kemmer. F.N., *The Nalco Water Handbook*, McGraw Hill, New York, (1979).

141. Bandara. J. et al., *Appl. Catal. B*, 34, (2001) 307-320.

142. Cunningham. J. and Sayyed. G., *J. Chem. Soc., Faraday Trans.* 86 (1990) 3941.

143. Stone. A., Torrents. A., Smolen. J. and Hadley. J., *J. Environ. Sci. Technol.* 27 (1993) 895–902.

144. Davis. A.P. and Huang. C.P., *Langmuir* 6 (1990) 857–862.

145. Pennel. K.D., Rhue. R.D. and Johnson. C.T., *Environ. Sci. Technol.* 26 (1992) 756–761.

146. Goss. K., *Environ. Sci. Technol.* 26 (1992) 2287–2292.

147. Goss. K., *Environ. Sci. Technol.* 27 (1993) 2127–2132.

148. Cornell. R.M., Schwertmann. U. and Coll. U., *Polym. Sci.* 256 (1980) 1711–719.

149. Morrison. S.R., *The Chemical Physics of Surfaces*, Plenum Press, New York, (1977).

150. Sposito. G., *The Environmental Chemistry of Aluminum*, CRC Press, Boca Raton, FL, (1996).

151. Anpo. M. and Matsura. M., *Photochemistry on Solid Surfaces,* Elsevier, Amsterdam, (1989).

152. Corma. A., Rodellas. C. and Fornes. V., *J. Catal.* 88 (1984) 374.

153. Cerrsin. L., Fax. B.J. and Lord. R. C., *J. Chem. Phys.* 21 (1953) 1170.

154. Lee. E.H., *Catal. Rev.* 8 (1973) 285.W. Weuss, *Surf. Sci.* 377 (1997) 943.

155. Weiss. W., *Surf. Sci.* 377 (1997) 943.

156. Shaikhutdinov. Sh.K., Joseph. Y., Kuhrs. C., Ranke. W. and Weiss. W., *Farraday Discuss.* 114 (1999) 363.

157. Hirano. T., *Appl. Catal.* 26 (1986) 65.

158. Kuhrs. C., Arita. Y., Weiss. W., Ranke. W. and Schlogl. R., *Top. in Catal.* 14, 1-4 (2001) 111-123.

159. Weiss. W. and Schlogl. R., *Top. in Catal.* 13 (2000) 75-90.

160. Lenoble. V., Boutas. O., Deluchat. V., Serpaud. B. and Bollinger. J., *J. Coll. and inter. Sci.*, 255 (2002) 52-58.

161. Kaltreider. R. C., Davis. A. M., Larivi`ere. J. P. and Hamilton. J.W., *Environ. Health Perspect.* 109 (2001) 245.

162. Jain. C. K. and Ali. I., *Water Res.* 34 (2000) 4304.

163. Pattanayak. J., Mondal. K., Mathew. S. and Lalvani. S. B., *Carbon* 38 (2000) 589.

164. Sancha. A. M., O'Ryan. R. and Perez. O., *in "Proceedings of the Santiago Symposium, September 1998," IAHS*, Publ. No. 260, p. 17 (2000).

165. Clifford. D. and Lin. C.-C., *"Arsenic (III) and Arsenic (V) Removal from Drinking Water in San Ysidro, New Mexico"* EPA/600/S2-91/011. U.S. EPA, incinnati, (1991).

166. Guenegou. T., Tambute. A., Jardy. A. and Caude. M., *Analusis* 26 (1998) 352.

167. Wang. Y. and Reardon. E. J., *Appl. Geochem.* 16 (2001) 1241.

168. Borho. M. and Wilderer. P., *Water Sci. Technol.* 34 (1996) 25.

169. Meng. X., Bang, S. and Korfiatis. G. P., *Water Res.* 34 (2000) 1255.

170. Subramanian. K. S., Viraragavan. T., Phommavong. T. and Tanjore. S., *Water Qual. Res. J. Canada* 32 (1997) 551.

171. Hug. S. J., Canonica. L., Wegelin. M., Gechter. D. and Von Gunten. U., *Environ. Sci. Technol.* 35 (2001) 2114.

172. Celis. R., Hermosin. M. C. and Cornejo. J., *Environ. Sci. Technol.* 34 (2000) 4593.

173. Lothenbach. B., Furrer. G., Scharli. H. and Schulin. R., *Environ. Sci. Technol* 33 (1999) 2945.

174. Herrera. P., Burghard. R. C. and Phillips. T. D., *Vet. Microbiol.* 74 (2000) 259.

175. Dentel. S. K., Jamrah. A. I. and Sparks. D. L., *Water Res.* 32 (1998) 3689.

176. Bouras. O., Chami. T., Houari. M., Khalaf. H., Bollinger. J. C. and Baudu. M., *Environ. Technol.* 23 (2002) 504.

177. Lenoble. V., Boutas. O., Deluchat. V., Serpaud. B. and Bollinger. J., *J. Coll. and inter. Sci.*, 255 (2002) 52-58.

178. Makansi, J., *Power* 137 (March) (1993) 23.

179. Paik. S.C. and Chung. J.S., *Appl. Catal. B* 8 (1996) 267.

180. Zhu. T., Dreher. A. and Stephanopoulos. M.F., *Appl. Catal. B* 21 (1999) 103.

181. Rosenberg. H.S., Engdahl. R.B., Oxley. J.H. and Genco. J.M., *Chem. Eng. Prog.* 71 (5) (1975) 66.

182. Goar. B.G., *Oil Gas J.* 25 (August) (1975) 96.

183. Gall. R.L. and Piasecki. E.J., *Chem. Eng. Prog.* 71 (5) (1975) 72.

184. Brown. G.W., Roderick. D. and Nastri. A., *Oil Gas J.* 18 (1991) 41.

185. Lepsoe. R., *Ind. Eng. Chem.* 32 (1940) 910.

186. Salis. J. and Berk. D., *Ind. Eng. Chem. Res.* 27 (1988) 1951.

187. Mulligan. D.J. and Berk. D., *Ind. Eng. Chem. Res.* 28 (1989) 926.

188. Roesner. G., *Die Chemische Fabrik* 10 (1937) 101.

189. Khalafalla. S.E., Foerster. E.F. and Haas. L.A., *Ind. Eng. Chem.*, Prod. Res. Dev. 10 (1971) 133.

190. Khalafalla. S.E. and Haas. L.A., *J. Catal.* 24 (1972) 121.

191. Okay. V.C. and Short. W.L., *Ind. Eng. Chem., Prod. Res. Dev.* 12 (1973) 291.

192. Hibbert. D.B. and Tseung. A.C.C., *J. Chem. Soc., Faraday. Trans. I* 74 (1978) 981.

193. Happel. J., Hnatow. M.A., Bajars. L. and Kundrath. M., *Ind. Eng. Chem., Prod. Res. Dev.* 14 (1975) 154.

194. Happel. J., Leon. A.L., Hnatow. M.A. and Bajars. L., *Ind. Eng. Chem., Prod. Res. Dev.* 16 (1977) 150.

195. Bazes. J.G.I., Caretto. L.S. and Nobe. K., *Ind. Eng. Chem., Prod. Res. Dev.* 14 (1975) 264.

196. Hibbert. D.B., *Catal. Rev. Sci. Eng.* 34 (1992) 391.

197. Wang. C.-H., Lin. S.-S., Hwang. W.-U. and Weng. H.-S., *Ind. Eng. Chem. Res.* 41 (2002) 666.

198. Ma. J., Fang. M. and Lau. N.T., *Appl. Catal. A* 150 (1997) 253.

199. Boswell. M.C., *Canadian Patent* 301554 (1930).

200. Boswell. M.C., *US Patent* 1880741 (1932).

201. Boswell. M.C., *US Patent* 2026819 (1936).

202. Doumani. T.F., *US Patent* 2361825 (1944).

203. Doumani. T.F., Deery. R.F. and Bradley. W.E., *Ind. Eng. Chem.* 36 (1944) 329.

204. "*Ullmann's Encyclopedia of Industrial Chemistry*," 5th ed. VCH, Weinheim. (a) Kahlich, D., Wiechern, U., and Lindner, J., Vol. A22, p. 239 (1993); (b) Thiemann, M., Scheibler, E., andWiegand, K.W., Vol. A17 (1991) 332.

205. Trent. D. L., *in* "*Kirk–Othmer Encyclopedia of Chemical Technology*," 4th ed., Vol. 20, p. 271. Wiley, New York, (1996).

206. Duma. V., Ph.D. Thesis, in preparation, Technical University Chemnitz, Germany.

207. Koper. O., Li. Y. X. and Klabunde. K. J., *Chem. Mater.*, 5 (1993) 500.

208. Li. Y. X., Koper. O., Atteya. M. and Klabunde. K. J., *Chem. Mater.*, 4 (1992) 323.

209. Li. Y. X. and Klabunde. K. J., *Lumgmuir*, 7 (1991) 1368.

210. Klabunde. K. J., Khaleel. A. and Park. D., *High Temp. and Mater. Sci.*, 33 (1995) 9.

211. Li. Y. X. and Klabunde. K. J., *Chem. Mater.*, 4 (1992) 611.

212. Sen. B., Falconer. J. L., Mao. T. F., Yu. M. and Flesner. R. L., *J. Catal.*, 126 (1990) 465-476.

213. Hegde. R. J. and Barteau. M. A., *J. Catal.*, 120 (1989) 387-400.

214. Stobbe. D. E., Van Buren. F. R., Van Dillen. A. J. and Geus. J. W., *J. Catal.*, 135 (1992) 533-562.

215. Kim. D. S., Segawa. K., Soeya. T. and Wachs. I. E., *J. Catal.*, 136 (1992) 539-553.

216. Stobbe. D. E., Buren. F. R., Stobbe-Kreemers. M. W., Schokker. J. J., Van Dillen. A. J. and Geus. J. W., *J. Chem. Soc. Faraday Trans.*, 87 (1991) 1623-1629, 1631-1637.

217. Stile. A. B., *Catalyst supports and supported catalysts, theoretical and applied concepts*, Butterworths, London, 1987.

218. Edreva-Kandjiera. R. M., Vuurman. M. A. and Johannes. C., *J. Mol. Catal.*, 76 (1992) 299-305.

219. Siegel. R. W., Ramasamy. S., Hahn. H., Ting. L. and Gronsky. R., *J. Mater. Res.*, 1988, 3, 1367.

220. El-Shall. M. S., Slack. W., Vann. W. and Hanely. D., *J. Phys. Chem.*, 1994, 98(12), 3067.

221. Xu. H., Tan. S. and Leo. N. T., *Trans. Nonferrous Met. Soc. China*, 2(1), 58-60 (English) 1992.

222. Baraton. M. I. and El-Shall. M. S., *Nanostruct. Mater.*, 1995, 6, 301.

223. Edelstein. A. S., Hadjipanayis. G. C. and Siegel. R. W. (editors), *Nanophase Materials*, Kluwer Academic Publisher, Dordrecht, 1994, pp. 73-80.

224. Huh. M. Y., Kim. S. H., Ahn. J. P., Park. J. K., Kim. B. K., *Nanostruct. Mater.*, 1999, 11(2), 211.

225. Cow. G. M. and Gonsalves. K. E. (editors), *Nanotechnology, moleculary Desighned mataerials*, American Chemical Society, Washongton, D. C., 1996, pp. 79-99.

226. Rouanet. A., Pichelin. G., Roucan. C., Snoeck. E., Monty. C., *in* G.C. Hadjipanayis, R. W. Siegel (editors), *Nanophase Materails*, Kluwer Academic Press, Dordrech, 1994, pp. 85-88.

227. Kodas, T. T., *Adv. Mater.*, 1989, 6, 180.

228. Hadjipanayis, G. C. and R. W. Siegel (editors), Nanophase Materials, Kluwer Academic Publishers, Dordrecht, 1994, pp. 109-116.

229. Janackovic. Dj., Jakoanvic. V., Kostic-Gvozdenovic. Lj., Uskokovic. D., *Nanostruct. Mater.*, 1998, 10(3), 341.

131

230. Messing. G. L., Zhang. S. C., Jayanthi. G. V., *J. Am. Ceram. Soc.,* 1993, 76(11) 2707.

231. Jayanthi. G. V., Zhang. S. C. and Messing. G. L., *J. Aerosol Sci. Technol.,* 1993, 19(4) 478.

232. Messing. G. L. and Gardner. T. J., *Am. Ceramic Soc. Bull.,* 1987, 64, 1498.

233. Pollinger. J. P. and Messing. G. L., *J. Aerosol. Sci. Technol.,* 1993, 19(4) 217.

234. Kodas. T. T., Datye. A., Lee. V. and Engler. E., *J. Appl. Phys.,* 1989, 65, 2149.

235. Cow. G. M. and Gonsalves. K. E. (editors), Nanotevhnology, Molecularly Designed Materials, American Chemical Society, Washington, D.C., 1996, pp. 64-78.

236. Ulrich. G. D. and Riehl. J. W., *J. Colloid Interface Sci. Technol.,* 1982, 87, 257.

237. Lindackers. D., Janzen. C., Rellinghaus. B., Wassermann. E. F., Roth. P., *Nanostruct. Mater.,* 1998, 10(8) 1247.

238. Skanadan. G., Chen. Y. J., Glumac, N. and Kear. B. H., *Nanostruct. Mater.,* 1999, 11(2) 149.

239. Itoh. H., Utampanya. S., Stark. J. V., Klabunde. K. J. and Schlup. J. R., *Chem. Mater.,* 1993, 5, 71.

240. Palkar. V. R., *Nanostruct. Mater.,* (1999) 11(3) 369.

241. Interrante. L. V. and Hampden-Smith. M. J. (editors), Chemistry of Advanced Materials: an Overview, Wiley-VCH, New York, 1998.

242. Barringer. E. A. and Bowen. H. K., *J. Am. Ceram. Soc.,* (1982) 65 C-199.

243. Sunil. D., Gafney. H. D., Rafailovich. M. H., Sokolov. J., Gambino. R. J. and Huang. D. M., *J. of non-Cryst. Solids,* 319 (2003) 154-162.

244. Gesser. H. D. and Gosswami. P. C., *Chem. Rev.*, (1989) 89, 765.

245. Charty. M., Henry. M. and Livage. J., *Mater. Res. Bull.*, (1994) 29, 517.

246. Kumazawa. H., Inoue. T. and Sasa. E., *Chem. Eng. J.*, (1994) 55, 93.

247. Hench. L. L. and West. J. K., *Chem. Rev.*, (1990) 90, 33.

248. Yi. G. and Sayer. M., *Ceram. Bull.*, (1991) 70, 1173.

249. Avnir. D., Acc. *Chem. Res.*, (1995) 28, 328.

250. Chandler. C. D., Roger. C. and Hampden-Smith. M. J., *Chem. Rev.*, (1993) 93, 1205.

251. Brinker. C. J. and Scherer. C. W., *Sol-Gel Science*, Academic Press, San Diego, CA, 1990.

252. Segal. D., *Chemical Synthesis of Advanced Ceramic Materials*, Cambridge University Press, Cambridge 1989.

253. Klein. L. (editor), *Sol-Gel Optics: Processing and Applications*, Kluwer, Boston, 1993.

254. Narula. C. K., *Ceramic Precursor Technology and its Applications*, Marcel Decker, New York, 1995.

255. Smith. W. F., *Principles of Materials Science Engineering*, McGraw-Hill Book Company, Singapore (1986).

256. Newnham. R. E., McKinstry. S. E. and Ikawa. H., *Mater. Res. Soc. Symp. Proc.* 175, 161 (1990).

257. Birringer. R., *Mater. Sci. Eng.* A117, 32 (1989).

258. Gleiter. H., *J. Appl. Crystallogr.* 24, 79 (1991).

259. Mayo. M. J., Chen. D.-J. and Hague. D. C., *Nanomaterials: Synthesis, Properties and Applicatons*, ed. Cammarata, pp. 8, 165, J. W. Arrowsmith Ltd., Bristol, UK (1996).

260. Li. G. S., Smith. R. L., Inomata. H. and Arai. K., *Mater. Research Bull.*, 37 (2002) 949-955.

261. Trovarelli. A., *Catalytic Science Series, Catalysis by ceria and related materials*, Vol.2, London, 2002, p. 69.

262. Anderson. J.R., *Structure of Metallic Catalysts*, Academic Press, London, 1975.

263. Geus. J.W. and van Veen. J.A.R., in: R.A. van Santen, P.W.N.M. van Leeuwen, J.A. Moulijn, B.A. Averill (Eds.), *Catalysis. An Integrated Approach*, Second Revised and Enlarged Edition, Elsevier, Amsterdam, 1999, p. 459.

264. Che. M., in: L. Guczi, F. Solymosi, P. Tétényi (Eds.), *New Frontiers in Catalysis*, Elsevier, Amsterdam, 1993, p. 31.

265. De Jong. K. P., *Curr. Opin. Solid Stat Mater. Sci.* 4 (1999) 55.

266. Geus. J.W., *Stud. Surf. Sci. Catal.* 16 (1983) 1.

267. De Jong. K.P., *Stud. Surf. Sci. Catal.* 63 (1991) 19.

268. Jos van Dillen. A., Robert J. A. M., Lensveld. D. J., Geus. J. W. and de Jong. K. P., *J. Catal.*, in press.

269. Kotter. N. and Riekert. L., *Stud. Surf. Sci. Catal.* 3 (1978) 51.

270. Nagayama. H., Honda. H. and Kawahara. H., *J. Electrochem. Soc.*, (1988) 135, 2013.

271. Hishinuma. A., Goda. T., Kitaoka. M., Hayashi, S. and Kawahara. H., *Appl. Surf. Sci.*, (1991) 48/49, 405.

272. Deki. S., Aoi. Y., Okibe. J., Yanagimoto. H., Kajinami. A. and Mizuhata. M., *J. Mater. Chem.*, 7 (9) 1997, 1769-1772.

273. K. J. Klabunde, *Nanoscale Materials in chemistry*, (2001) 95.

274. David and J. E. Welch, *Trans. Faraday*, 52 (1956) 1642.

275. L. J. Bellamy, *The infrared spectra of complex molecules*; John Wiley & Sons Inc.: New York, 1954; chapter 6, p 85.

276. K. E. Lawson, S. Corportion, S. Base, N. M. Albuquerque, *Infrared absorption of inorganic materials*; Reinhold Publishing Corp.: New York, 1961; p 62.

277. Abbas A. Khaleel and Kenneth J. Klabunde, *Chem, Eur. J.*, 2002, 8 (17), 3991-3997.

278. K. Chen, l. Dong, Q. Yan and Y. Chen, *J. Chem. Soc. Faraday Trans.*, 1997, 93(12), 2203-2206.

279. Tanilmis, T; Atalay, S; Alpay, H. E., *J. of Hazard. Mater.*, 2002, B90, 157-167.

280. S.E. Manahan, *Environmental Chemistry*, Lewis, New York, 2000.

281. Hooker, P, D.; Klabunde, K, J., *Environ. Sci. Tech.*, 1994, 28, 1243-1247.

282. Lee, C. C.; Huffman, G.L. *Environ. Prog.* 1989, 8, 190.

283. Lee, C. C.; Huffman, G.L. In *Innovative Hazardous waste treatment technology series,* Vol. 1, thermal Processes; Freeman, H. M., Ed.; Technomic: Lancaster, Basel, 1990; p 1.

284. Imamura, S.; Tarumoto, H.; Ishida, S. *Ind. Eng. Chem. Res.* 1989, 28, 1449.

285. Getty, E. E.; Petrosius, S. C.; Drago, R. S. *J. Mol. Catal.* 1991, 67, 127.

286. Hung, L. S.; Pfefferle, L.D. *Environ. Sci. Technol.* 1989, 23, 1085.

287. Kinner, L. L; McGowin, A.; Manahan, S. E. *Environ. Sci. Technol.* 1993, 27, 482.

288. Illman, D. L. *Chem. Eng. News* 1993, July 12th, 26.

289. Miller, H, L; Dwight, W, S; Cundy, V, A; Matula, R, A, *Hazard. Waste*, 1984, 1, 1.

290. Masel, R. I. *Principles of adsorption and reactions on solid surface*; John Wiley and Sons Inc.: New York, 1996.

291. Corodi, E. M.; Falconer, J. L., *J. Catal.* 1996, 162, 104.

292. Sokoll, R.; Hobert, H.; Schmuck, I. *J. Catal.* 1990, 121, 1536.

293. Clark, F. T.; Springman, M. C.; Willcox, D.; Wachs, I. E. *J. Catal.* 1993, 139, 1.

294. Khaleel, A.; Li, W.; Klabunde, K. J. *Nanostruct. Mater.* 1999, 12, 463.

295. Khaleel, A.; Kapoor, P. N.; Klabunde, K. J. *Nanostruct. Mater.* 1999, 11 (4), 459.

296. Jacoby, M. *Chem. Eng. News* 1998, November 23, 38.

297. Dagani, R. *Chem. Eng. News* 1999, June 7, 25.

298. Johnson, B. F. G. *Coord. Chem. Rev.* 1999, 190, 1269.

299. Khaleel, A; Dellinger, A. *Environ. Sci. Tech.* 2002, 36, 1620-1624.

300. Paul D. H, Klabunde K. J, *Environ. Sci. Tech.* 1994, 28, 1243-124.

301 Tanabe K., Solid *acids and bases*, academic press: New York, 1970.

302 Tanabe K., *Catalysis, science and technology*, New York, 1981.

303 Claudine N., *Physics and chemistry at oxide surfaces*, Cambridge University Press, 1996.

304 Parks G. A., *Chem. Rev.*, 1965, 65, 177.

305 Auroux A. and Gervasini A., *J. Phys. Chem.*, 1990, 94, 6371.

306 Sanderson R. T, *Inorg. Chem.*, 1964, 3, 925.

307   Tanabe K., and Fukuda Y., React. Kunet. *Catal. Lett.*, 1974, 1, 21.

308   Sanderson R. T., *Chemical Periodicity*, Rheinhold: New York, 1960.

309   Vinek H., Noller H., Ebel M. And Schwarx K., *J. Chem. Soc. Faraday Trans. I*, 1977, 73, 734.

310   Thiel P. A. and Madey T. E., *Surf. Sci. Rep.*, 1987, 7, 211.

311   Brookes N. B., Thornton G. and Quinn F. M., *Solid State Comm.*, 1987, 64, 383.

312   Onishi H., Egawa C., Aruga T. and Iwasawa Y., *Surf. Sci.*, 1987, 191, 479.

313   Sanders H. E., Gardner P., King D. A and Morris M. A., *Surf. Sci.*, 1994, 304, 159.

314   Boehm H. P., *Discuss. Faraday Soc.*, 1971, 52, 264.

315   Coluccia S., Lavagnino S. and Marchese L., *Mater. Chem. Phys.*, 1988, 18, 445

316   Shido T., Asakura K. and Iwasawa Y., *J. Chem. Soc. Faraday Trans. I*, 1989, 85, 441.

317   Morrow B. A., Stud. *Surf. Sci. Catal. A*, 1990, 57, 161.

318   Knozinger E., Jacob K. H. and Hofmman P., *J. Chem. Soc. Faraday Trans.*, 1993a, 89, 1101.

319   Knozinger E., Jacob K. H., Singh S. and Hofmman P., *Surf. Sci.*, 1993b, 290, 388

320   Bourgeois S., Jomard F. and Oerdereua M., *Surf. Sci.*, 1992, 279, 349.

321   Ketteler G., Weiss W., Ranke W. and Shlögl R., *Phys. Chem. Chem. Phys.* 3 (2001), 1114.

322   Fellows R. A., Lennie A. R., Raza H., Pang C. L., Thornton G. and Vaughan D. J., *Surf. Sci.* 445 (2000), p. 11.

323   Condon N. G, Leibsle F. M, Lennie A. R., Murray B. W., Vaughan D. J. and Thornton G., *Phys. Rev. Lett.* 75 (1995), 1961.

324   Condon N. G., Leibsle F. M., Lennie A. R., Murray P. W., Parker T. M., Vaughan D. J. and Thornton G., *Surf. Sci.* 397 (1998), 278.

325 Ritter M. and Weiss W., *Surf. Sci.* 432 (1999), p. 81

326 Wang X. G-, Weiss W., Shaikhutdinov Sh.K, Ritter M., Petersen M., Wagner F., Schög R. and Scheffler M., *Phys. Rev. Lett.*,81 (1998), 1038.

327 Shaikhutdinov Sh.K and Weiss W., *Surf. Sci.*, 432 (1999), L627.

328 Smentkowski V. S., Cheng C. C and Yates J. T, Jr., *Surf. Sci.*, 215 (1989), L279

329 Camillone N., Adib K., Fitts J.P., Rim K.T., Flynn G.W., Joyce S.A., Osgood R.M., *Surf. Sci.*, 511 (2002) 267-282.

330 Adib. K, Camillone. N, Fitts. J.P, Rim. K.T, Flynn G.W, Joyce S.A, Osgood R.M, Surf. Sci., 497 (2002) 127–138.

331 Wolf. D, Phys. Rev. Lett. 68 (1992) 3315.

332 Rohr. F, Wirth. K, Libuda. J, Cappus. D, Ba¨umer. M, Freund. H.-J, Surf. Sci. 315 (1994) L977.

333 Pojani. A, Finocchi. F, Goniakowski. J, Noguera. C, Surf. Sci. 387 (1997) 354.

334 Weiss. W, Barbieri. A, Van Hove. M. A, Somorjai. G. A, Phys. Rev. Lett. 71 (1993) 1848.

335 Barbieri. A, Weiss. W, Van Hove. M.A, Somorjai. G.A, Surf. Sci. 302 (1994) 259.

336 Lennie. A.R, Condon. N.A, Leibsle. F.M, Murray. P.W, Thornton. G, Vaughan. D.J, Phys. Rev. B 53 (1996) 10 244.

337 WyckoV. R.W.G, Crystal Structures, 2nd ed., Vol. I, Interscience, New York, 1982.

338 Cornell. R.M, Schwertmann. U, The Iron Oxides, VCH, Weinheim, 1996.

339 Ritter. M, Weiss. W, Surface Science 432 (1999) 81–94.

جامعة الإمارات العربية المتحده

عمادة الدراسات العليا

برنامج ماجستير علوم البيئة

دراسات لدور تركيب أكاسيد الحديد في التحفيز لعمليات البيئة

رسالة مقدمة من الطالبة:

عائشة علي سيف راشد النايلي

إلى جامعة الإمارات العربية المتحدة

إستكمالا لمتطلبات الحصول على درجة الماجستير في علوم البيئة

مشرفي الرسالة

د. عباس أحمد خليل	د. براين مورفي
الأستاذ المساعد	الأستاذ المساعد
بقسم الكيمياء	بقسم الكيمياء
كلية العلوم	كلية العلوم
جامعة الإمارات العربية المتحدة	جامعة الإمارات العربية المتحدة

2004